RICE UNIVERSITY

Multi-Failure Mode Risk Assessment of the Houston/Galveston Bridge System to Hurricane Threats

by

Candase Dawn Arnold

A THESIS SUBMITTED
IN PARTIAL FULFILLMENT OF THE
REQUIREMENTS FOR THE DEGREE

Master of Science

APPROVED, THESIS COMMITTEE

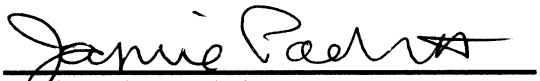

Jamie Padgett, Chair
Assistant Professor of Civil and
Environmental Engineering

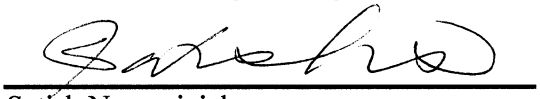

Satish Nagarajaiah
Professor of Civil and Environmental
Engineering and Mechanical Engineering
and Material Science

Philip Bedient
Professor of Civil and Environmental
Engineering

HOUSTON, TEXAS
December 2011

ABSTRACT

Multi-Failure Mode Risk Assessment of the Houston/Galveston Bridge System to Hurricane Threats

by

Candase Dawn Arnold

This research implements the first Houston/Galveston area hurricane risk assessment of bridges for multiple failure modes: bridge deck uplift and bridge scour. Due to recent hurricane damage of bridges, emergency managers need to understand the potential state of the bridge network immediately following a storm for effective mitigation and post-event planning. To that end, this study builds a new database of bridge information necessary for vulnerability modeling, adapts current deterministic models of bridge deck uplift and scour for a probabilistic framework and expands the scour models to include a qualitative estimate for embankment scour. The study area bridges are tested under various hurricane scenario events to reveal the likelihood of damage. Potential applications include retrofit prioritization, real-time spatial damage modeling and better informed preparation. By understanding the risk hurricanes pose to the bridge system, emergency officials can better plan rescue and recovery efforts before a storm impacts the Texas coast.

Acknowledgments

There are many people without whom this thesis would not have reached fruition. First, I'd like to thank my advisor Dr. Jamie Padgett for all her guidance and help with my research, my thesis and my career path. Thank you for taking me on as an undergraduate research assistant all those years ago. Next, I'd like to thank Dr. Satish Nagarajaiah and Dr. Philip Bedient for agreeing to serve on my committee.

Additionally, my thanks go out to all those who helped me in this research project: my fellow graduate student, Navid, several contacts at TxDOT who helped procure inspection files and bridge plans, but especially Michael Carlson and Kenny Ozuna, all of my collaborators at the SSPEED Center and undergraduate research assistants, Benjamin Berryhill and Andrew Lo. I would also like to express my gratitude for all of my fellow graduate students who helped me through my research and time as a graduate student at Rice, especially: Jay Ghosh, Emily McCarthy, Blaine Fuselier and Citlali Tapia.

Finally, I would like to thank my family and my fiancé, Peter, for all of their support during my time at Rice.

Contents

Acknowledgments iii

Contents iv

List of Figures vii

List of Tables xi

List of Equations xiii

Introduction 1

1.1. Motivation and Scope of Research 2

1.2. Overview of Thesis 4

Literature Review 6

2.1. Empirical Evidence of Common Failure Modes from Previous Hurricane Events ... 6

2.2. Bridge Deck Uplift Failure Mode: Mechanics and Research 12

2.2.1. Surge and Wave Forces Acting on Bridge Decks 13

2.2.2. Research on Surge and Wave Forces Prior to Hurricane Katrina 14

2.2.3. Research on Surge and Wave Forces since Hurricane Katrina 16

2.3. Scour Failure Mode 17

2.3.1. Mechanics of Scour 17

2.3.2. Current Scour Practices and Hydraulic Engineering Circulation-18 19

2.3.3. SRICOS/HEC-18 (clay) Method 20

2.3.4. Pier Scour Research 22

2.3.5. Abutment Scour Research 24

2.3.6. Embankment Scour Research 26

2.4. Hurricane Risk Assessment Models for Bridge and Roadway Systems 27

Data Collection and Inventory Analysis 33

3.1. Importance of Data Mining 33

3.2. Data Sources Mined for Houston/Galveston Database 35

3.2.1. National Bridge Inventory 35

3.2.2. Geographical Information Systems Data and Defining the Houston/Galveston Bay Area 37

3.2.3. TxDOT Data: Inspection Files and As-Builts 41
3.2.4. Soil Type Data: SoilMart Online Database 45
3.2.5. Bridge Site Visits 46
3.2.6. Storm Surge and Wave Scenarios from the UT-Austin ADCIRC Modeling Group 47
3.3. Building the Houston/Galveston Bay Area Database 48
3.3.1. Method for Calculating Parameters in the Houston/Galveston Database 50
3.3.1.1. Determining Bridge Type 50
3.3.1.2. Calculating Height above Water 52
3.3.1.3. Calculating Water Depth 56
3.3.1.4. Calculating Channel Bottom Elevation 58
3.3.2. Determining Bridge Subsets for Modeling Purposes 58
3.4. Statistical Analysis of Houston/Galveston Bridge Inventory Database 59
Vulnerability Modeling of Bridge Deck Uplift 64
4.1. Background on Fragility Modeling and Methodology for Uplift 65
4.1.1. Demand Modeling in the Bridge Deck Uplift Model 67
4.1.2. Capacity Modeling in the Bridge Deck Uplift Model 71
4.2. Fragility Surfaces for Bridge Deck Uplift Vulnerability 74
Probabilistic Approach to Scour Vulnerability Modeling 78
5.1. Overview of the Probabilistic Scour Models 78
5.2. Probabilistic Pier Scour Modeling 80
5.2.1. Uncertainties in Input Parameters and Bias in the Model 85
5.2.2. Capacity Limit States for Fragility Analysis 89
5.2.3. Fragility Analysis of Piers in the Houston/Galveston Bay Area 90
5.3. Probabilistic Abutment Scour Modeling 96
5.3.1. Uncertainties in the Input Parameters 102
5.3.2. Capacity Limit States for Abutment Fragility Analysis 103
5.3.3. Fragility Analysis of Abutments in the Houston/Galveston Bay Area 104
5.4. Qualitative Approach to Embankment Scour 107
5.4.1. Qualitative Risk Levels for Embankment Scour Assessment 108
Case Study of the Houston/Galveston Bay Area Bridge System 111
6.1. Case Study Methodology 111

6.1.1. Definition of the Houston/Galveston Bay Area 111
6.1.2. Definitions of Scenario Events 112
6.2. Results of Case Study Analysis 114
6.2.1. Bridge Inundation Results 114
6.2.2. Bridge Deck Uplift Results 117
6.2.3. Comparison of Bridge Deck Uplift and Inundation Results for Structural Damage 120
6.2.4. Pier Scour Results 121
6.2.5. Abutment Scour Results 123
6.2.6. Local Scour Risk from Pier and Abutment Scour 125
6.2.7. Embankment Scour Results 127
6.3. Overall Risk Maps for the Houston/Galveston Case Studies 128
6.4. Conclusions from the Case Study Results 131
Applications of the Houston/Galveston Bay Area Risk Assessment 132
7.1. Assessment of the Viability of Post-Event Re-Entry Routes 132
7.2. Predictive/Real-Time Risk Assessment 138
7.3. Retrofit Prioritization and Aids to Mitigation Efforts 140
7.4. Application Conclusions 141
Conclusions and Opportunities for Future Work 142
8.1. Summary and Conclusions 142
8.2. Suggestions for Future Work 145
References 147
Appendix A- Definitions of Damage States 152
Appendix B- Assumptions on Missing Data 153
Appendix C- Parameters of Fragility Curve Fitting for Pier Scour 155
Appendix D- Parameters of Fragility Curve Fitting for Abutment Scour 159
Appendix E- Risk Maps of Houston/Galveston Case Study 163

List of Figures

Figure 2.1: Failure Modes Evidenced in Hurricane Katrina (Padgett et al., 2008) (a.) Bridge Deck Uplift/Unseating; (b.) Impact; (c.) Scour under Approaches; and (d.) Inundation of Electrical/Mechanical Equipment. 8

Figure 2.2: Schematic of Scour at Bridges (Briaud, 2006). 19

Figure 2.3: Fragility Curves for Bridge Damage Conditioned upon Surge Elevation Based on Empirical Data from Hurricane Katrina (Padgett et al., 2009). 30

Figure 3.1: Map of Houston/Galveston Bay Area with LiDAR Data. 40

Figure 3.2: Example of Inspection File Report for On-System Bridge. 43

Figure 3.3: Example of As-Built Interior Bent Page for Mining Pier Information. 44

Figure 3.4: Example of Calculation of Height above Water from As-Built. 54

Figure 3.5: Example of Height above Water from Channel Profile. 55

Figure 3.6: Schematic of Height above Water and Water Depth Calculations for Flat Bridges 57

Figure 3.7: Schematice of Height above Water and Water Depth Calculation for "Changing Elevation" Bridges. 57

Figure 3.8: Pie Chart of the Houston/Galveston Bay Area Bridges by Classification Type. 60

Figure 3.9: Pie Chart of the Houston/Galveston Bay Area Bridges by Age. 61

Figure 3.10: Pie Chart of the Houston/Galveston Bay Area Bridges by Height above Water. 62

Figure 3.11: Pie Chart of the Houston/Galveston Bay Area Bridge by Soil Type. 63

Figure 4.1: Schematic of Static Reliability Assessment for Span Unseating. Adapted from Ataei and Padgett (2010b). 66

Figure 4.2: Fragility Surfaces for MSSS Concrete Girder Bridges (a.) without Vertical Connections; and (b.) with Vertical Connections 77

Figure 4.3: Fragility Surface for (a.) MSSS Concrete Box Beam Multiple Bridge without Vertical Connections; and (b.) MSC Steel Girder Bridge with Vertical Connections. 77

Figure 5.1: Schematic Overview of the Probabilistic Scour Assessment. 80

Figure 5.2: Schematic of Pier Scour in a Stream (USGS, 2009). 81

Figure 5.3: Example Graph of Scour Depth Verses Time from SRICOS Method (Briaud et al., 2004). 84

Figure 5.4: Fragility Curve Fitting for a Bridge Pier in Sandy Soil. 92

Figure 5.5: Fragility Curve Fitting for a Bridge Pier in Clay Soil 92

Figure 5.6: Tornado Plot of Sources of Uncertainty in Bridge 10. 94

Figure 5.7: Tornado Plot of Sources of Uncertainty in Bridge 122. 95

Figure 5.8: Schematic of Abutment Scour Vortexes (Ayres, 2004). 97

Figure 5.9: Examples of Abutment Types (a.) Sloping Spill Through; (b.) Vertical Wall; (c.) Wing Wall with Angled Wings; and (d.) Wing Wall with Perpendicular Wings (Nielson, 2005). 99

Figure 5.10: Fragility Curve Fitting for a Bridge Abutment in Sandy Soil. 105

Figure 5.11: Fragility Curve Fitting for a Bridge Abutment in Clay Soil. 106

Figure 5.12: Examples of Embankment Scour (a.) and (b.) behind Abutments and under Approach Spans; and (c.) under Roadways (DesRoches, 2006). 108

Figure 6.1: Map of the Houston/Galveston Bay Area with Bridges Characterized by Height above Water 112

Figure 6.2: Map of Houston/Galveston Bay Area Denoting Hurricane Scenario Landing Points 113

Figure 6.3: Map of Inundated Bridges in the "Super Ike" Scenario. 117

Figure 6.4: Map of Bridge Deck Uplift Failure Probabilities in the "Super Ike" Scenario 119

Figure 6.5: Map Comparing Bridge Deck Uplift Failure Probability and Inundation for the "Super Ike" Scenario. 121

Figure 6.6: Map of Pier Scour Failure Probabilities in the "Super Ike" Scenario. 123

Figure 6.7: Map of Abutment Scour Failure Probabilities in the "Super Ike" Scenario. 125

Figure 6.8: Map of Embankment Risk Levels for the "Super Ike" Scenario. 128

Figure 6.9: Map of Risk from Uplift and Local Scour in the Hurricane Ike Scenario. 129

Figure 6.10: Map of Risk from Uplift and Local Scour in the Ike +30% Scenario. 130

Figure 6.11: Map of Risk from Uplift and Local Scour in the "Super Ike" Scenario.. 130

Figure 7.1: Map of Overall Failure Probabilities from Hurricane Ike Scenario with Major Routes Overlaid. 134

Figure 7.2: Map of Overall Failure Probabilities from Ike + 30% Scenario with Major Routes Overlaid. 137

Figure 7.3: Map of Overall Failure Probabilities from "Super Ike" Scenario with Major Routes Overlaid. 138

Figure E.1: Map of Inundated Bridges in the Hurricane Ike Scenario. 163

Figure E.2: Map of Inundated Bridges in the Ike + 30% Scenario. 164

Figure E.3: Map of Failure Probabilities from Uplift in the Hurricane Ike Scenario. 164

Figure E.4: Map of Failure Probabilities from Uplift in the Ike +30% Scenario 165

Figure E.5: Comparison Map of Uplift and Inundation for Hurricane Ike Scenario. 165

Figure E.6: Comparison Map of Uplift and Inundation for Ike +30% Scenario. 166

Figure E.7: Map of Failure Probabilities for Pier Scour in the Hurricane Ike Scenario. 166

Figure E.8: Map of Failure Probabilities for Pier Scour in the Ike +30% Scenario. 167

Figure E.9: Map of Failure Probabilities for Abutment Scour in "Ike" Scenario. 167

Figure E.10: Map of Failure Probabilities for Abutment Scour in Ike + 30% Scenario. 168

Figure E.11: Map of Failure Probabilities for Local Scour in Hurricane Ike Scenario. 168

Figure E.12: Map of Failure Probabilities for Local Scour in Ike + 30% Scenario. 169

Figure E.13: Map of Failure Probabilities for Local Scour in "Super Ike" Scenario. 169

Figure E.14: Map of Embankment Scour Risk Levels for Hurricane Ike Scenario. 170

Figure E.15: Map of Embankment Scour Risk Levels for Ike + 30% Scenario. 170

List of Tables

Table 2.1: Number of Bridges and Costs of Failure Modes in Hurricane Katrina. 8

Table 2.2: Severity of Bridge Damage from Failure Modes in Hurricane Katrina. 9

Table 2.3: Number and Severity of Bridges Damaged from Failure Modes during Hurricane Ike. 12

Table 3.1: Pertinent Data Mined from NBI for Houston/Galveston Database. 37

Table 3.2: GIS Files Obtained and Their Sources for Houston/Galveston Database. 40

Table 3.3: List of Information Mined from Each: NBI Inspection, Scour Inspection and As-Built File. 42

Table 3.4: Data Obtained from Bridge Site Visits. 47

Table 3.5: Parameters Collected for Houston/Galveston Database 49

Table 3.6: Material Types and Structure Types of Bridge Decks (NBI, 2010) 51

Table 3.7: Basic Classification Guide for Bridges in the Houston/Galveston Bay Area. 52

Table 3.8: Detailed Classification Guide for Bridges in the Houston/Galveston Bay Area. 52

Table 4.1: Sources and Distributions of Uncertainty in the Bridge Deck Uplift Model. Taken from Ataei and Padgett (2010b). 74

Table 4.2: Capacity Related Inventory Data for Uplift Fragility Example Bridges. 76

Table 5.1: Variables and Distributions with Uncertainties Accounted for in Probabilistic Pier Scour Model 86

Table 5.2: Definitions of Soil Types Found in the Houston/Galveston Region. 88

Table 5.3: Assumptions on Critical Water Velocity Values and Bounds for Initial Erosion Rate (Briaud et al., 2009). 88

Table 5.4: Variables and Distributions with Uncertainties Accounted for in Probabilistic Abutment Scour Model. 103

Table 6.1: Number of Bridge Inundated, Not Inundated and in the Surge Zone for Each of the Three Scenario Events 116

Table 6.2: Number of Bridges in Each Failure Category for Each Hurricane Scenario Event from Bridge Deck Uplift. 118

Table 6.3: Number of Bridges in Each Failure Probability by Height above Water in the "Super Ike" Scenario. 119

Table 6.4: Number of Bridges in Each Failure Category for Each Hurricane Scenario Event from Pier Scour. 122

Table 6.5: Number of Bridges in Each Repair Category for Each Hurricane Scenario Event from Pier Scour. 122

Table 6.6: Number of Bridges in Each Failure Category for Each Hurricane Scenario Event from Abutment Scour. 124

Table 6.7: Number of Bridges in Each Repair Category for Each Hurricane Scenario Event from Abutment Scour. 124

Table 6.8: Number of Bridges in Each Failure Category for Each Hurricane Scenario Event from Local Scour. 126

Table 6.9: Number of Bridges in Each Repair Category for Each Hurricane Scenario Event from Local Scour. 126

Table 6.10: Number of Bridges in Each Risk Level for Each Hurricane Scenario Event from Embankment Scour. 128

Table 7.1: Matrix of Routes Analyzed for Each Hurricane Scenario Event with Likely Accessibility Rating. 136

Table A.1: Definitions of Damage States, Adapeted from Padgett et al. (2008) 152

Table C.1: Parameters of Fragility Curve Fitting for Pier Scour. 155

Table D.1: Parameters of Fragility Curve Fitting for Abutment Scour. 159

List of Equations

Equation 4.1: Probability of Damage Given Intensity Measures (Ataei and Padgett, 2010b). 65

Equation 4.2: Maximum Quasi-Static Vertical Force per Unit Length (AASHTO, 2008). 67

Equation 4.3: Variables $\overline{W}$, x and y (AASHTO, 2008). 68

Equation 4.4: Wave Length Calculation (AASHTO, 2008). 68

Equation 4.5: Impulse/Slamming Force (AASHTO, 2008). 69

Equation 4.6: Maximum Uplift Force with Bias Estimation (Ataei and Padgett, 2010b). 69

Equation 4.7: Dimensionless Wave Height and Wave Period in the Longuet-Higgins Joint Probabilisty Distribution. 70

Equation 4.8: Weight per Unit Length of Bridge Span (Ataei and Padgett, 2010b) ... 71

Equation 4.9: Vertical Connection Strength (Ataei and Padgett, 2010b). 72

Equation 4.10: Resistive Force of Dowel Bar Connections (Ataei and Padgett, 2010b). 72

Equation 4.11: Capacity of Bridge Deck (Ataei and Padgett, 2010b). 73

Equation 5.1: Maximum Potential Pier Scour from Briaud and Oh (2010). 81

Equation 5.2: Effective Pier Width (Briaud and Oh, 2010). 82

Equation 5.3: Coefficient K_1 for Pier Type (Briaud and Oh, 2010). 82

Equation 5.4: Coefficient K_{sp} to Account for Spacing between Piers (Briaud and Oh, 2010). 83

Equation 5.5: Correction Factor for Water Depth, K_w (Briaud and Oh, 2010). 83

Equation 5.6: Froude Numbers of Pier Given Assumed Velocity, V_1, and Critical Velocity, V_c (Briaud and Oh, 2010) 83

Equation 5.7: Pier Scour, y_{final}, for a Given Duration Event (Briaud et al., 2004)..... 84

Equation 5.8: Scour Depth Calculation with Bias Removal and Model Error Estimator (Bolduc et al., 2008)..... 89

Equation 5.9: Maximum Abutment Scour Equation from Briaud and Oh (2010)..... 97

Equation 5.10: Correction Factor for Abutment Shape (Briaud and Oh, 2010)..... 98

Equation 5.11: Correction Factor for Abutment Angle, K_2 (Briaud and Oh, 2010).... 99

Equation 5.12: Correction Factor for Abutment Setback from Water (Briaud and Oh, 2010).....100

Equation 5.13: Correction Factor for Channel Type (Briaud and Oh, 2010).....100

Equation 5.14: Correction Factor for Flow Pressure (Briaud and Oh, 2010).....100

Equation 5.15: Reynold's Number Equation for Channel (Briaud and Oh, 2010)....101

Equation 5.16: Froude Numbers for Assumed Velocity, V_1, and Critical Velocity, V_c (Briaud and Oh, 2010).....101

Equation 5.17: Embankment Scour Risk Levels.....109

Equation 6.1: Upper Bound Series Estimation of Local Scour Risk. 125

Equation C.1: Forms of the Pier and Abutment Fragility Curves 155

Chapter 1

Introduction

In coastal regions, hurricanes can inflict substantial damage to structures, infrastructure and communities, with significant direct and indirect consequences. Among the affected infrastructure, hurricanes greatly impact coastal transportation systems by destroying bridges and sections of roadway, and hindering rescue and recovery efforts after the event. To that end, this research focuses on determining the risk that hurricanes pose to the Houston/Galveston bay area transportation infrastructure by conducting a thorough inventory analysis to support vulnerability modeling, developing or adapting new models of bridge reliability and applying them to a regional suite of bridges for various scenario hurricane events. These models of bridge reliability are the first probabilistic models of their type to be adapted for use across large geographical regions, such as the Houston/Galveston bay area. The risk assessment framework proposed considers multiple failure modes of the bridges in the chosen area; namely, bridge deck uplift, the movement

of the bridge deck from its supports, and scour, the erosion of soil beneath roadways and bridge supports, in order to give a more complete idea of the state of the bridge and roadway network after a hurricane.

1.1. Motivation and Scope of Research

Understanding the vulnerability of bridge and roadway infrastructure to hurricane events is critical to support pre-event planning for risk mitigation, as well as post-event action. During this post-event activity phase, the transportation infrastructure system is essential as a means to transport emergency care and relief equipment into coastal communities, such as Galveston Island and Bolivar Peninsula, access victims and critical facilities, and eventually support long term recovery and rebuilding. Thus, the roadway system must be resilient enough to withstand the hurricane event or officials must know about potential issues in the infrastructure system and be able to plan accordingly. Furthermore, heightened understanding of the risk of damage can enable effective targeting of resources, such as retrofit or upgrade, in advance of an event to mitigate adverse consequences.

Hurricane Katrina, in 2005, revealed that the coastal bridge and roadway network is vulnerable to hurricane induced surge and wave forces, as 45 bridges failed during the event, several of which required extensive repair or rebuilding (DesRoches, 2006). This sparked recent research into the causes of bridge failures during hurricanes and how the bridge deck interacts with the surge and wave produced by the storm. The current research in bridge performance during

hurricanes has been instrumental in determining the forces that a single bridge will face during a hurricane event, but, with few exceptions, these studies do not address any failure modes of the bridge other than deck movement nor do they present a framework to evaluate the risk of damage across a large region (like that affected by Hurricane Ike). Reconnaissance teams sent in after Hurricane Katrina found that while many of the bridges in Katrina failed due to bridge deck movement or electrical failures in movable bridges, a significant percentage of bridges also failed due to abutment scour and approach span undermining (DesRoches, 2006).

In order to help facilitate risk mitigation and planning efforts, quantification of the risk of damage to bridge and roadway infrastructure is needed across a regional area. These risks may be associated with unseating of bridge decks, scour of bridges, undermining of soils supporting the roadways, and even debris. This thesis provides a framework for probabilistic assessment of bridge and approach roadways for multiple failure modes viable for risk assessment across a regional portfolio of bridge and roadway infrastructure susceptible to coastal storms. Integral to this framework, this study conducts a rigorous review of bridge details to characterize the inventory in the Houston/Galveston area, and provides an archetype database of bridge information necessary for vulnerability modeling of any regional portfolio. A recently proposed probabilistic approach for assessment of bridge deck unseating is adapted for application to the case study region, while a new approach for fragility assessment of scour potential is proposed that integrates a probabilistic framework with current deterministic methodologies to account for uncertainty in the soil parameters, hydraulic parameters, and bridge geometry.

Additionally, the inherent bias from the original models is removed in order to accurately assess the risk that the hurricane forces pose to the bridge network while accounting for model error. Finally, in recognition of the role that roadway and bridge approach damage play in posing a risk to post-event performance of the transportation network, qualitative estimates of embankment scour are provided.

The proposed multi-failure mode framework for bridge deck uplift and scour vulnerability is then applied to a regional assessment of the Houston/Galveston bay area for several scenario hurricane events, examining the spatial distribution of damage, accessibility of post-event re-entry routes, and critical facility access in the Galveston, Bolivar and Clear Lake regions. The risk assessment framework developed in this study is formulated as a database driven model with algorithms that can be utilized for any region. Although three case study scenarios are examined in this thesis, the Houston/Galveston bay area inventory analysis and fragility models derived can be readily incorporated with advanced hurricane modeling software for emergency officials to have a more holistic view of the hurricane and its effects on the transportation infrastructure applied to future probabilistic or deterministic storms.

1.2. Overview of Thesis

This thesis is broken up into eight chapters. Chapter 2 reviews reconnaissance reports from Hurricanes Katrina and Ike, as well as the current literature on estimation of storm surge and wave forces, scour depth at bridge piers and

abutments and the current risk assessment models used in hurricane emergency planning. Chapter 3 conducts an in-depth inventory analysis for bridge infrastructure in the Houston/Galveston bay area including all of the sources of data used in the models. Chapter 4 describes the bridge deck uplift fragility approach that is used in this study and how it is adapted for use on the regional level. Chapter 5 details the framework proposed for probabilistic analysis of scour, and examines the scour analysis approach for piers, abutment and embankments as well as the sources of uncertainty in these models. Chapter 6 presents the results of applying the bridge deck and scour fragility models in a risk assessment of the Houston/Galveston bay area for three scenario hurricane events, and evaluates the state of transportation infrastructure for hindcast and hypothetical storms. Chapter 7 delves into the practical applications of this research, especially in emergency planning and analysis of post-event entry routes onto Galveston Island among other areas and applications. Finally, chapter 8 summarizes the conclusions of this study and lists future opportunities for research and application.

Chapter 2

Literature Review

2.1. Empirical Evidence of Common Failure Modes from Previous Hurricane Events

Many hurricanes in the past several decades have caused damage to the bridge infrastructure systems, such as Hurricane Camille in 1969, Hurricane Ivan in 2004 (Douglass et al., 2004), the Songda Typhoon in 2004 and Hurricane Irene in 2011(AP, 2011), just to name a few. However, two hurricanes in particular, Hurricane Katrina and Hurricane Ike, have focused national and local attention, respectively, on understanding and improving bridge and roadway performance during coastal storm events.

Hurricane Katrina made landfall on August 29, 2005 on the southern coast of Louisiana with winds over 140 MPH and surge that reached up to 35 feet (DesRoches, 2006). Hurricane Katrina is the most expensive tropical cyclone on

record in the US (not adjusted for inflation) (Blake et al., 2011). While the flooding of New Orleans and loss of life that accompanied the failure of the levee system protecting the city of New Orleans has received the most national attention, also important was the performance of the bridge and roadway networks during Hurricane Katrina and the damages evident (DesRoches, 2006).

During Hurricane Katrina, 45 bridges were damaged, including one bridge that was under construction at the time. Of these bridges, most were movable spans that had their electrical and mechanical equipment submerged with storm surge, but these bridges accounted for a small portion of the emergency repair costs and, indeed, were seen to have slight damage. Table 2.1 shows the causes of damage and emergency rebuilding costs associated with bridges during Katrina with some bridges having multiple failure modes (DesRoches, 2006, Padgett et al., 2008). When bridges had multiple failure modes the cost of emergency repairs was assigned to both causes' costs; therefore, the table below cannot be taken as total cost of the hurricane but rather as relative costs of different failure modes. Figure 2.1 below show the various failure modes seen in Hurricane Katrina. Also, Table 2.2 shows the number of bridges at each level of severity of damage for each cause; see Appendix A for definitions of damage states.

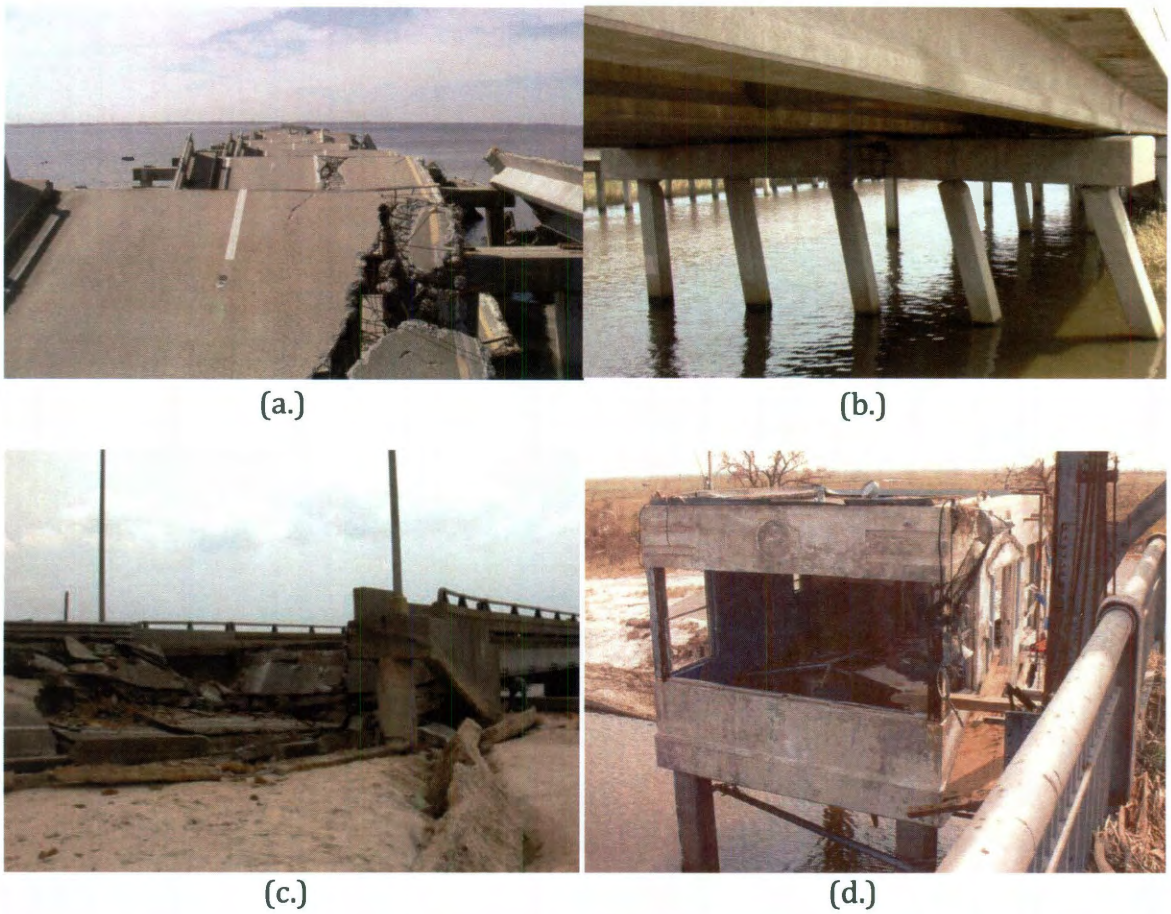

(a.) (b.)

(c.) (d.)

Figure 2.1: Failure Modes Evidenced in Hurricane Katrina (Padgett et al., 2008) (a.) Bridge Deck Uplift/Unseating; (b.) Impact; (c.) Scour under Approaches; and (d.) Inundation of Electrical/Mechanical Equipment.

Failure Mode	Number of Bridges	Cost of Emergency Repairs
Unseating/ Shifting of Spans	10	$584.9 million
Scour	13	$52.14 million
Impact	6	$11.51 million
Inundation of Electrical or Mechanical Equipment	27	$14.87 million

Table 2.1: Number of Bridges and Costs of Failure Modes in Hurricane Katrina- Adapted from Padgett et al. (2008).

Failure Mode	Slight	Moderate	Extensive	Complete
Unseating/ Shifting of Spans	0	2	3	5
Scour	0	2	10	1
Impact	0	4	2	0
Inundation of Electrical or Mechanical Equipment	8	13	6	0

Table 2.2: Severity of Bridge Damage from Failure Modes in Hurricane Katrina- Adapted from Padgett et al. (2008).

As is evidenced in these tables, while inundation claimed the highest number of bridges, the inundation did not usually lead to complete damage of the bridge in question and, despite the increased number of bridges, did not account for the majority of emergency repair costs (Padgett et al., 2008). One reason why more bridges failed from inundation than from other failure modes in Hurricane Katrina is the vast numbers of movable bridges in Louisiana, Alabama and Mississippi (NBI, 2010). The same is not true of all coastal bridge networks, and is not the case in the Houston/Galveston area. The two failure modes that had the highest relative emergency costs and, following inundation, had the highest number of bridges damaged were unseating/shifting of bridge spans and scour at bridges and approaches.

From the 10 bridges that failed predominantly from their spans shifting, roughly 1000 spans were displaced or taken completely off their supports by surge and wave forces (Padgett et al., 2009). Some of the common features of the bridges that failed due to deck unseating were low clearance above the mean water level, simply-supported bridge decks, lack of vertical reinforcement between sub and

super-structure and lack of horizontal resistance such as shear keys (Padgett et al., 2009, DesRoches, 2006, Okeil and Cai, 2008, Robertson et al., 2007). The second costliest mode of failure, scour, was not examined in too much detail after Hurricane Katrina, but it is an important failure mode of the bridges since excessive scour at the bridge or roadway can cause a disconnect in the transportation network.

Additionally, while not tabulated here, the cause of almost all the roadway damage seen in Hurricane Katrina was due to soil undermining of the roadways which led to the collapse of roadway sections and debris accumulated on roadways (DesRoches, 2006). The erosion of soil beneath roadways is closely related to embankment scour that occurs at bridges and will be looked at in more detail in the scour Section 5.4 of this thesis. Debris removal from roadways is a key component of post-event recovery, as debris hinders rescue efforts to enter communities; however, debris modeling is outside of the scope of this thesis and can be explored in future work. Hence, while the greatest cost of rebuilding the transportation system after Hurricane Katrina was associated with bridges, the damage done to the roadways was also extensive and caused disruption to recovery efforts (DesRoches, 2006). Even though Hurricane Katrina prompted the most research into understanding the forces that hurricanes exert on bridge structures, it was during Hurricane Ike that the direct risks to the Houston/Galveston area transportation system were realized.

Hurricane Ike landed on shores of the Texas coastline on September 13, 2008 as a strong Category 2 storm with wind speeds of 110 MPH and surge levels

reaching 20 feet (Stearns and Padgett, 2011, FEMA, 2008). While hitting Galveston and Houston hard, leaving millions flooded and without power, Hurricane Ike did the most damage to the Bolivar Peninsula where almost every house was leveled by the surge and wave forces (FEMA, 2008). Although at a different scale than Hurricane Katrina before it, Hurricane Ike impacted the transportation infrastructure in the Houston/Galveston bay area (Stearns and Padgett, 2011). In total, 53 bridges were damaged during Hurricane Ike, mostly small, local, timber structures but also three larger concrete and steel bridges (Stearns and Padgett, 2011). Although a direct comparison to the damages seen in Hurricane Katrina is not warranted because the bridges documented in Katrina were all large state-owned bridge structures compared to mostly locally or privately owned timber structures, it is still important and valuable to observe the failure modes of the bridges in Hurricane Ike since this research project focuses on the most likely risks to the major transportation routes in the Houston/Galveston bay area.

During Hurricane Ike, almost all the bridges that failed did so due to deck unseating or scour related problems, with very few bridges failing due to impact or submergence of electrical equipment. Table 2.3 shows the distribution of damaged bridges along with the causes for damage (Stearns and Padgett, 2011). The highest number of bridges failed due to deck unseating and also caused the most extreme damage, as was also seen in Hurricane Katrina. However, scour was more thoroughly evidenced and was a close second in the number of bridges damaged although the level of damage was less. Through these two hurricanes, and Hurricane Ike in particular, it is seen that bridge deck unseating and scour related damages are

the two most prevalent and costly failure modes of bridge structures during coastal storm events and thus it is those two failure modes that this research addresses jointly to conduct a more comprehensive risk assessment of the Houston/Galveston bay area.

Cause	Slight	Moderate	Extensive	Complete	Total
Unseating/ Shifting of Spans	0	0	1	25	26
Scour	3	3	18	0	24
Impact	1	2	3	0	6
Inundation of Electrical Equipment	0	1	0	0	1

Table 2.3: Number and Severity of Bridges Damaged from Failure Modes during Hurricane Ike- Adapted from Stearns and Padgett (2011).

2.2. Bridge Deck Uplift Failure Mode: Mechanics and Research

The movement of bridge spans from their supports has consistently been the costliest and, in some cases, the most frequent damage seen in hurricanes events in the coastal United States. Due to this fact, understanding the forces that act on the bridge deck during hurricanes is of utmost importance to being able to estimate failure probabilities for a region. Prior to Hurricane Katrina, most work on wave and storm surge forces was limited to quantifying forces on offshore platforms since they often experience higher surge and wave values being in the Gulf of Mexico and because they are vital to the oil and gas industries (Bea et al., 1999, Bea et al., 2001, Sarpkaya and Isaacson, 1981). After Hurricane Katrina exposed the vulnerability of the coastal bridge system, a great deal of research was conducted to understand the

forces that storm surge and waves exert on the decks of these coastal bridges since the models of forces used for offshore platforms were inadequate to fully understand the interaction of the waves with the bridge decks (Douglass et al., 2006, Aguíñiga et al., 2008, Cuomo et al., 2009, Chen et al., 2009, Marin and Sheppard, 2009, Bradner et al., 2011). Following these and other experiments, the combined forces of storm surge and waves acting on a bridge deck have been characterized into four distinct components: drag, inertia, buoyancy and slamming forces, with all the forces except buoyancy acting in both the horizontal and vertical directions.

2.2.1. Surge and Wave Forces Acting on Bridge Decks

Drag forces occur as a result of the flow velocity around the bridge deck and are related to the area of the bridge deck in contact with fluid flow based on angle and direction. The inertial forces experienced by the bridge deck are "proportional to the time rate of change of linear momentum of the water mass impacting the structure" (Marin and Sheppard, 2009). This is generally the mass of the water displaced by the structure along with what is referred to as the added mass: a portion of the water surrounding the bridge deck that changes with time to reflect the dynamic interaction of the fluid with the bridge deck. As noted in most physics based models, and by Marin and Sheppard (2009), the inertial force on a fully submerged structure is usually constant, but for partially submerged structures, this force varies in time as both the mass of the water displaced and the added mass changes. The force acting on the structure that is the easiest to calculate and understand is the buoyancy force: the weight of the water displaced by the bridge

deck acting in the vertical direction. The drag, inertial and buoyancy forces are called quasi-static forces because they have frequencies that are on the same order as that of the waves. The last component of force acting on the structures is the slamming force which is primarily due to trapped air between the wave and the bottom of the bridge deck. The combination of the vertical forces reducing the effective weight of a given bridge deck and the horizontal forces pushing the deck off its supports can often lead to the displacement or removal of many simply supported bridge spans as seen extensively during Hurricane Katrina (Okeil and Cai, 2008, DesRoches, 2006).

2.2.2. Research on Surge and Wave Forces Prior to Hurricane Katrina

As mentioned earlier, before 2005, most scholarly interest in wave forces was related to the fields of protecting offshore structures and jetties from hurricane forces (Sarpkaya and Isaacson, 1981, Kaplan et al., 1995, Bea et al., 1999, French, 1979). For these offshore platforms, horizontal forces were the most important, especially slamming forces as these can move equipment and destroy the platform decks. Vertical wave forces, however, were considered to be of less importance because most platforms decks have grated floors that reduce the vertical loads on the structure to values on par with the horizontal loads and because, for the most part, horizontal platforms are well anchored to their substructures (Bea et al., 1999). The results of the work on offshore platforms include many varying methodologies for calculating forces on horizontal platforms based on empirical

data and physics based models, but they are not immediately applicable to the case of coastal bridges.

Even though research on offshore platforms constituted most of the work done on wave force prior to 2005, wave forces on docks and bridge-like structures were being investigated as early as 1963 when El Ghamry (1963) modeled the effect of wave forces on docks, and found that the uplift forces generated by waves on docks were very sensitive to wave height and wave length (El Ghamry, 1963). Additionally, Denson conducted small-scale laboratory tests on bridge decks in both 1978 and 1980, the first research to directly look at bridge decks (Denson, 1978, Denson, 1980). While his work found some interesting conclusions that would be repeated after Hurricane Katrina (i.e. that wave moments caused most of the damage from Hurricane Camille and that anchorage could have prevented said damage), there are limitations of his work, including the fact that the results from the wave basin tests of his two experiments varied greatly. While this early work on both offshore platforms and, to a limited extent, bridge decks is valuable to an analysis of the demand caused by wave forces, many of the methodologies developed cannot be directly applied to coastal bridge decks because of limited experimental testing in the case of the few projects utilizing bridge deck geometry and because of differences in geometry and coastal bathymetry in the case of work on offshore platforms.

2.2.3. Research on Surge and Wave Forces since Hurricane Katrina

With Hurricane Katrina in 2005, the subject of wave force research was focused on bridge structures due to multitude of bridges damaged during the storm. In addition to reconnaissance to understand why the bridges failed (DesRoches, 2006), Hurricane Katrina also prompted researchers to investigate and review existing work done on wave forces, which was completed by groups at the University of South Alabama (Douglass et al., 2006) and at Texas A&M University Kingsville (Aguíñiga et al., 2008). These reports called for more experimental testing of bridge decks, both small and large-scale, as well as experimental tests that varied wave periods, wave length and wave height (Douglass et al., 2006, Aguíñiga et al., 2008). Since then, research has been conducted to quantify the wave forces on large-scale bridge structures, using a 1:5 scale through Bradner's work (Bradner et al., 2011), as well as 1:10 scale experiments to understand the slamming force of trapped air under bridge superstructures (Cuomo et al., 2009). Additionally Marin and Sheppard adapted Kaplan's physics-based method for offshore structures to analyze bridge deck geometries (Marin and Sheppard, 2009). As a result of these endeavors to better characterize wave loads on bridge decks, the American Association of State Highway and Transportation Officials (AASHTO) developed the first specifications for design of bridges subjected to coastal storms in 2008 (AASHTO, 2008). The AASHTO specifications give guidance to designers by consolidating the wave force research into a methodology to calculate the maximum vertical and horizontal forces exerted by a given wave or storm surge, based primarily on the work of Marin and Sheppard (2009). The work presented in the AASHTO specifications is the basis

of the bridge deck uplift model presented in this thesis and will be explored in greater depth later.

2.3. Scour Failure Mode

As seen in both Hurricanes Katrina and Ike, scour is consistently the second most frequent and costliest failure mode and thus the mechanics of it must be understood in order to assess the risk scour poses to the bridge and roadway network.

2.3.1. Mechanics of Scour

Scour is the erosion of soil from under or around bridge supports, mainly piers, abutments or embankments. Hurricanes notwithstanding, scour is a critical issue in the US and accounts for more general bridge failures than any other cause (Briaud, 2006). In hurricane events, however, scour can have highly detrimental effects on the bridge and roadway system, mainly through embankment scour where the soil directly behind the abutment can erode causing the approach spans or roadway to collapse.

To understand bridge scour, an understanding of the mechanics of soil erosion must first be obtained. When water starts to flow over and around soil particles, three things happen: 1.) at the interface between water and soil particles, shear and drag forces develop, 2.) because of the flow of water around the soil particle, the normal force exerted on the soil particle decreases, and 3.) both the normal and shear stresses at the boundaries fluctuate with time (Briaud and Oh,

2010). With these three conditions occurring, the shear forces can overcome the forces holding the soil particles together and erosion can occur. Hence, there is a threshold force that must be exceeded (usually given as a specific water velocity, used in this study, or shear stress) in order for erosion to initiate. With an understanding of how scour is initiated, bridge scour in a more general sense can be discussed. Bridge scour is usually broken up into general scour, contraction scour and local scour. General scour can occur with or without the presence of a bridge and is erosion along the waterbed. One example of this occurs when improvements to a channel cause increased water velocity and thus erosion of the soil on the bottom and banks of the channel. Contraction scour occurs when a channel or waterway is constricted by embankments from a bridge causing water velocity to increase and erosion to occur (Briaud and Oh, 2010). This thesis is not concerned with these types of scour as they occur over the life-cycle of the bridge or even without a bridge, so the presence of a hurricane does little to increase the probability of these scour types. The last scour type, local scour, includes the three types of erosion studied in this project: pier, abutment and embankment scour. Local scour is defined as erosion around a localized point, such as the bridge pier or abutment and is caused by the increased turbulence of the water around the impeding objects. Additionally, embankment scour occurs when the soil sloping from the body of water to the abutment or underneath approach spans erodes. Below is a simple schematic that shows general, contraction and local scour in relation to a bridge structure.

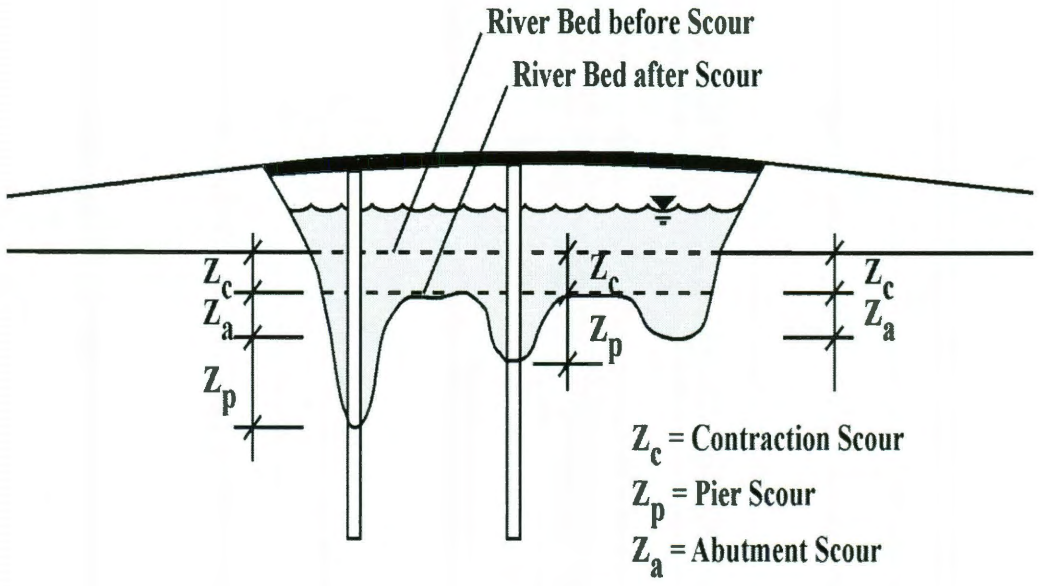

Figure 2.2: Schematic of Scour at Bridges (Briaud, 2006).

2.3.2. Current Scour Practices and Hydraulic Engineering Circulation-18

After the Shoharie Creek Bridge failure in 1987, the Federal Highway Administration (FHWA) required that every bridge over a "scourable stream" be inspected for vulnerability to scour (Harrison and Morris, 1991). To help with this inspection, the FHWA produced a technical advisory and two technical publications providing guidance to city and state officials developing a scour inspection and evaluation program. Of these publications, it is Hydraulic Engineering Circulation-18 (HEC-18)- "Evaluating Scour at Bridges" that is of the most use in this study as it lays out a plan, for both new and existing bridges, to estimate the maximum scour depth a bridge will see in its lifetime (Richardson and Davis, 2001). However, while this publication is highly useful to design engineers and inspectors alike, the equations presented there are deterministic in nature and give no indication as to what the most likely depth of scour will be for a bridge, given a certain lifespan.

Also, the method presented in HEC-18 is based on tests done in sand-flumes and thus will be highly conservative for bridges whose piers are located in cohesive soils which are known to have a much slower erosion rate (Briaud et al., 2001b). Finally, while still widely used as a scour depth indicator, the original HEC-18 method, called HEC-18 (sand), does not include any time-dependency or allow for a hydrograph of the channel at a given bridge to be used as an input; instead an average water velocity is chosen as representative for the life of the bridge and the maximum scour depth that the pier could ever experience is calculated. For the purposes of this study, scour depth has to be estimated from a short-term, high velocity event to verify if hurricanes can significantly affect the scour depth at bridge piers or abutments, leading to repair or failure. This requires a slightly different approach, which is laid out in Briaud et al. (2004), called the SRICOS method or HEC- 18 (clay), as it is now incorporated as one of the options presented in HEC-18.

2.3.3. SRICOS/HEC-18 (clay) Method

The SRICOS method was developed to better understand the scour at bridges with cohesive soil types; thereby addressing a missing element in the previous HEC-18 (sand) method which was based solely on sand flume tests. This method used flume tests of bridges in silts and clays, the soil types considered cohesive. Silts and clays are defined as those soil samples that have more than 50% of a soil sample pass through a 0.075 mm sieve, with silts ranging from 0.075 mm to 0.002 mm and clays being less than 0.002 mm in size (Briaud et al., 2004). These two soil types were

chosen because they are known to erode much more slowly than sands and thus, while a bridge located in sand may reach maximum scour depth with just one flood event, a bridge in a cohesive soil could never reach its potential maximum scour depth estimated by the HEC-18 (sand) method (Briaud et al., 2004). However, with the new HEC-18 (clay) method, in order to properly estimate the scour depth, the erosion rate of the soil must first be determined so as to calculate how quickly a bridge will approach its maximum scour depth over time. This was accomplished through the creation of the Erosion Function Apparatus (EFA), which is a mechanical apparatus that pushes a given soil sample through a Shelby tube (like a push-up ice cream pop) into flowing water and measures how long it takes for 1 mm of the soil to erode. This test is done with varying water velocities until a full range of erosion rates (in mm/hr) can be determined for a range of water velocity (Briaud et al., 2001b). This EFA output and the maximum scour depth are the basic inputs to the SRICOS method.

SRICOS assumes that the time dependent scour depth at the bridge is hyperbolic, based on the initial scour rate (determined from the EFA graph of erosion rate vs. water velocity or shear stress) and the maximum scour depth. Based on the initial erosion rate of the soil in question, the scour depth would increase hyperbolically over time until the maximum scour depth is reached. The SRICOS method, because of its ability to determine the time-dependent scour depth at a bridge site, is used as the basis of the probabilistic pier and abutment scour models presented in Chapter 5. However, specific literature about each of the scour types is presented below.

2.3.4. Pier Scour Research

Pier scour, which is the most common in non-flood events and is the best understood of the scour phenomena, occurs when flowing water erodes the soil around a pier causing a hole to form around the pier which exposes the pile, elongates the effective length of the pier and reduces the capacity of the pier to resist lateral forces (Chiew, 2008). There are a plethora of equations, outside of the two methods presented above, to determine the scour depth at piers, but many of these equations are used for design purposes to estimate the maximum scour depth a pier would experience rather than the scour depth due to a certain event or during a certain duration. The equations also, in many cases, include a factor of safety which is desirable for design but which hampers estimations of potential scour depth for existing bridges (Johnson, 1995). For example, the most commonly used scour equation at piers, HEC-18 (sand), was originally created for bridges in the design phase and contains a built in safety factor.

The SRICOS method discussed above has already been simplified by in the work of Briaud et al. (2010) and Govindasamy et al. (2008) to be applied with limited data source, and allows, with some caveats, for the initial erosion rate of the soil to be estimated based upon soil type, eliminating the need for site specific soil samples (Govindasamy et al., 2008). Additionally, Bolduc et al. (2008) took the SRICOS method and, using Bayesian models, developed a logistic, probabilistic model that accounted for the bias in the original equation (Bolduc et al., 2008). Such bias removal and error estimation are key for application of the predictive

equations in reliability assessment. However, even with the improvements of Briaud et al. (2010), Govindasamy et al. (2008) and Bolduc et al. (2008), the SRICOS method has not been applied to a large suite of bridges in a probabilistic way as to ascertain the likelihood of meeting or exceeding a particular scour depth.

In addition to various models that calculate scour for a given bridge site, there are also many models that give a relative scour ranking based on items in the National Bridge Inventory (NBI) database (Morris and Pagan-Ortiz, 1997, Harrison and Morris, 1991, Stein et al., 1999). These models usually indicate scour vulnerability in bridges based on rankings of the condition of bridge super and substructure, channel adequacy, cost of rebuilding, and average daily traffic. While these simplified models include the costs of each bridge when ranking scour vulnerability and can easily be applied to a regional set of bridges, they only rank risk based on biannual reports made to the Nation Bridge Inventory and take into account normal water flows around the bridges, not the increased velocity of hurricane storm surge. Also, these models are intended to be used as an indicator of a bridge's lifetime susceptibility to scour, not the susceptibility to a specific event. Thus, while a valuable tool to determine scour critical bridges, they do not accurately embody the risk that hurricane storm surge poses in causing additional scour at bridge piers and are used in this study for identification purposes only (i.e. identifying which bridges are scour critical before a hurricane event and if increased water levels and velocities cause additional scour at these bridges as opposed to those bridges with generally low scour vulnerability).

Even though pier scour has received the most research attention, in Hurricanes Katrina and Ike it was not seen as a large failure mode of the bridges and there is evidence that the surge during a hurricane does not increase scour depth at piers enough to cause major issues in most cases (Froehlich and Fisher, 2000). In fact, it was discovered that while the hurricanes bring in high water velocity to the piers, the short duration of the storm actually causes scour from hurricanes to play less of a role in pier scour than normal tidal flows do (Froehlich and Fisher, 2000). Thus, while pier scour will be estimated in this study, it will likely only play a role in the failure of those bridges which are already known to be scour critical and discovering a method to measure scour at abutments and embankments is of primary importance.

2.3.5. Abutment Scour Research

Abutment scour is much more complex than pier scour and less research has been conducted on how to measure scour at abutments. There are theories that abutment scour can be estimated in a similar manner to pier scour with slightly different assumptions (Melville, 1997), but there are also theories that postulate that no comparison can be drawn between pier and abutment scour because of the eddies that can form due to abutment type and shape since the water cannot flow freely around the abutment as it can around piers (Chiew, 2008). With that in mind, it is difficult to find an accepted method or equation for determining abutment scour at a bridge with very precise data much less a simplified method for determining the scour vulnerability of bridges across a region. Most studies of abutment scour have

been limited to computer simulations or very controlled laboratory experiments for a small subset of abutment types (Oh et al., 2009). Nonetheless, abutment scour seems to be more prevalent than pier scour during hurricane events since it undermines the soil at the toe of the abutment and can cause more immediate damage to the bridge structure.

One method for determining abutment scour was put forth by Froehlich (1989) and is based on a multiple linear regression analysis that was run on laboratory measurements of abutment scour for two conditions at the bridge site: live-bed and clear water. Live-bed scour occurs when the scour hole at the abutment is replenished by material roughly the same size as the supporting soil. Clear water scour occurs when the material that is carried by the flow is much smaller than the soil that initially supported the abutment (Froehlich, 1989). Froehlich (1989) developed an equation for each type of scour at the abutment based on the shape of the abutment, inclination angle, flow around the abutment, area of the abutment, and the particle diameters of the soil. These equations require many parameters to be known about the soil and the properties of the bridge abutment, but it is possible to create a probabilistic form of these equations that utilizes the uncertainties in the parameters to estimate the scour at each bridge. Another method stems from the SRICOS method and is applied to abutments through additional input information to account for abutment type, shape and setback from the water's edge and increased complexities in the core equations to include the eddy effects around the abutments (Briaud and Oh, 2010). Despite the increased complexities from the pier scour equations, the SRICOS method for abutment scour is generally less conservative (i.e.

does not have a built in factor of safety) than other predictive models (Oh et al., 2009), and is adopted in this study to be consistent across both pier and abutment scour.

2.3.6. Embankment Scour Research

Finally, embankment scour encompasses both the soil erosion of the embankments leading up to the bridge abutment and the undermining of soil beneath the approach spans to the bridge. By far, this was the most severe of the forms of scour evidenced in Hurricane Katrina (DesRoches, 2006), and to a lesser extent in Hurricane Ike. One possible reason for this could be that the soil beneath the approach spans does not often experience water flowing perpendicular to the roadway on a regular basis unlike the soil at the piers and abutments (because most flow generated from rainfall will be overland flow that will run in the direction of the roadway towards the stream/river in most cases, whereas piers and abutments experience perpendicular water flow regularly due to the flow of the stream/river) and thus has greater potential for the storm surge velocity to be able to move the soil particles. Another reason could be that, especially in older bridges, there is a higher likelihood that a bridge pier or abutment could have already experienced water velocities equal or greater than that of the storm surge and thus have already reached its maximum scour depth, resulting in little or no additional scour (Briaud et al., 2001a). Regardless of the reason why embankment scour is usually the most severe in hurricane events, this undermining of soil at the approach spans can cause the roadway that the soil is supporting to collapse, and the bridge to be impassable

(DesRoches, 2006). Currently there are no widely accepted models to predict embankment scour at bridges that can be applied on a regional scale for hurricane storm surge. There are some studies on embankment erosion of levies during hurricanes, but they are not applicable to small scale bridge embankments (Powledge et al., 1989a, Powledge et al., 1989b). Therefore, part of the research for this study will be to adapt the current knowledge from SRICOS and erosion rates of soils to develop a qualitative approach to embankment scour that defines risk levels for the bridges in the study area.

2.4. Hurricane Risk Assessment Models for Bridge and Roadway Systems

Understanding the forces that act on the bridge under wave action or estimation of scour given surge and fluid flow is only the first step to understanding how coastal storms affect the road and bridge transportation systems. The next step is being able to quantify the likelihood of damage to all the bridges in a region. This is done through a vulnerability/risk assessment. Because predicting the performance of bridges under hurricane loading has a significant amount of inherent uncertainty, the vulnerability of said bridges is best defined in probabilistic terms. In fact, the very concept of *risk*, which refers to the potential for damages or losses that can be associated with an event, implicitly requires the identification of the hazard potential as well integration of the hazard potential with the probability of damage and/or the effects of the damage (Ellingwood and Wen, 2005). Alternatively, studies

based on scenario events can be applied to gain a better understanding of the consequences and failure potential under the case study storms. Nationwide risk assessment packages, such as HAZUS-MH offered by FEMA (Basoz and Mander, 1999), address multiple hazards; however, these packages do not currently contain appropriate input models to assess risks to bridge and transportation infrastructure posed by hurricanes.

While much work has been done to understand the risk to bridges in other natural hazards, like earthquakes, through the application of empirical or analytical fragility curves in a risk assessment (Basoz and Kiremidjian, 1999, Alipour et al., 2010, Yang et al., 2009, Kang et al., 2008, Kiremidjian et al., 2007, Lee et al., 2011, Rokneddin et al., 2011, Zhou et al., 2010), very little work has been conducted to quantify the risk that hurricanes pose to the coastal infrastructure systems. Until recently, the traditional "risk assessment" methods for a coastal region given a storm surge were based on inundation maps of some sort (CCSP, 2008). Sometimes the inundation would be based both on storm surge simulations and the elevation of the bridge, but most of the time inundation maps only included surge information and any bridge in the surge zone was considered at risk, without any quantification of the susceptibility to damage or consequences of the event other than documenting the surge height. The few studies that have examined risk to transportation systems from hurricanes have usually been limited to analysis empirical evidence (Padgett et al., 2009, Douglass et al., 2004); however, Chen et al. (2007) presented a methodology for emergency risk management that focuses on

understanding the vulnerability of roadways to hurricane storm surge and wave forces (Chen et al., 2007).

Following Hurricane Katrina a few empirical fragility curves were derived based on the damage to the Louisiana bridge system, the first of their kind; however, these fragility curves were not differentiated by bridge type or design details, instead giving a probability of damage state exceedance for a given surge height generic to bridges typical to the region (Padgett and Arnold, 2009, Padgett et al., 2009). Figure 2.3 provides an example of the empirical fragility curves calculated based on statistical analysis of the observed damages and hindcast surge elevations from Hurricane Katrina (Padgett et al., 2009). Given the limitation of statistically significant data for differing bridge types, damage levels and design details, analytical and simulation based fragility analysis of bridges under hurricane loading has been prompted. Specifically, Ataei and Padgett (2011) proposed a method for bridge deck unseating fragility analysis, which is adopted in this study. Further details on this method are summarized in Chapter 4 of this thesis; however this method and other analytical fragility analysis of coastal bridges under hurricane threats cannot be conducted without a comprehensive database of coastal bridge information. Therefore, a major portion of this research is to build a database for the Houston/Galveston area that facilitates the development of bridge specific analytical fragility curves for bridge deck uplift. Such fragilities can be integrated with probabilistic hazard estimates or scenario hurricane events, marking a significant advance over existing risk assessment models for coastal bridge and transportation infrastructure limited to presence in an inundation zone.

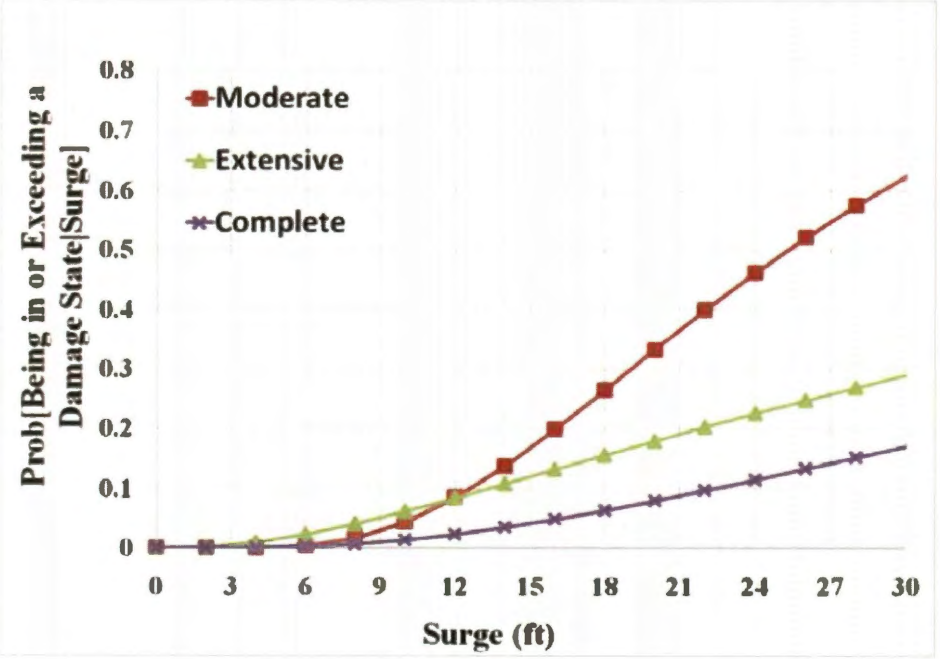

Figure 2.3: Fragility Curves for Bridge Damage Conditioned upon Surge Elevation Based on Empirical Data from Hurricane Katrina (Padgett et al., 2009).

As far as scour is concerned, calculating scour depth has been used during the design phase to determine the maximum scour depth, and more recently, due to many scour-related bridge failures, during inspections to determine if a bridge is scour critical and in need of scour countermeasures. The Department of Transportation requires all water crossing bridges to be inspected for scour regularly because of the risk that scour poses to bridges across the whole of the US; however, the method for inspecting bridges varies from state to state and relies mostly on visual inspection with calculations only taking place if a bridge is considered at risk for scour (Govindasamy et al., 2008). Additionally, the scour calculated for these bridges is based on normal flows and not on an extreme event like a hurricane, and focuses on pier scour which has been seen in past hurricanes to

be a subordinate mode of failure to abutment or embankment scour (Froehlich and Fisher, 2000). There is a need to understand the risk that hurricanes pose to undermining the soil around bridges and under roadways to be able to have a clearer picture of risk to the transportation network; which is met by developing probabilistic models of pier and abutment scour and determining risk levels for embankment scour based on soil type and water velocity. There have been a few studies in creating probabilistic forms of existing scour methods (Johnson and Dock, 1998, Bolduc et al., 2008); however, these methods have been limited to pier scour and are not entirely applicable to a regional suite of bridges because the uncertainties assumed in Johnson and Dock (1998) are specific to Bonner Bridge in North Carolina.

While significant research has been conducted on understanding the forces at an individual bridge for uplift or scour, there is a current need for emergency officials and decision makers to have a regional assessment of the risk that hurricanes pose to the overall inventory of bridges in a transportation system. This research project addresses this pressing need by applying probabilistic methods to account for uncertainty in the estimation of both uplift and scour to a new regional database of information in order to obtain risk maps for scenario hurricane events in the Houston/Galveston area. Many risk assessments of transportation systems (other than inundation maps) have focused primarily on evacuation from hurricane prone regions (Dueñas-Osorio et al., 2010); however, the risk assessment presented in this study focuses on the state of the bridge network immediately following a hurricane event, allowing for better informed decision making about post-event

recovery efforts and facilitating the prioritization of bridges for retrofit or rebuilding. This type of risk assessment, while routinely conducted for other hazards (Rokneddin et al., 2011), has not been applied to hurricane prone regions.

Chapter 3

Data Collection and Inventory Analysis

3.1. Importance of Data Mining

One of the most crucial aspects of conducting a regional risk assessment is collecting all the necessary data to support analysis of the various types of vulnerability. Although historically, regional risk assessment of other types of hazards have conducted general fragility analyses of bridge classes, and then assigned each bridge in a region a class fragility (Basoz and Kiremidjian, 1999, Nielson, 2005, Choi et al., 2004), this study attempts to enable a more refined, bridge specific fragility assessment. The structural reliability models under surge/wave as well as the scour estimates require detailed information about a given bridge not easily inferred by generic bridge classes defined by material and construction type. Therefore this study aims to characterize the important data to support regional risk assessment of bridge infrastructure in coastal regions. Collecting this data is easy enough for a

single bridge or even a small sub-set of bridges, but when applied to an entire region, such as the Houston/Galveston bay area, the matter of data collection becomes of upmost importance. Thus, much time and consideration is given to mining the pertinent data from many data sources as well as to performing site visits to bridges where data was unavailable or inadequate. This endeavor to develop a database structure for vulnerability assessment is intended to serve as a model for other coastal regions, and identify viable data sources to support such efforts.

The current bridge deck modeling, scour depth prediction and soil erosion calculations are all extremely data intensive. Even with a simplified analysis, data and data collection are vital to an accurate risk assessment since the reliability of the model rests on the amount of uncertainty inherent in the input data. Many sources of information already exist in the form of the National Bridge Inventory (NBI) database and the Texas Department of Transportation (TxDOT) records; however, detailed information is also required for girder type and area, vertical reinforcement and soil type. Additionally, given the size and extent of the region in question, site visits to all 155 bridges would be unfeasible, thus a major portion of this research was to locate and piece together a comprehensive database of information that would include structural information as well as soil details and general characteristics for all the water-crossing bridges in the Houston/Galveston area. Collecting all of this information required compiling the NBI data for the state of Texas, spending months in the Houston branch TxDOT office gathering bridge inspection files and as-built files for every bridge available, finding a reliable source

that would give soil type near each bridge in the area, and conducting a few specified bridge site visits when all other data sources were exhausted. This section will go into detail describing all the sources of data in the new Houston/Galveston database (which is available upon request), what assumptions were made with each and how these sources led to the final database.

3.2. Data Sources Mined for Houston/Galveston Database

3.2.1. National Bridge Inventory

The National Bridge Inventory is a national database of bridges on public roads, including interstates, US highways, state and county roads that resulted from the enactment of the National Bridge Inspection Program to support safety inspection and evaluation of highway bridges (NBI, 2010). The database includes the bi-annual inspection data listed by state, and although it was not intended to support hazard risk assessment studies, it can provide a valuable starting point for any regional data collection. NBI is publicly accessible (NBI, 2010); however, some fields, such as the bridge identification number, are stripped to help ensure some safety and security of the data. There are over 100 items listed in the NBI data for each bridge, as described in the NBI Coding Guide (FHWA, 1995), although not every item is populated for each bridge. However, for the purposes of this study, only specific items were necessary (see Table 3.1). A complete description of all the items in the NBI database can be found in its coding guide online (FHWA, 1995), but a few distinctions must be made about the specific data pulled for this study (NBI, 2010).

Firstly, there are two main types of structures, those owned by state authorities, called on-system bridges, and those owned by private or local owners called off-system bridges. This is an important segregating factor because there is typically far more information collected from on-system bridges than off-system ones. Another note is that the publicly available dataset was cross checked with additional data from TxDOT to ensure details such as the nearest mile marker, road carried, facility crossed and structure identification number (all data which had been stripped or duplicated in the online dataset) was valid. Pertinent items were extracted for all the bridges from NBI, and narrowed down into the Houston/Galveston bay area, as discussed in the next section. Table 3.1 below gives the NBI data label for each piece of information pulled as well as the item number associated with it (NBI, 2010).

Data Label	Item Number
Structure Number- Includes identifiers for TxDOT districts, county, control area as well as a unique 3 digit identifier at the end that is stripped in the online database	8
Features Crossed- The body of water, roadway or railroad crossed by the bridge	6
Facility Carried- The road/railroad carried by the bridge	7
Location- Gives a distance in miles from the nearest major intersection or landmark	9
Latitude and Longitude	16,17
Owner- Type of agency that actually owns the structure, generally denotes on and off system structures	22
Year Built	27
Skew- The acute angle of the constructed bridge	34

Data Label	Item Number
Navigable Vertical Clearance- Only tabulated for bridges that have boat traffic under them, a first estimate for height above water	39
Service Under Bridge- Yields the operation of facilities under the bridge and is particularly useful for denoting water-crossing bridges	42B
Structure Type- Includes both the material type (concrete, steel, etc) and structure design	43A,B
Approach Structure Type- Includes both the material type (concrete, steel, etc) and structure design	44A,B
Number of Main Spans	45
Number of Approach Spans	46
Length of Maximum Span	48
Structure Length	49
Bridge Width	51

Table 3.1: Pertinent Data Mined from NBI for Houston/Galveston Database.

3.2.2. Geographical Information Systems Data and Defining the Houston/Galveston Bay Area

The next source of data consists of many geographical information systems (GIS) layers that are utilized in ArcMap to set the boundaries of the Houston/Galveston bay area, to extract the elevation at each bridge, and to visualize the spatial distribution of many of the data parameters and results (i.e. bridge type, soil type and probability of failure). ArcMap is a geographical information system which can take the file of bridge data from NBI and create a map of the bridge locations and data, along with some files that provide background and a geospatial reference for the bridge locations. For the purposes of this study, many GIS files were obtained from the GIS/Data Center at the Rice University Library, a full list of which is below

(Table 3.2), including datasets on all the roadways, counties, inlets and bays of south Texas, as well as advanced LiDAR (Light Detection and Ranging) data for elevations of the entire region. After putting together a map of the Houston/Galveston bay area using the GIS files listed below, the research study area was defined as the entire Island of Galveston, Bolivar Peninsula and everything within a one mile radius of the edge of the Houston Ship Channel, Trinity Bay, East Bay and West Bay. This ensured that all the bridges that could potentially experience significant surge or wave heights were included without excessive data collection outside the surge zone.

With the bay area now defined, the database of all Texas bridges was refined using a buffer tool in ArcMap so that only the bridges in the bay area were included. Furthermore, the key information obtained from GIS was the ground elevation at each bridge and the soil type at each location; the source of the soil type data will be discussed in Section 3.2.4 below. For the elevation, LiDAR elevation maps with a horizontal precision of +/- 10 ft were used, obtained from the United States Geological Survey (USGS) online seamless server (USGS, 2011). The information from USGS is contained in small parcels, so several areas of LiDAR data were overlapped to eventually arrive at a map of the complete bay area region (see Figure 3.1 below of LiDAR data). The USGS obtains these LiDAR elevations by sending pulses of a laser from LiDAR instruments fitted to various aircraft and measuring the time it takes to detect the returning light beam. When the LiDAR maps are made, they have all the buildings and landmarks on them; however, the data is post-processed to remove structures and foliage to create a bare earth map. However, a significant drawback to the LiDAR elevation is that the laser beams to not reflect

completely off of water and thus do not give accurate elevations of either the water or the channel bottom. Because of this and the fact that the bridge locations from NBI are generally located at the center of the bridge (and thus, over water), the LiDAR elevation pulled directly from the given location would describe neither the water level elevation, nor the channel elevation. Thus, it was necessary to manually find the elevation (or create a new file of bridge locations using the first approach span) for each bridge at the first approach of the bridge. Also, taking the elevation at the beginning of the bridge assured that the elevation would be of the roadway level and not the ground beneath the bridge (as the bridge would be stripped out to give the bare earth map). This is an important distinction since items pulled from NBI and TxDOT files give the height from the bridge to the ground or water level and it is important to be consistent in the methodology for gathering the elevation data.

Figure 3.1: Map of Houston/Galveston Bay Area with LiDAR Data.

GIS File	Data Source
State of Texas	Texas State Data Center
Counties of Texas	Texas State Data Center
Bathymetry of Texas Coastline	NOAA
Outline of Texas Coastline	NOAA
Galveston roads	Texas State Data Center
Houston Roads	Texas State Data Center
Major Roads throughout state	Rice GIS/ Data Center
LiDAR Elevation data	USGS Seamless Server
Texas Waterways	Texas State Data Center

Table 3.2: GIS Files Obtained and Their Sources for Houston/Galveston Database.

3.2.3. TxDOT Data: Inspection Files and As-Builts

The most important data source for regional database construction is the information from the local Department of Transportation (DOT) on bridges that it inspects and maintains. For this study, detailed inspection reports and bridge plans were obtained from TxDOT, primarily from the Houston District and Beaumont District offices. Inspection files were procured for all the water crossing bridges in the Houston/Galveston bay area. Beyond inspection files, bridge plans as actually constructed, called as-builts, were obtained for on-system bridges from TxDOT's in-house database, TxDocs Online. These two data sources provide almost all of the necessary data for the bridge deck uplift vulnerability model, and it is from these sources that the most data is mined. The inspection files contain the bi-annual inspection form used to populate the NBI database, but usually go further in describing the type of bridge deck, the span lengths, and in most cases include a channel profile, which is highly useful in determining the distance between the water surface and the bridge deck as well as the channel elevations. Additionally, many of the bridges have been inspected for possible scour issues and this inspection is also included in the file, yielding valuable information such as pier type, abutment type and soil type. What cannot be mined from the inspection files in terms of structural attributes can usually be found in the as-built. For this study, the pages of most interest were the bridge overview pages along with the pages on bents and abutments where details such as the vertical reinforcement between bridge deck and substructure, girder type and size, pile size and length and pier type and size can be obtained. Table 3.3 below details which parameters can be found in

each of the inspection files and as-builts. Following that, Figures 3.2 and 3.3 show examples of inspection file pages and as-built pages to assist any future regional data collection. From Figure 3.2 of the inspection file, note the red boxes which denote some of the details gathered for this specific bridge (i.e. bridge length, deck, width, deck type, and longest span). The as-built example in Figure 3.3 shows where to find typical pier size, dowel information (usually called bar D), and girder depth.

NBI Inspection	Scour Inspection	As-Built
Span Lengths	Pier Type	Span Lengths
Girder Types	Pier Geometry	Pier/Pile Size
Height of Deck	Soil Type	Height above Water
Height of Asphalt	Abutment Shape	Vertical Reinforcement
Channel Profile	Attack Angle	Presence of Shear Keys
Number of girders	Number of Piers	Abutment Shape/ Setback
Previous damage	Presence of Rip Rap	Soil Type

Table 3.3: List of Information Mined from Each: NBI Inspection, Scour Inspection and As-Built File.

Texas Department of Transportation

Modified 12-5-2000)
for Microsoft Word 7.0, WIN95 & NT

Bridge Inventory Record

District: 20 County: 036 Cont-Sec: 0508-02 Structure: 032 Route: IH 10
Feature Crossed: Lost/Old River & FM 565 Inspector's Signature: Date: 7/19/06
Company Name: *JPH Consulting*
Location: 2.6 Mi. E of FM 3180 Maintenance Section: 01
Latitude: N 29°49' 50.39" Longitude: W 94°48' 1.00" Milepoint: 19.7405
General Description:
65 simple span prestressed concrete beam bridge on concrete pile bents. Bridge is on a 4-lane, 2-way controlled access main lanes with a high ADT (46,800 vpd).

Bridge Length: 5078 ft. Deck Width: 118 ft. Lanes On: 4 Lanes Under: 2
Skew Angle: 0 Deg. ☐ Lf. Fwd. ☐ Rt. Fwd. Bridge Rail: T501
Clear Width Between: 112 ft. ☐ Curbs, ☒ Rails, ☐ Pvmt Edges Approach Rdway Width: 58 ft.
Deck Type: 8" Concrete Deck
Surfacing: N/A Vertical Over-Clearance: ft. ☒ Unimpaired
Stringers: Spans: 1 - 65
Type: Prestressed Concrete Beams Size: See Plans Number: See Plans
Spacing: See Plans Controlling Span Length (C-C bearings): 80' - 0" ft.
Stringers: Spans:
Type: Size: Number:
Spacing: Controlling Span Length (C-C bearings): ft.
Stringers: Spans:
Type: Size: Number:
Spacing: Controlling Span Length (C-C bearings)- ft.
Est Deck Overtopping Freq: ☒ >100 ☐ 11 - 100 ☐ 3 - 10 ☐ < 3
Est Approach Overtop. Freq: ☒ >100 ☐ 11 - 100 ☐ 3 - 10 ☐ < 3
Horizontal / Vertical Alignment: Good / Good
Date Built / Design Load: 1992 / HS20 (per plans)
Regulatory / Advisory Speeds: 65 mph (posted) / N/A
Posted Load Restriction: ☒ None
Comments:

Signature *Date*

Bridge Inventory Record (page 1 of 2)

Figure 3.2: Example of Inspection File Report for On-System Bridge.

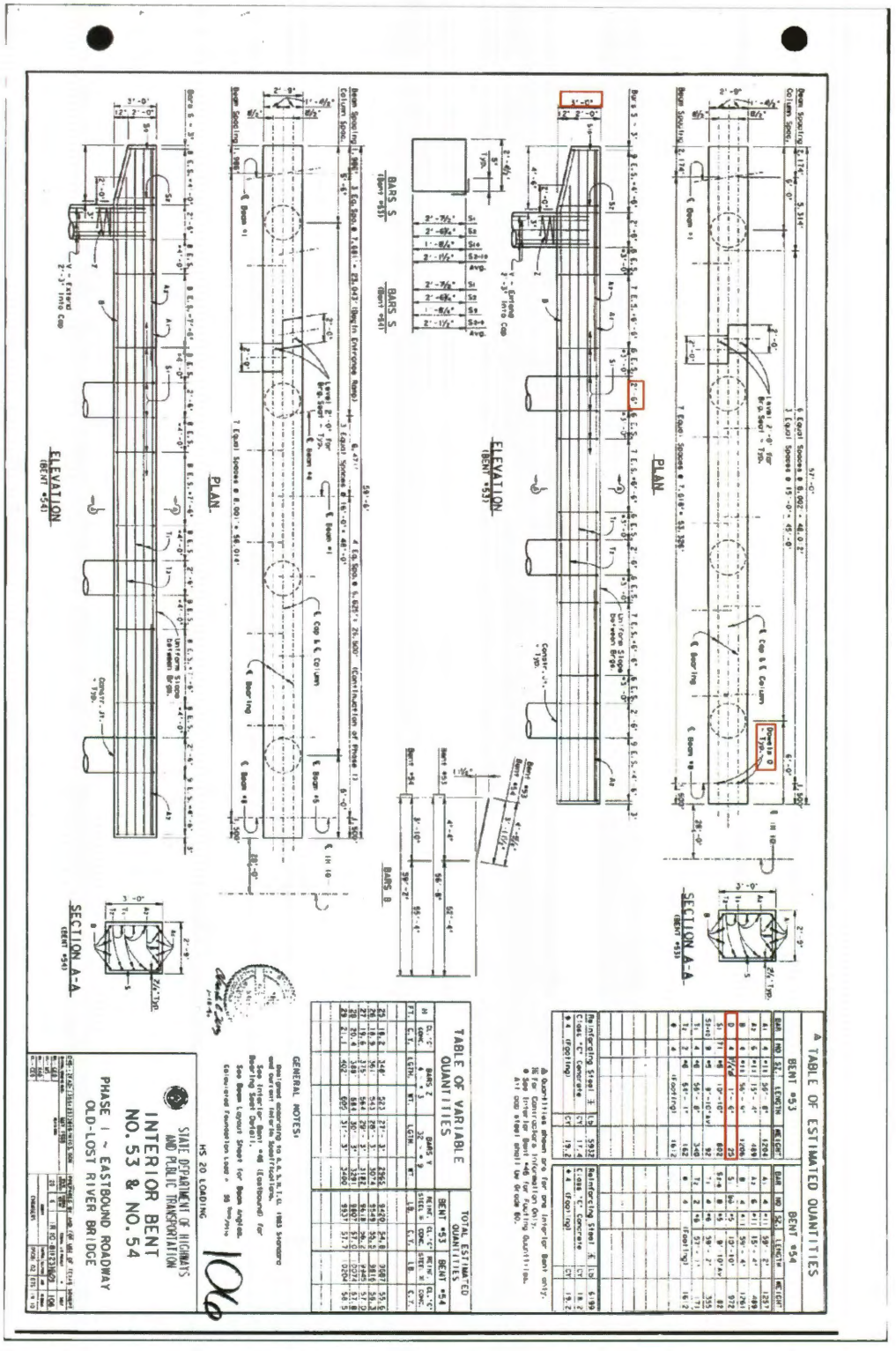

Figure 3.3: Example of As-Built Interior Bent Page for Mining Pier Information.

3.2.4. Soil Type Data: SoilMart Online Database

To conduct the scour analysis, at the minimum the general soil type for every bridge in the database must be obtained. Ideally, soil samples would be collected and tested for each site to characterize the erosion rate. However, to practically support a regional assessment with over 150 bridges in the Houston/Galveston bay area, soil erosion rates will be inferred based on soil type and past testing of similar classes of soil. The estimated initial erosion rates based on soil type are adopted from the simplified analysis of Briaud et al. (2009) and discussed further in Chapter 5 of this thesis. For many bridges, the soil type is contained in the TxDOT scour inspection file, but not for every bridge in the bay area region; thus, there is a need for a reliable and consistent source documenting soil type throughout the Houston region. This source of soil type information was found in SoilMart (NCRS, 2011), an online database with basic soil types for large areas of land. There are some limitations to the SoilMart database; the soil type obtained from a representative sample is generalized across wide swaths of land (up to several hundred acres) and so site specific variation in soil type verses the representative sample can exist. Additionally, the representative samples are only obtained for the first five feet of depth, so it does not give an accurate view of the soil stratification. However, for the purposes of this study, general soil types from the SoilMart database are adopted so as to assign an erosion rate for the scour susceptibility analysis. It is acknowledged that future studies could conduct more refined site specific geotechnical investigation. From the online database, soil types were downloaded for the Galveston, Harris, Chambers and Liberty counties.

3.2.5. Bridge Site Visits

Even with the many sources of data that were mined for bridge geometry, channel properties and soil type, not every parameter could be determined for each bridge. Where the data mining process did not yield enough information for the regional risk assessment, bridge site visits were conducted. For this study, seventeen bridges were visited to determine soil type (if the SoilMart database and the scour inspection did not agree), pier geometry and type, and most importantly, abutment geometry, type and setback from the water. Information on the abutments of the bridges is the most difficult to locate in the traditional sources listed above, and thus limited abutment data was the primary driving force for conducting bridge site visits, although, once there, other parameters were also collected for verification purposes. Because lack of abutment data was the deciding factor on bridge site visits, the bridges were chosen based on their anticipated susceptibility to abutment scour. Bridges included in these site visits had to have previous scour damage, be located in highly erodible soil, such as sand, and not be inundated based on the surge levels from a hindcast Hurricane Ike scenario event. This last proviso was added because when the bridge deck is inundated, embankment scour or soil erosion of the approach spans is a far more likely and dangerous risk than abutment scour (Briaud, 2011). Where there were bridges not included in the site visits that were still missing key information, the missing data was inferred based on the parameters from similar bridges in the area. Specifics on assumptions of missing data can be found in Appendix B. Table 3.4 below lists the information that was

gathered at each bridge site. The bridge site visits constitute the final data gathering mechanism for bridge and channel geometry.

Data Gathered at Bridge Site Visits
Soil Type
Pier Type
Pier Size
Attack Angle of Water to Pier and Abutment
Abutment Type
Abutment Setback from Channel's Edge

Table 3.4: Data Obtained from Bridge Site Visits.

3.2.6. Storm Surge and Wave Scenarios from the UT-Austin ADCIRC Modeling Group

The probabilistic models of unseating and scour developed in this study can be integrated with probabilistic or scenario events to assess risks to the bridge and transportation infrastructure. For the case studies presented in this thesis, scenario hurricane events are considered based on input obtained from collaborators through the SSPEED Center (CHG, 2010). The UT-Austin Computational Hydraulics Group simulates coastal storms' movement and strength using Advanced CIRCulation models for surge and wind parameters and SWAN models for wave parameters (CHG, 2010).

Three scenario events in the Houston/Galveston bay area were considered: the original hind cast Hurricane Ike; Hurricane Ike with 30% stronger wind speeds

at the original landing location; and a worst case scenario event called "Super Ike," which included 30% stronger wind speeds than Ike and a more southern landing position so as to impact Houston and Galveston more directly. For each of these scenarios, the output from the ADCIRC and SWAN modeling was post-processed and the following data was obtained for each bridge: peak surge elevation and wave height, wave period and water velocity at each time step in the simulation. The mesh developed by the UT-Austin Computational Hydraulic Group is the most precise mesh to be made for the Texas coast, with the grid for near-shore measurements about 50m by 50m. Additionally, the model and mesh for the Texas coat was validated on storms Alicia (1972), Brett (1999), Allen (1980), Carla (1961), Rita (2005) and Ike (2008), even modeling the "fore-runner effect" seen in Hurricane Ike (Dawson, 2010). However, despite the increased accuracy of this ADCIRC model for the Texas coast, given the larger mesh size, there is uncertainty in the surge elevation and wave heights at the bridge site that must be accounted for in the predictive structural and scour models when looking at scenario events.

3.3. Building the Houston/Galveston Bay Area Database

With the various data sources identified, the database for the bridges of interest must be populated. From the NBI database and the defined area of the Houston/Galveston bay area, 155 bridges were identified as water-crossing (by NBI data) in the bay area, not including culverts and tunnels. Using the sources above and the data collected from them, the parameters given in Table 3.5 were collected or calculated for each bridge span of each bridge in the area. For those parameters

that were calculated or determined using other data, a more thorough description follows the table.

Parameter	Source/ Method of Calculation
Bridge Type	NBI/ Using number of spans, material type and girder type
Number of Spans	NBI
Span Lengths	Inspection Files, As-Built
Bridge Deck Width	NBI, Inspection Files
Deck Material	NBI
Bridge Skew	NBI
Year Built	NBI
Location (Lat/Long)	NBI
Connection Details- dowel bar diameter and length	As-Built
Deck Height/Asphalt Height	Inspection Files, As-Built
Girder Type/ Size	Inspection Files, As-Built
Number of Girders	Inspection Files, As-Built
Height above Water	Calculated from Channel Profile, As-Built
Water Depth	Calculated from Channel Profile
Bridge Deck Elevation	ArcMap
Channel Elevation	Calculated from Bridge Deck Elevation and Channel Profile
Scour Rating	Scour Inspection
Soil Type	SoilMart, Scour Inspection, As-Built, Site Visits
Pier Type/ Size	Scour Inspection, As-Built, Site Visits
Number of Piers	Scour Inspection, As-Built, Site Visits
Pile Lengths/ Size	Inspection Files, As-Built
Attack Angle of Water to Pier	As-Built, Scour Inspection, Site Visits/ Calculated based on maps
Abutment Type/ Size	Inspection Files, As-Built, Site Visits
Abutment Setback from Water	As-Built, Site Visit
Channel Type	As-Built
Surge Height	UTA ADCIRC
Wave Height	UTA SWAN
Wave Period	UTA SWAN

Table 3.5: Parameters Collected for Houston/Galveston Database.

3.3.1. Method for Calculating Parameters in the Houston/Galveston Database

3.3.1.1. Determining Bridge Type

Many of the parameters listed above are easily found in the available data sources; however, some parameters are calculated based on available data, such as bridge type, height above water, water depth and channel elevation. Determining bridge type is one of the more important facets of categorizing bridges in a regional area to ensure that the distribution of construction types is representative of other coastal regions, and to draw inferences based on observational data from past storms. For example, Hurricane Katrina revealed the vulnerability of low elevation multi-span simply supported bridges (Padgett et al., 2009). The first divide in bridge type is number of spans, easily determined from NBI. The second categorizing factor is the bridge material: concrete, steel or timber; and the last factor is the girder or deck type. The simplest categories for bridge type are as follows and can be determined by the number of spans and material alone: Single Span (SS), Multi-Span Simply Supported (MSSS) Concrete/Steel, and Multi-Span Continuous (MSC) Concrete/Steel. A more detailed analysis of bridge types is usually desired and thus, from the structure type in NBI, more specific categories of bridge type can be defined as follows: SS Concrete Box Multiple, SS Concrete Girder, SS Concrete Slab, MSSS Concrete Box Multiple, MSSS Concrete/Steel Girder, MSSS Concrete Slab, and MSC Concrete/Steel Girder. Unless listed as continuous in the material type, i.e. concrete continuous or steel continuous, each bridge is assumed to be simply

supported. All bridges that do not fall into the explicitly labeled categories above, for example, timber, masonry, aluminum or iron bridges as well as trusses, arches and suspension bridges, are categorized as Other. Additionally, culverts and tunnels were excluded from the analysis. Table 3.6 lists the material and structure types found in NBI. Below that Tables 3.7 and 3.8 define which material and structure types determine which classifications for a bridge.

Material Type (MT) and NBI ID		Structure Type (ST) and NBI ID	
0	Concrete	1	Slab
2	Concrete Continuous	3	Stringer/ Multi-Beam or Girder
4	Steel	5	Girder and Floorbeam System
6	Steel Continuous	7	Tee Beam
8	Prestressed Concrete	9	Box Beam or Girders- Multiple
10	Prestressed Concrete Continuous	11	Box Beam or Girders- Single
12	Wood or Timber	13	Frame
14	Masonry	15	Orthotropic
16	Aluminum, Wrought Iron or Cast Iron	17	Truss- Deck
18	Other	19	Truss- Thru
		20	Arch- Deck
		21	Arch- Thru
		22	Suspension
		23	Stayed Girder
		24	Movable Lift
		25	Movable- Bascule
		26	Movable- Swing
		27	Tunnel
		28	Culvert
		29	Mixed Types
		30	Segmental Box Girder
		31	Channel Beam
		32	Other

Table 3.6: Material Types and Structure Types of Bridge Decks (NBI, 2010).

Classification - Basic	Spans	Material Type	Structure Type
SS Concrete	1	1,5	Any
MSSS Concrete	>1	1,5	Any
MSC Concrete	>1	2,6	Any
SS Steel	1	3	Any
MSSS Steel	>1	3	Any
MSC Steel	>1	4	Any
Other	Any	7,8,9,0	Any

Table 3.7: Basic Classification Guide for Bridges in the Houston/Galveston Bay Area.

Classification- Detailed	Spans	Material Type	Structure Type
SS Concrete Box Multiple	1	1,5	5
SS Concrete Girder	1	1,5	2,3
SS Concrete Slab	1	1,5	1
MSSS Concrete Box Multiple	>1	1,5	5
MSSS Concrete Girder	>1	1,5	2,3
MSSS Concrete Slab	>1	1,5	1
MSC Concrete Girder	>1	2,6	2,3
MSSS Steel Girder	>1	3	2,3
MSC Steel Girder	>1	4	2,3
Other	Any	7,8,9,0	7-22, 0

Table 3.8: Detailed Classification Guide for Bridges in the Houston/Galveston Bay Area.

3.3.1.2. Calculating Height above Water

An extremely important value for determining inundation and relative surge level is the distance between the mean water level and the deck or underside of the bridge.

For this study, the height above water was usually determined in one of two ways, either from the channel profile or from the bridge profile in the as-built. The channel profile lists various points along the bridge length, usually every span, and a measured distance to the channel bottom, along with an average of the distance to the water level. Height above water for most spans is simply the measured distance to the water level; however, the height to the ground below the bridge span was substituted for height above water for spans with no water beneath them. For those bridges where a channel profile was not available, an estimate of height above water was taken from the bridge overview pages in the as-built. Using Adobe PDF and its measurement tools, the relative distance between the bridge deck and the water level could be ascertained from the as-built and the actual distance then calculated by using the scale provided on the bridge plans. In the example of the as-built below (Figure 3.4), note the red arrows which measure the distance from deck to water on the plan. Additionally, in Figure 3.5 of the channel profile, the key aspects are blocked in red for an example span.

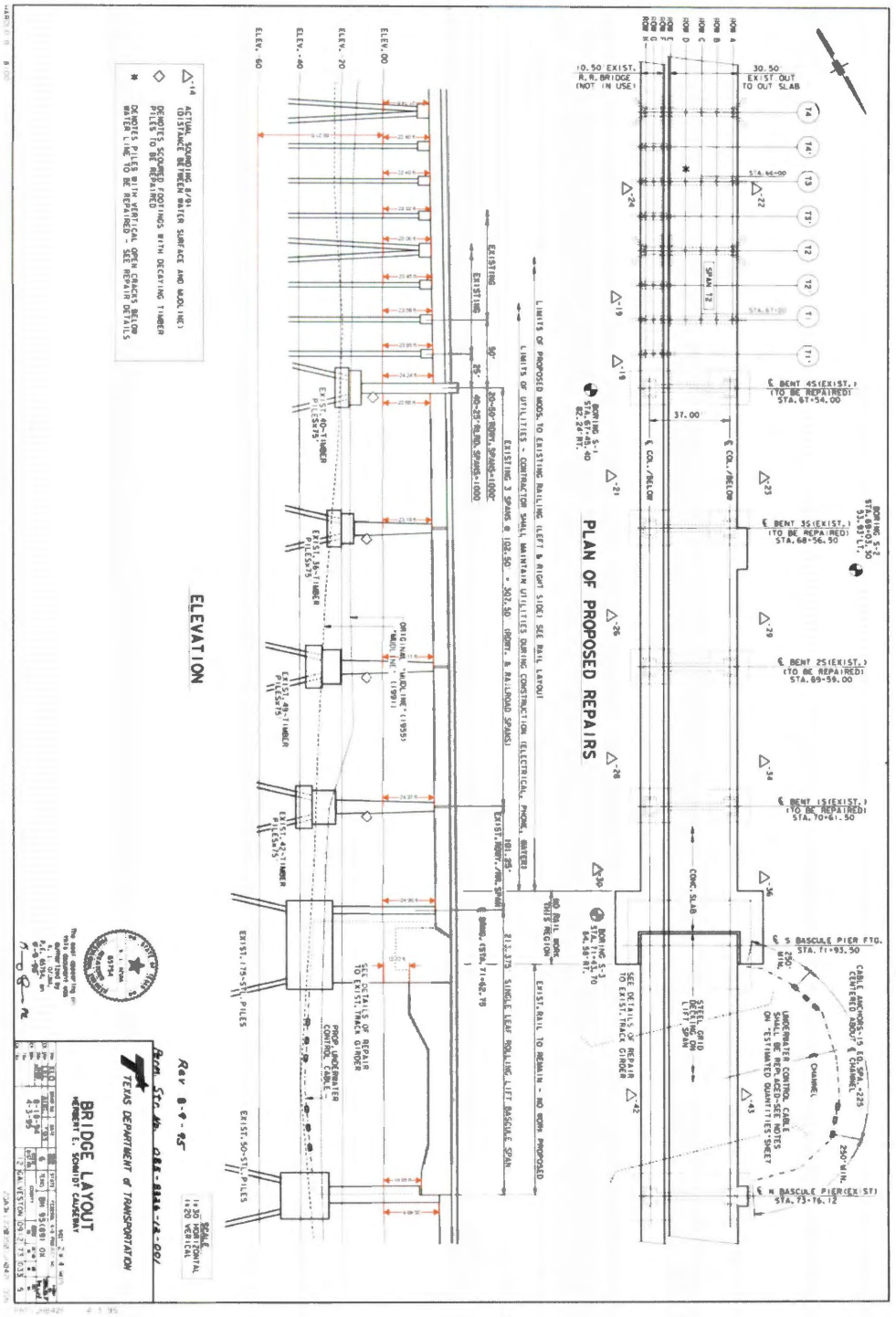

Figure 3.4: Example of Calculation of Height above Water from As-Built.

Texas Department of Transportation

CHANNEL CROSS-SECTION MEASUREMENTS RECORD

Bridge I.D.: 20-036-0508-02-032

Facility: IH 10

Feature X'ed: Old/Last River & FM 565

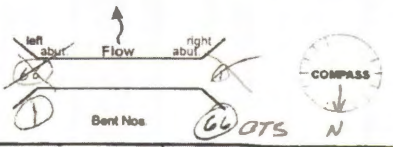

Sheet 2 of 2

Bent #	Notes (Item 44)	Total Horiz. Dist.	Entar Design — Prime Consultant — Date: 5/30/08 — ☑ Upstream ☐ Downstream				Store Structural — Prime Consultant — Date: 6-13-10 — ☑ Upstream ☐ Downstream				Prime Consultant — Date: — ☐ Upstream ☐ Downstream				Prime Consultant — Date: — ☐ Upstream ☐ Downstream			
			Distance from Last Bent	Top Ref.	Bot. Ref.	Vertical Distance	Distance from Last Bent	Top Ref.	Bot. Ref.	Vertical Distance	Distance from Last Bent	Top Ref.	Bot. Ref.	Vertical Distance	Distance from Last Bent	Top Ref.	Bot. Ref.	Vertical Distance
36		2703'	80'	A	H	16.7'	B3	A	H	17.1'								
37		2783'	80'			16.6'	30			16.8'								
38		2863'	80'			16.5'	29			16.8'								
39		2943'	80'			16.5'	28			16.7'								
40		3023'	80'			15.6'	27			16.2'								
41		3103'	80'			15.8'	26			16.0'								
42		3183'	80'			15.5'	25			15.8'								
43		3263'	80'			16.9'	24			17.1'								
44		3343'	80'			22.0'	23			23.2'								
45		3423'	80'			21.1'	22			21.0'								
46		3503'	80'			20.9'	21			21.6'								
47		3583'	80'			21.5'	20			21.8'								
48		3663'	80'			21.5'	19			23.0'								
49		3743'	80'			23.1'	18			23.3'								
50		3823'	80'			22.1'	17			23.0'								
51		3903'	80'			22.7'	16			23.5'								
52		3983'	80'			22.4'	15			23.4'								
53		4063'	80'			22.0'	14			23.7'								
54		4143'	80'			22.1'	13			22.4'								
55		4223'	80'			21.4'	12			21.5'								
56		4303'	80'			21.4'	11			21.3'								
57		4383'	80'			21.2'	10			22.0'								
58		4463'	80'			21.9'	9			22.0'								
59		4543'	80'			20.2'	8			23.8'								
60		4623'	80'			20.5'	7			21.2'								
61		4703'	80'			20.6'	6			20.5'								
62		4783'	80'			20.0'	5			20.2'								
63		4863'	80'			18.5'	4			18.7'								
64		4943'	80'	↓	↓	16.3'	3		↓	16.7'								
65		5023'	80'	↓	↓	14.8'	B2		H	14.5'								
66	E ABUT	5078'	55'	A	H	6.8'	—		—	—								
							~32	↓	H	14.6'								
1	East Abut	—	—	—	—	—	A1	A	I	7.0'								
							—	A	B	2.7'								
							—	A	F	7.0'								
							@83	A	G	16.2'								

2008 Bents #'s are incorrect (Backwards to Layout) 05S 6-13-10

If measurements were taken with any device other than a drop line or tape measure, please describe method on reverse side of form. Please record any important comments on the reverse side.

Reference Features:

A. Top of Railing C. Top of Curb E. Sidewalk G. Water Surface I Rigid Rip-Rap K. _____

B. Edge of Deck D. Top of Parapet F. Top of Cap H. Channel J. Rubble Rip-Rap L. _____

Figure 3.5: Example of Height above Water from Channel Profile.

3.3.1.3. Calculating Water Depth

Similar to height above water seen in the figures above, water depth was calculated primarily from the channel profile. For most bridges calculating the water depth is straightforward. If the bridge is flat, or does not change elevation over its length, the water depth for each span is found by subtracting the height above water from the given distance between the bridge deck and the channel bottom (see Figure 3.6). Most bridges fall into this category, and any bridge with less than 8 spans was assumed relatively flat. However, calculating the water depth becomes more complicated when elevation change in the bridge is taken into account and some assumptions must be made. First, for most of the longer bridges with elevation change, the height above water for each span was calculated from the as-built (see Figure 3.4 above) rather than from the channel profile to account for the changing bridge elevation. From there the distance to the channel bottom of each span was still obtained from the channel profile, and the water depth could be calculated by subtracting the height above water (see Figure 3.7). The biggest assumption made here is that the height above water does not change significantly over time, since the as-built is from the date of construction, unlike the channel profile measurements which are completed on a bi-annual basis.

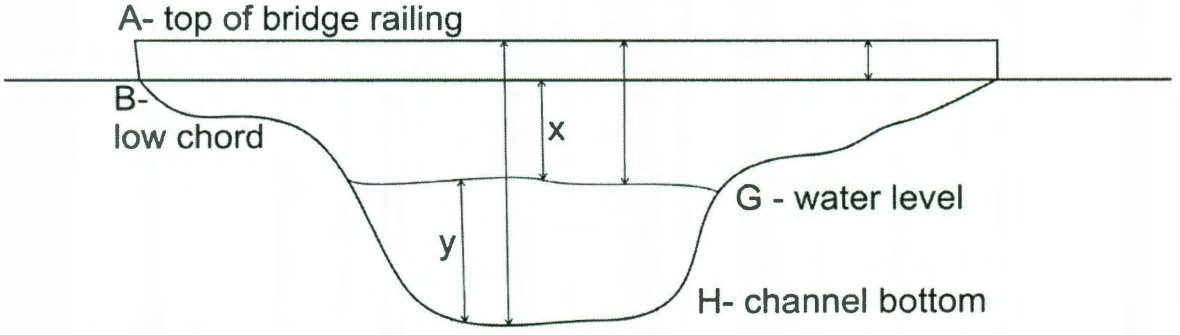

Given: A-B, A-G, and A-H from channel profile
x is the height above water
y is the water depth
if (A-G) > (A-H) then,
x=(A-G) - (A-B), otherwise
x=(A-H) - (A-B)
y=(A-H) - x - (A-B)

Figure 3.6: Schematic of Height above Water and Water Depth Calculations for Flat Bridges.

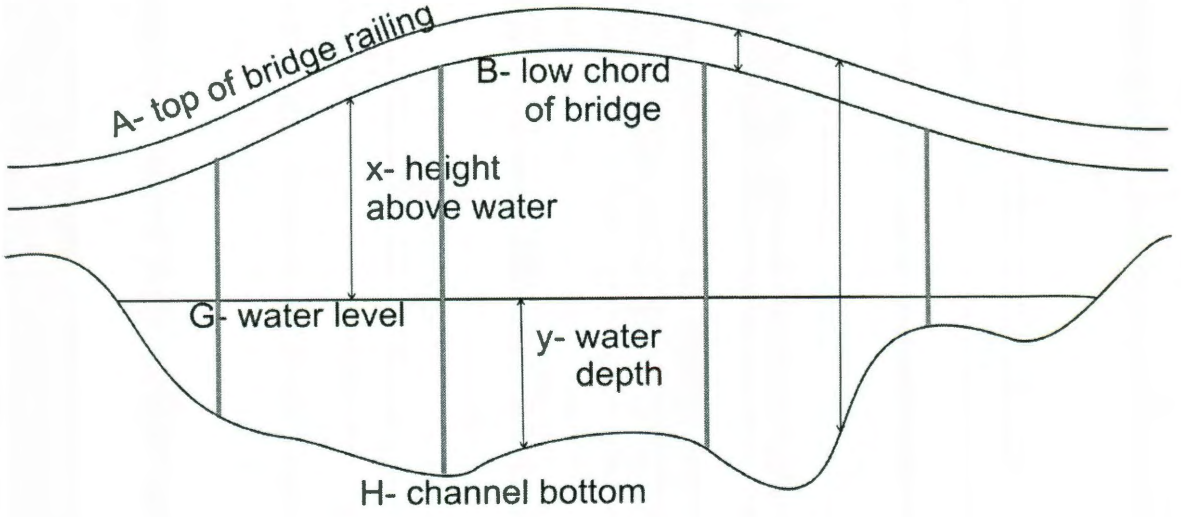

Given A-B, A-H, x from as-built
Assume G is a constant elevation
y = (A-H) - x - (A-B)

Figure 3.7: Schematice of Height above Water and Water Depth Calculation for "Changing Elevation" Bridges.

3.3.1.4. Calculating Channel Bottom Elevation

After the height above water and the water depth was obtained for each bridge span, the channel elevation was determined by taking the elevation of the bridge deck for flat bridges and subtracting both the height above water and the water depth. For bridges whose elevation changes, the elevation from LiDAR was taken beneath the bridge at the channel level so as to assume a constant water level, and the channel elevation was found by subtracting the water depth, and the bridge elevation by adding the height above water, as illustrated in the figure above.

3.3.2. Determining Bridge Subsets for Modeling Purposes

Once all the data had been collected for each bridge in the bay area, subsets of the database must be created for each of the four vulnerability models based on the data available. For instance, the bridge deck uplift model is not suited for running timber structures or skewed structures at this time. Thus, the uplift data set of bridges contains 136 bridges for which there is sufficient data and model applicability. However, the subset for bridge deck uplift could be expanded in the future if models appropriate for timber and skewed bridges are created. Likewise, pier scour analysis is only relevant for those bridges with more than one span, as single span bridges generally have no piers in the water; thus, the data set for pier scour is 123 bridges. The abutment scour model is only valid for bridges whose abutments are not already protected by scour countermeasures like riprap. Hence the subset for abutment scour is 109 bridges. Finally, embankment scour analysis is conducted for the complete 155 bridge database.

3.4. Statistical Analysis of Houston/Galveston Bridge Inventory Database

After gathering all the pertinent data, a basic statistical analysis was conducted to better characterize and understand the bridges in the area and to draw some initial insights on the susceptibility of the Houston/Galveston bay area to hurricane threats. Some statistics were calculated using the entire database of 155 bridges (those pertinent to scour and general vulnerability, such as age of structure) while other statistics such as bridge superstructure classification were calculated using the database of 136 bridges that were included in the bridge deck uplift. First, the bridges were classified following the detailed classification scheme described above. Figure 3.8 shows the distribution of bridges by detailed classification type. As has been demonstrated in both Hurricane Katrina and Hurricane Ike, Multi-Span Simply Supported Bridges (MSSS) are typically the most vulnerable to bridge deck uplift due to the lack of continuity between spans and the limited vertical resistance connecting each span to the substructure (Padgett et al., 2009, Stearns and Padgett, 2011). When looking at the Houston/Galveston bay area, it is seen that 68% of the bridges in the area are MSSS classified, and may be of critical importance when evaluating the risk to uplift. Upon a closer look closer at the detailed classifications, it can be seen that over half of the MSSS bridges are Concrete Girder type, but the other half consist of Concrete Box Beam and Concrete Slab. Because of this, the bridge deck uplift model incorporates all of these superstructure types in order to fully characterize the risk to the bridges in this area.

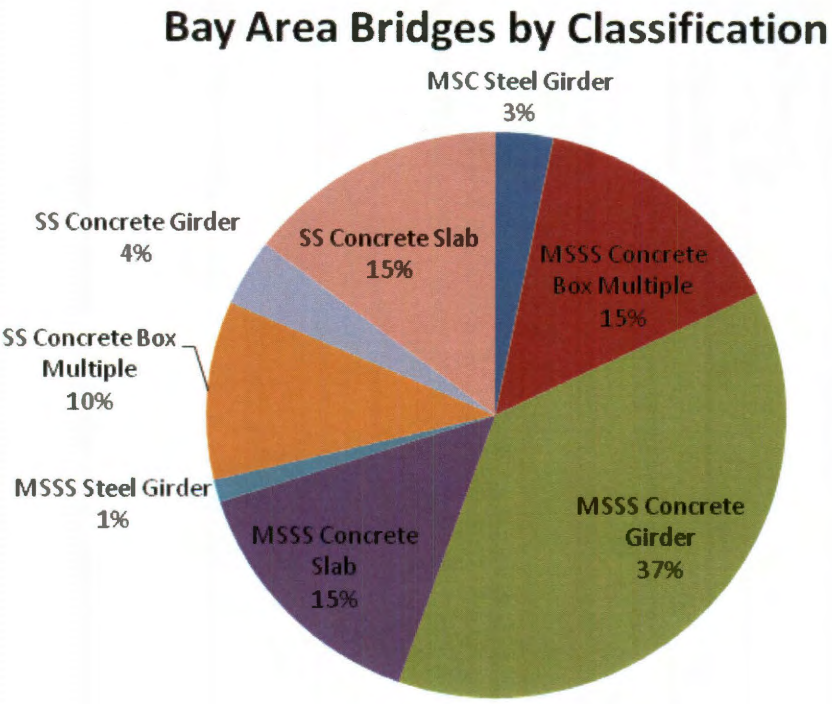

Figure 3.8: Pie Chart of the Houston/Galveston Bay Area Bridges by Classification Type.

Figure 3.9, presented below, shows the distribution of bridges in the Houston/Galveston bay area based on the age of the structure. From this, it is clear that over half of the bridges in the Galveston bay area are over 35 years old. While not considered in this thesis, future research could investigate the risks from both extreme events and deterioration of aging structures in the Houston/Galveston bay area, such as has been done for bridges in earthquake prone areas (Rokneddin et al., 2011).

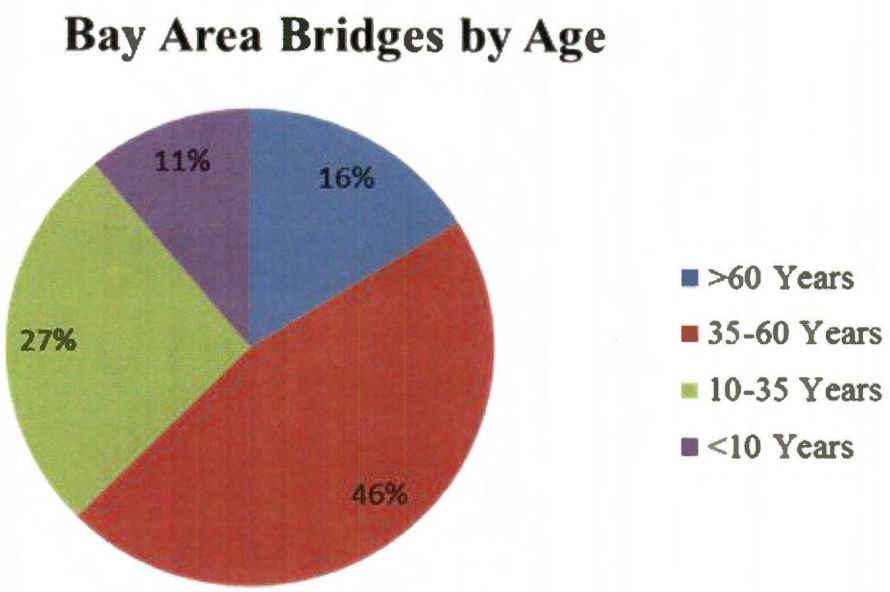

Figure 3.9: Pie Chart of the Houston/Galveston Bay Area Bridges by Age.

Also, a parameter of interest for both scour and uplift is the distance between the bridge deck and the water level. This information, when coupled with storm surge data, can determine the relative surge height of the bridge as well as whether or not the bridge is inundated, a measure of short-term impassability. Also, studies on the damages from Hurricane Katrina noted that the most severely damaged bridges had a low elevation over the water level (Padgett et al., 2009). As seen in Figure 3.10 below, 68% of the bridges in this area are less than 15 ft above the mean water level and thus would be inundated at that surge. Hurricane Ike reached surge heights of 14 ft some places in the Houston Ship Channel so an even stronger storm or one that would hit Houston and Galveston more directly may have more devastating results on the bay area transportation system.

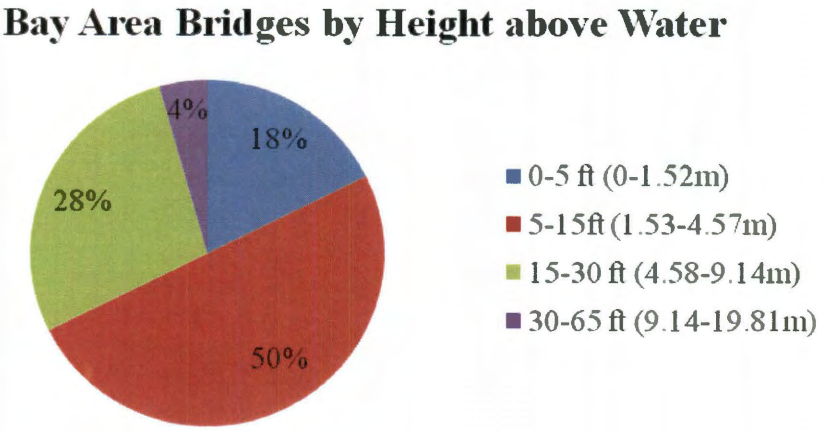

Figure 3.10: Pie Chart of the Houston/Galveston Bay Area Bridges by Height above Water.

For scour determination, one of the key parameters is the type of soil located at each bridge site; thus, a statistical view of the soil types in the Houston/Galveston bay area could yield unique insights into the scour problem (Figure 3.11). Based solely on the soil type, there is some reason to believe that the bridges in the Houston/Galveston region may be more resistant to scour than in other areas. From the statistics in Figure 3.11, the bay area bridge could experience less scour due to 58% of the bridges being located in clay soil which is the most erosion resistant of soil types, rock not included. However, 9% of the bridges are also found in the most erodible soil type, sand, and are therefore, the most susceptible to scour related problem.

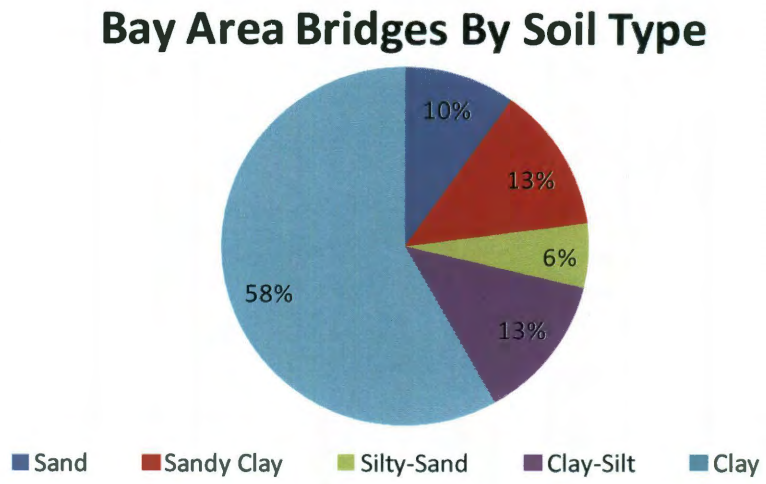

Figure 3.11: Pie Chart of the Houston/Galveston Bay Area Bridge by Soil Type.

As can be seen by a basic statistical analysis of the database, the case study bridges in the Galveston Bay Area are typically older, low elevation, multi-span simply supported bridges. Given the evidence from past hurricane events, these types of structures are particularly susceptible to unseating under storm surge and wave loading. Therefore, a hurricane risk assessment of the bay area bridges should explicitly consider probability of span shifting or unseating. Scour may be somewhat less pressing based on the predominant soil type, but given empirical evidence, the issue of scour cannot be discounted without a more thorough examination of the problem through probabilistic scour depth modeling.

Chapter 4

Vulnerability Modeling of Bridge Deck Uplift

With the database of the Houston/Galveston bay area completed, fragility models for the two failure modes are needed in order to assess the vulnerability of the bridges in the database. As seen in empirical evidence from past hurricanes, bridge span displacement or removal is the leading cause of complete bridge failure during coastal storm events, both in cost and frequency. As such, fragility models from bridge deck uplift are required to determine the failure probability for each bridge. However, while the new AASHTO specifications gives guidance to determining the wave and surge loads on new design, previously there have been no probabilistic models to determine the risk to existing bridges accounting for the uncertainty in both the bridge capacity and the hurricane demand. Ataei and Padgett (2010b) recently proposed a first methodology to develop fragility surfaces for the span shifting and unseating failure mode of coastal bridges. Their model will be used in

the regional assessment conducted herein to evaluate the performance of bridges during hurricanes. Although further details on the probabilistic model can be found in Ataei and Padgett (2010b), an overview of the methodology is provided below along with details of how it is applied to the Houston/Galveston bay area.

4.1. Background on Fragility Modeling and Methodology for Uplift

Fragility modeling aims to determine the conditional probability of failure for a structure given a level of hazard intensity measure (IM). Fragility curves or surfaces are obtained by comparing the capacity (C) of a structure to the demands (D) experienced across a range of IMs, thereby determining a failure probability of the structure at each IM value. Ataei and Padgett (2010b) showed that the unseating fragility of coastal bridges is best depicted by a fragility surface with a vector of intensity measures (Ataei and Padgett, 2010a).

$$P\left[Damage \middle| \ Z_c, H_{MAX}\right] = P[\,D > C \middle| \ Z_c = s_1, H_{MAX} = s_2] \ ,$$

Equation 4.1: Probability of Damage Given Intensity Measures (Ataei and Padgett, 2010b).

where Z_c is the relative surge elevation, $H_{max}$is the maximum wave height, and s_1, s_2 are the values at which the failure probability is being computed. To evaluate this conditional probability statement, Ataei and Padgett (2010b) found that an assessment of static vertical uplift demands relative to probabilistic capacity models, instead of a full dynamic analysis for each bridge, was sufficient to assess

unseating fragility of typical low capacity connection bridges as found in the Houston/Galveston bay area bridge inventory. This approach thus reduces the computations needed to conduct a regional risk assessment, enabling bridge specific fragility assessment and making the model more efficient for quickly determining which bridges are in the most danger of failure.

The methodology adopted compares the vertical capacity of each bridge span to the vertical uplift force caused by storm surge and waves, and failure is defined as the force exceeding the capacity. Figure 4.1 below shows the methodology schematically and more details on the approach to evaluate both demand, capacity and associated uncertainties are discussed in the following subsections (Ataei and Padgett, 2010b).

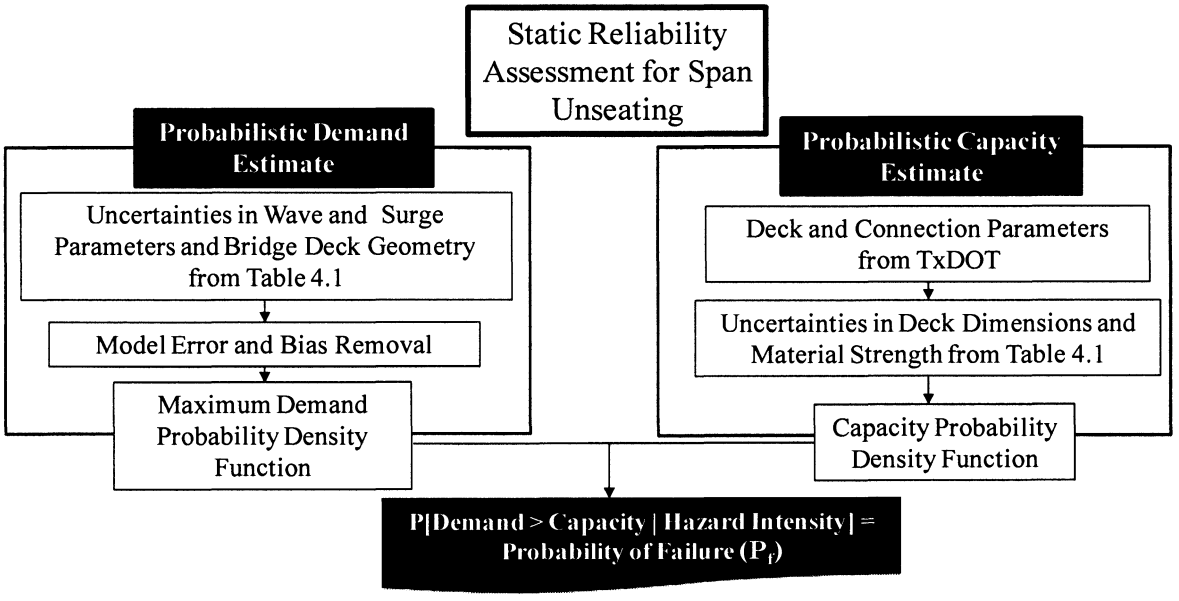

Figure 4.1: Schematic of Static Reliability Assessment for Span Unseating. Adapted from Ataei and Padgett (2010b).

4.1.1. Demand Modeling in the Bridge Deck Uplift Model

Ataei and Padgett (2010b) provide a detailed discussion of the approach for probabilistic analysis of the demand generated by hurricane induced surge and wave as adopted in this study. Their model builds heavily upon the new AASHTO (2008) guide specifications for bridges vulnerable to coastal storms in which estimates of the peak forces on bridge decks are presented based on extensive studies by Marin and Sheppard (2009). These models were tested with field data of the I-10 Escambia Bay Bridge and a physics- based model to show accuracy in theory and practice. A review of the AASHTO wave force estimates is provided forthwith.

As mentioned earlier, the vertical force on a bridge is composed of four parts, an impact force due to trapped air between the water and the bridge deck, as well as the quasi-static forces of drag, inertia and buoyancy. The maximum quasi-static vertical force per unit length is estimated as:

$$F_{V-MAX} = \gamma_w \overline{W} \beta \left(-1.3 \frac{H_{MAX}}{d_s} + 1.8 \right) \left[1.35 + 0.35 \tanh(1.2T_p - 8.5) \right] \left(\begin{array}{c} b_0 + b_1 x + \frac{b_2}{y} + b_3 x^2 \\ + \frac{b_4}{y} + \frac{b_5 x}{y} + b_6 x^3 \end{array} \right) (TAF)$$

Equation 4.2: Maximum Quasi-Static Vertical Force per Unit Length (AASHTO, 2008).

where γ_w is the unit weight of water, H_{MAX} is the wave height, d_s is the total water depth during the storm surge, and T_p is the wave period. B is a coefficient that takes

into account the position of wave crest with respect to the bridge deck. Coefficients b_0 to b_6 are defined by the geometric properties of the deck, and *TAF* is a factor to adjust the vertical quasi static force for the effects of entrapped air. Additionally, $\overline{W}$, x and y are given below:

$$\overline{W} = \left[\lambda - \left(\frac{\lambda}{H_{MAX}}\right)\left(Z_c + \frac{H_{MAX}}{2}\right)\right]$$

$$\text{If } \frac{\overline{W}}{W} < 0.15, \text{ then } \overline{W} = 0.15W$$

$$x = \frac{H_{MAX}}{\lambda} \quad \text{and} \quad y = \frac{\overline{W}}{\lambda}$$

Equation 4.3: Variables $\overline{W}$, x and y (AASHTO, 2008).

where Z_c is the relative surge elevation, positive if the storm water level is below the bottom of the cross section, W is the bridge width and λ is the wave length. Wave length is usually difficult to determine when predicting or hindcasting hurricanes, however a relationship between wave period and wave length has often been suggested in past research. For example, AASHTO suggests the following equation to relate wave length and period:

$$\lambda = \frac{gT_p^2}{2\pi}\sqrt{\tanh\left(\frac{4\pi^2 d_s}{T_p^2 g}\right)}$$

Equation 4.4: Wave Length Calculation (AASHTO, 2008).

where g is the gravitational constant, and d_s and T_p are defined as before. The impulse like force, also known as the slamming force, is also defined by AASHTO per unit length by:

$$F_s = A\gamma_w H_{MAX}^2 \left(\frac{H_{MAX}}{\lambda}\right)^B$$

Equation 4.5: Impulse/Slamming Force (AASHTO, 2008).

where A and B account for the position of both the surge and wave crest with respect to the bridge deck. For a full account of the peak wave force equations, along with equations for the many coefficients, see AASHTO (2008).

With these models, the maximum uplift force, F_{vt} can be calculated by summing the slamming force with the quasi-static force and removing the bias in the estimation of these forces along with accounting for the error inherent in the model itself. Equation 4.6 shows this below where Δb used to account for the bias in the determination of the wave forces and ε_1 is a random variable with lognormal distribution used here to capture the model error.

$$F_{vt} = (F_{V-MAX} + F_s + \Delta_b)\varepsilon_1$$

Equation 4.6: Maximum Uplift Force with Bias Estimation (Ataei and Padgett, 2010b).

The bias function and model error are adopted directly from Ataei and Padgett (2010a), who conducted a statistical analysis of experimental data relative to AASHTO predictive equations. These analyses enable an application of the predictive equations for peak demands on bridge deck in the probabilistic analysis, and remove conservatism traditionally inherent to code based equations.

Based on the findings of Ataei and Padgett (2010a), two parameters are considered as the intensity measures that the demand and subsequent fragility surfaces are conditioned upon- relative surge height, Z_c and wave height, H_{max}.

Most hindcast models of storms provide information on wave height as the significant wave height instead of maximum wave height called for in the model. Thus, the maximum wave height, H_{max}, is determined to equal to1.8 H_s (AASHTO 2008). The wave period is then correlated to the maximum wave height by the Longuet-Higgins (1983) joint probability distribution: $f(\xi,\eta) = L(\xi/\eta)^2 \exp\{-\frac{\xi^2}{2}[1+(1-\frac{1}{\eta})^2 \frac{1}{\nu^2}]\}$ where ξ and η are dimensionless wave height and wave period respectively, and are given by the equations below:

$$\xi = H/\sqrt{m_0}\ ; \quad m_0 = (H_s/4)^2;$$
$$\eta = T/\overline{T}$$

Equation 4.7: Dimensionless Wave Height and Wave Period in the Longuet-Higgins Joint Probabilisty Distribution.

where L is a constant, defined as $(1+\frac{\nu^2}{4})\frac{1}{\sqrt{2\pi\nu}}$; m_0 is the first spectral moment, $\overline{T}$ is the mean wave period, and ν is the bandwidth of the wave spectral density. In addition to accounting for this uncertainty in wave period for a given wave height, other random variables are also considered in the fragility analysis, shown in Table 4.1. To remain consistent across both demand and capacity modeling, the deck thickness is taken as a uniform distribution where the thickness can vary from 95% to 105% of the value in the database. All other structural parameters are taken as

deterministic in the demand modeling. The next section describes the capacity analysis procedure adopted and associated random variables.

4.1.2. Capacity Modeling in the Bridge Deck Uplift Model

The capacity model presented in Ataei and Padgett (2010b) calculates the capacity of a bridge deck to resist vertical forces and consists of the weight of the deck and vertical connections between the deck and the substructure of the bridge. The weight per unit length of each span can be calculated using Equation 4.8 below.

$$W_s = (d_b W + A_g \times n_g)\gamma$$

Equation 4.8: Weight per Unit Length of Bridge Span (Ataei and Padgett, 2010b)

where W_s is the span weight per unit length, d_b is the deck thickness, W is the deck width, A_g is the cross section area of the girders, n_g is the number of girders and γ is the unit weight of the material. Uncertainties in the density of materials and in the thickness of the bridge deck are considered following the distributions given in Table 4.1. The girder type, height and number of girders given by TxDOT are taken as deterministic parameters because the most common girder types are pre-cast and made off-site.

Vertical connection between substructure and superstructure is usually manifested through anchor bolts or dowels bars in bridges in the coastal region. The contribution of this vertical connection, if it exists, can be determined by the pullout or yield strength of the bars. For anchor bolts, the equations are taken from ACI 318-Appendix D and given in Equation 4.9 below with uncertainty taken into account:

$$\text{Connection strength, } F_c = n_b \times \min\begin{cases}\text{Steel strength, } N_s = A_{se} f_{ut} \\ \text{Concrete breakout strength, } N_{cb} = \dfrac{A_N}{A_{No}} \psi_2 \psi_3 N_b \times \varepsilon_2 \\ \text{Pullout strength, } N_{pn} = \psi_4 N_p \times \varepsilon_3\end{cases}$$

Equation 4.9: Vertical Connection Strength (Ataei and Padgett, 2010b).

where n_b is the total number of bolts per span, A_{se} is the area of the bolt, f_{us} is the ultimate strength of the steel, A_N is the projected area of the failure surface for the anchor, A_{No} is the projected area of the failure surface of a single anchor remote from edges, N_p is the pullout strength in tension of a single bolt, ψ_2 to ψ_4 are modification factors. For more information, see explanations of the above equations in ACI 318 (ACI, 2005). Steel strength is based on mechanics of materials and thus no model error is associated with it. ε_2 and ε_3 are the model error terms as presented by Eligehausen et al. (2006) for concrete breakout and pullout strength respectively (Eligehausen et al., 2006). If the substructure and superstructure are connected via dowel bars the resistive force can be estimated by:

$$F_c = n_b \times \pi d_{se} l_{emb} \phi_b \le n_b \times A_{se} f_y;$$
$$\varphi_b = \frac{f_y d_{se}}{4 l_d}$$

Equation 4.10: Resistive Force of Dowel Bar Connections (Ataei and Padgett, 2010b).

where φ_b is the bond strength, d_{se} is the reinforcement diameter, l_{emb} is the embedment length of the dowel, f_y is the reinforcement yield strength, l_d is the development length estimated based on (12 – 1) in ACI 318 (ACI, 2005). The dowel bars are assumed to reach yielding if the embedment length is longer than the

development length, otherwise pullout governs The pullout equation above, like steel strength, is based on mechanics of materials and thus no model error is associated with it, only uncertainty in the input parameters. The capacity of the deck per unit length therefore is obtained by summing the weight and the connection force:

$$C = F_c / L_s + W_s$$

Equation 4.11: Capacity of Bridge Deck (Ataei and Padgett, 2010b).

Table 4.1 below lists the uncertainties accounted for in both the demand and capacity models, along with their various distributions.

Wave and surge parameters					
			Distribution Parameters		
Variable	**Symbol**	**Distribution**	**1**	**2**	**Unit**
Maximum wave height	H_{max}	Function of H_s	-	-	m
Wave Period	T_p	Longuett-Higgins	$\nu^1 = 0.3$	-	s
Wave length	λ	Function of T_p	-	-	m
Structural parameters					
Width	W	Deterministic	-	-	m
Deck type (Slab, girder)		Deterministic	-	-	-
Girder height	d_g	Deterministic	-	-	m
Deck thickness	d_b	Uniform	$l^2 = 95\%$	$u^3 = 105\%$	m
Concrete strength	f'_c	Normal	μ^4, from as built plans	$\sigma^5 = 4.3$	MPa
Steel strength	f_y	Lognormal	κ^6, from as built plans	$\zeta^7 = 0.08$	MPa
Concrete density[8]	γ_c	Normal	$\mu^4 = 23.53$	$\sigma^5 = 0.94$	kN/m^3
Steel density[9]	γ_s	Normal	$\mu^4 = 76.98$	$\sigma^5 = 0.77$	kN/m^3
Prediction models' error					
Wave load model error	ε_1	Lognormal	$\kappa^6 \approx 0$	$\zeta^7 = 0.08$	-
Anchor breakout/pullout model error	ε_2, ε_3	Normal	$\mu^4 \approx 1$	$\sigma^5 = 0.23$	-

[1] Wave spectral density.
[2] Lower bound for uniform distribution, in percentage.
[3] Upper bound for uniform distribution, in percentage.
[4] Mean value of normal distribution.
[5] Standard deviation of normal distribution.
[6] Logarithmic mean.

[7] Logarithmic standard deviation.
[8] (JCSS, 2001)
[9](Ellingwood and Hwang, 1985)

Table 4.1: Sources and Distributions of Uncertainty in the Bridge Deck Uplift Model- Ataei and Padgett (2010b).

4.2. Fragility Surfaces for Bridge Deck Uplift Vulnerability

As described in (Ataei and Padgett, 2010b), the fragility surfaces for each bridge span are evaluated across the range of combinations of surge elevations and wave heights. To propagate uncertainties in the random variables affecting capacity and demand, Monte Carlo sampling is conducted to obtain the distribution of the limit state function for each span, and then the distribution is integrated to estimate the probability of failure.

The failure probability of each span in a bridge identified, the failure probability of the entire bridge is merely the combination of the effect of each span, where the bridge is modeled as a series system and if one span fails, the entire system fails. The spans in this case are considered to be independent, with continuous spans considered to be a single span where they are continuous.

Ataei and Padgett (2010b) also looked at a fully dependent scenario for individual bridge spans and found that most of the bridges have narrow upper (independent) and lower (fully dependent) bounds with variations of less than 10% in the failure probabilities.

In theory, the probabilistic approach described above can be applied directly to a given set of input storm data to evaluate the failure probability of a bridge. In

this study, the fragility surfaces are instead derived for each bridge in the Houston/Galveston bridge inventory database. This approach has the advantage of decoupling the hazard assessment from the vulnerability modeling to enable any number of future hurricane scenarios to be evaluated for the region. The fragility surfaces of each bridge along with the relative surge height and wave height from scenario hurricane modeling procured from the Computational Hydraulics Group at UT-Austin are used to obtain the probability of failure for scenario regional risk assessment.

Four bridges from the Houston/Galveston bay area bridge inventory were chosen that demonstrate the differences in the fragility surfaces (Figures 4.2 and 4.3) based on bridge deck type and connectivity. Some selected database information for each of the three bridges is given in Table 4.2 below.

The differences in the fragility surfaces arise primarily out of differences in the capacity of the bridge to withstand the vertical uplift force. Therefore, the fields in Table 4.2 relate to the capacity parameters of weight and connectivity. Figures 4.2 (a.) and (b.) show two MSSS Concrete Girder type bridges: one with connectivity between the deck and the substructure of the bridge and one with no connectivity. It is clear from a comparison of the two figures that the connectivity decreases the vulnerability of the bridge from vertical uplift due to the increased capacity of the bridge. Figure 4.3 (a.) gives the fragility surface of an MSSS Concrete Box Beam Multiple bridge. Note that the fragility surface for the MSSS Concrete Box Beam bridge with no vertical connections is similar to the MSSS Concrete Girder bridge

with vertical connections. It was documented during laboratory experiments on bridge decks that the effect of trapped air beneath girders can sharply increase the vertical uplift force; however, air entrapment does not occur as much at concrete box beam bridges and thus, the vertical uplift forces are generally smaller (Cuomo et al., 2009). Finally, Figure 4.3 (b.) shows an MSC Steel Girder bridge to draw contrast between the fragilities of continuous bridges with that of simply-supported. The MSC Steel Girder bridge, due both to its vertical connections and its continuity of spans, shows the least amount of vulnerability to storm surge and wave uplift forces. Future work on bridge deck uplift could explore the relationship between the various bridge capacity parameters and the resulting fragility surfaces. The next chapter will discuss a similar methodology employed to estimate the scour depths at bridges in the Houston/Galveston bridge inventory.

Bridge ID	Classification Type	Vertical Connections	Median Span Length (ft)	Deck Width (ft)	Height above Water (ft)
12085B00535002	MSSS Concrete Girder	None	30	27	2.6
121020050807198	MSSS Concrete Girder	Dowels	30.33	35.7	5.9
121020AA3309001	MSSS Concrete Box Beam Multiple	None	23	28.3	3.5
120850050004220	MSC Steel Girder	Dowels	64	54.1	4.5

Table 4.2: Capacity Related Inventory Data for Uplift Fragility Example Bridges.

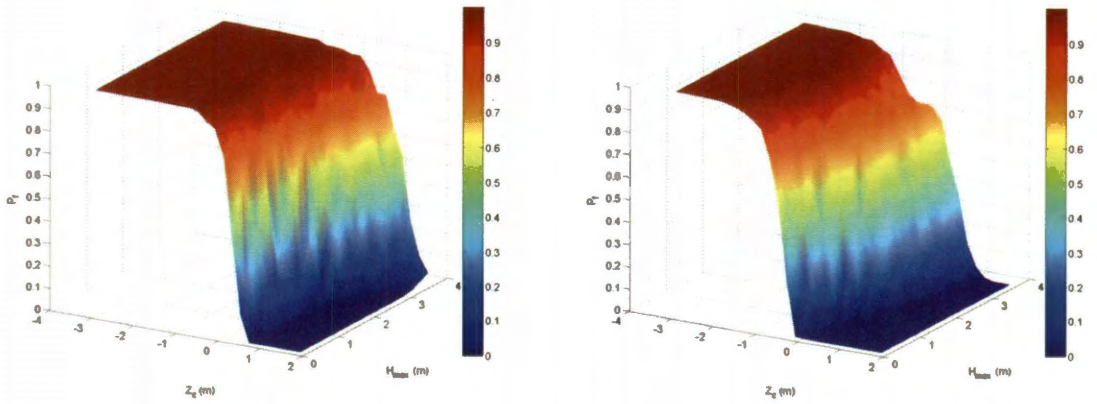

(a.) (b.)

Figure 4.2: Fragility Surfaces for MSSS Concrete Girder Bridges (a.) without Vertical Connections; and (b.) with Vertical Connections.

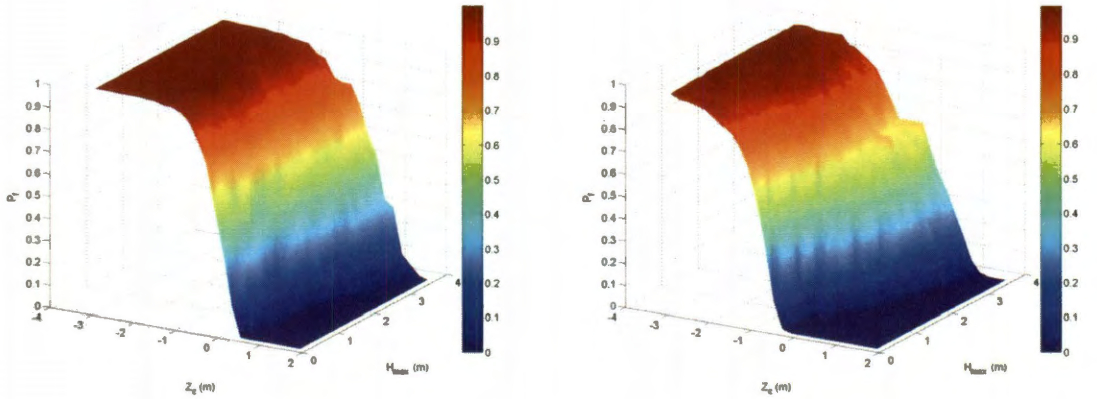

(a.) (b.)

Figure 4.3: Fragility Surface for (a.) MSSS Concrete Box Beam Multiple Bridge without Vertical Connections; and (b.) MSC Steel Girder Bridge with Vertical Connections.

Chapter 5

Probabilistic Approach to Scour Vulnerability Modeling

5.1. Overview of the Probabilistic Scour Models

The last aspect of the risk assessment for this region is scour vulnerability modeling. This chapter goes into detail about the specific scour model used, drawing from the SRICOS method originally presented by Briaud et al. (2004) and accounting for the uncertainties in the input parameters and the inherent bias in the original model to obtain a probabilistic estimate of scour depth. The scour analysis builds upon work by Briaud and Oh (2010), with the initial erosion rate estimates for each soil type stemming from the simplified SRICOS method for TxDOT, presented in Briaud et al. (2009). All input parameters come from the bridge and soil database developed for the Houston/Galveston bay area, described in Chapter 3. Previous methodologies are deterministic in nature and/or yield only the maximum scour depth a bridge

could possibly experience, often with emphasis on lifetime exposure rather than extreme event situations. The approach herein (illustrated in Figure 5.1) evaluates the probabilistic model of scour for a set of relevant hurricane hazard parameters. Scour fragility estimates are then derived for prescriptive limit states, which state the probability of meeting or exceeding a prescribed scour level given the water velocity from the hurricane.

First, the probabilistic pier and abutment models are discussed along with their associated input sources, uncertainties and limit states. Then, in both the pier and abutment model, fragility curves are presented to encompass a range of water velocities a bridge might experience during a hurricane event. Finally, a qualitative measure of embankment scour is described as a first pass at understanding the road and bridge systems susceptibility to embankment scour.

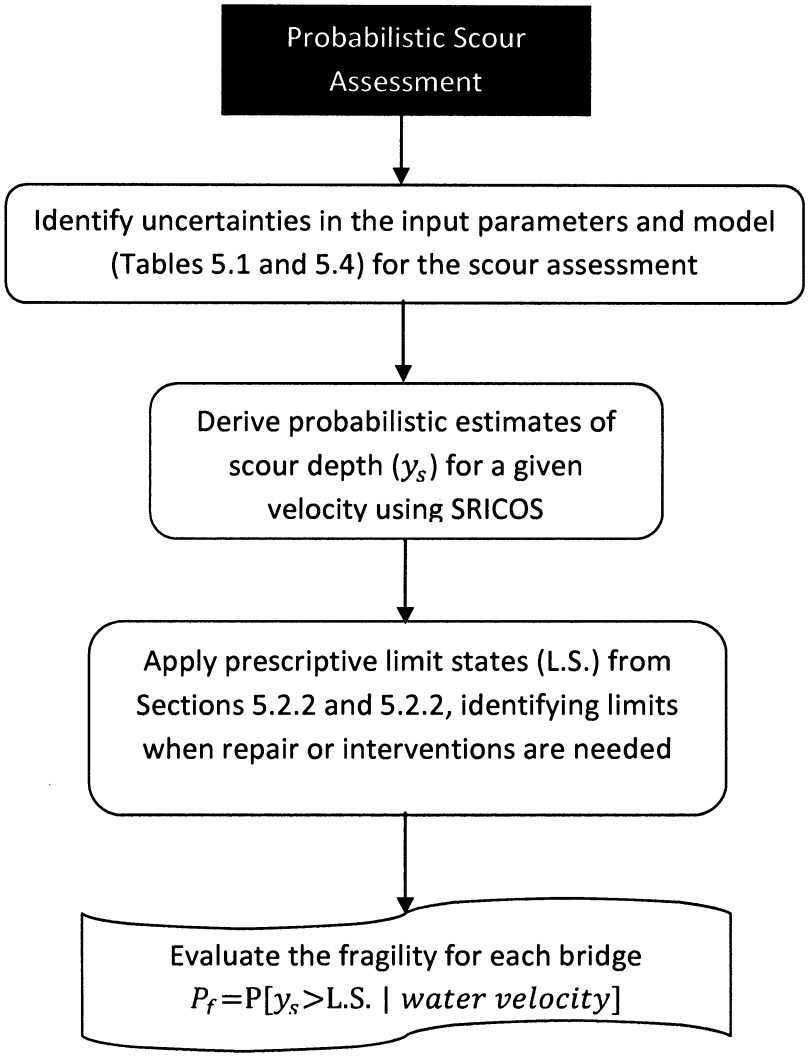

Figure 5.1: Schematic Overview of the Probabilistic Scour Assessment.

5.2. Probabilistic Pier Scour Modeling

The first application of the simplified SRICOS method is in determining the probable pier scour depth after a hurricane event. Pier scour is a form of local scour that occurs when water displaces soil particles around a bridge pier or pile, causing a hole to form (see Figure 5.2 for an example). This type of scour is dangerous in that the scour hole lengthens the pier which causes the both the pier and the pile

foundation to have a reduced capacity to resist lateral forces and, since pier scour occurs under water, this type of damage is not always immediately apparent, unlike deck displacement or soil erosion. Additionally, pier scour is the primary mode of scour failure in normal tidal and river flow events. Appropriately then, the SRICOS method was first designed for pier scour and is where this scour analysis starts.

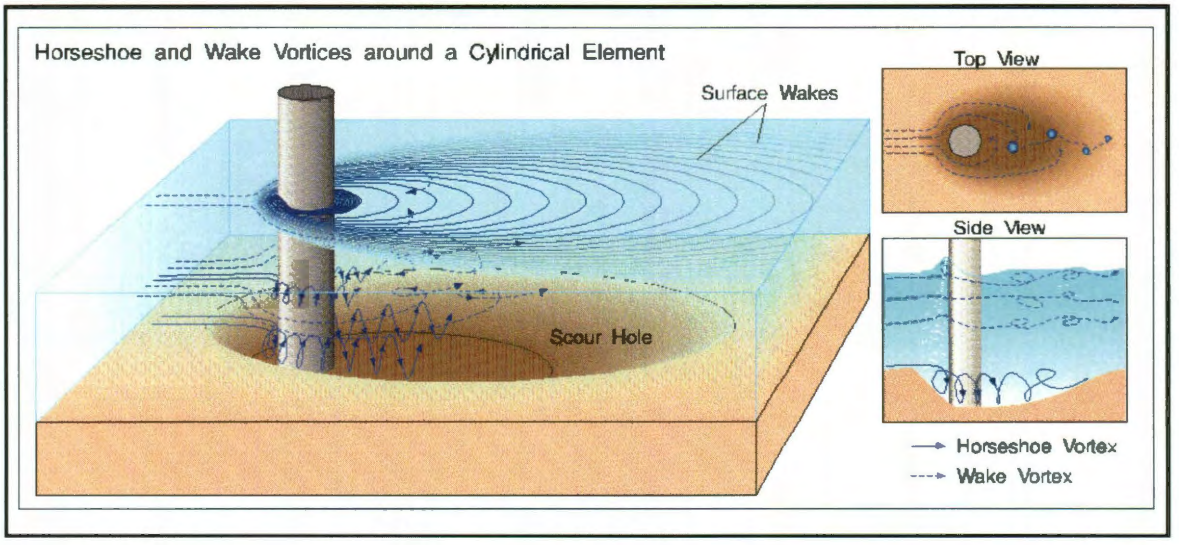

Figure 5.2: Schematic of Pier Scour in a Stream (USGS, 2009).

The pier scour equation from SRICOS is based on empirical scour findings and because of this is comprised mostly of coefficients determined by varying parameters of the bridge and/or water source. Maximum pier scour depth, via the SRICOS or HEC-18 (clay) method, is given by:

$$y_s = a' * K_1 * K_{sp} * K_l * K_w * 2.2 * (2.6 * Fr_{pier} - Fr_{c(pier)})^{.7}$$

Equation 5.1: Maximum Potential Pier Scour from Briaud and Oh (2010).

where a' is the effective pier width based on the angle of attack of the water, K_1 is the correction factor to account for pier type, K_{sp} is correction factor for the spacing of the piers, K_l is the correction factor that accounts for the aspect ratio of rectangular piers, K_w is the correction factor for the water depth effect, Fr_{pier} is the Froude number based on the velocity of the water approaching the pier, $Fr_{c(pier)}$ is the Froude number based on the critical water velocity and y_s is the maximum scour depth for given pier parameters. The effective pier width, $a'$is defined as:

$$a' = a * [\cos(\theta) + \frac{L}{a}\sin(\theta)]$$

Equation 5.2: Effective Pier Width (Briaud and Oh, 2010).

where a is the pier width, θ is the attack angle the water makes with the pier, and L is the length of the pier (not the height of the pier). For most piles, which are square or cylindrical, the effective width is the same as the pier width. To determine the correction factor, K_1, the differing pier types must be defined. In this study, there are three main piers types; round-nose, cylindrical and square-nose. Cylindrical is simply the piers that are cylinders, whereas square-nose accounts for all square and rectangular piers and round-nose includes all oval piers. With that in mind, the K_1factor is given by:

$$K_1 = \begin{cases} 1.0\ , for\ \theta > 30° \\ 1.0\ , for\ roundnose\ and\ cylinder \\ 1.1, for\ rectangular \end{cases}$$

Equation 5.3: Coefficient $K_1$for Pier Type (Briaud and Oh, 2010).

The spacing correction factor is usually 1.0 but for bridges where the piles or piers are close together the coefficient is given as:

$$K_{sp} = \begin{cases} 2.9 * \left(\frac{S}{a'}\right)^{-.91}, for\ \frac{S}{a'} < 3.2 \\ 1.0, \quad otherwise \end{cases}$$

Equation 5.4: Coefficient K_{sp} to Account for Spacing between Piers (Briaud and Oh, 2010).

In Equation 5.4 above, S is the spacing between piers. K_l in this study is 1.0 for all ranges of L/a from the work of Briaud and Oh (2010). The water depth correction factor is defined as:

$$K_w = \begin{cases} 0.89 * \left(\frac{y_1}{a'}\right)^{.35}, for\ \frac{y_1}{a'} < 1.43 \\ 1.0, \quad otherwise \end{cases}$$

Equation 5.5: Correction Factor for Water Depth, K_w (Briaud and Oh, 2010).

where y_1 is the water depth at the pier during the conditions examined (i.e. normal water depth for regular flow, storm water depth when looking at a specific storm event). The Froude numbers for the pier are given by Equation 5.6 below:

$$Fr_{pier} = \frac{V_1}{\sqrt{g * a'}}$$

$$Fr_{c(pier)} = \frac{V_c}{\sqrt{g * a'}}$$

Equation 5.6: Froude Numbers of Pier Given Assumed Velocity, V_1, and Critical Velocity, V_c (Briaud and Oh, 2010)

where V_1 is the given or assumed water velocity during the storm event, V_c is the critical water velocity at which scour begins, given by the assumptions in Section 5.2.1 below, and g is the gravitational constant (9.81 m/s). The maximum scour depth, y_s, can thus be obtained from Equations 5.1-5.6 above and then used in the SRICOS hyperbolic function (an example of which is given in Figure 5.3 below) to determine the scour depth of a pier given a storm of a specific duration and an initial erosion rate of the soil. This is shown in Equation 5.7 below:

$$y_{final} = \frac{t}{\frac{1}{\dot{z}_i} + \frac{t}{y_s}}$$

Equation 5.7: Pier Scour, y_{final}, for a Given Duration Event (Briaud et al., 2004)

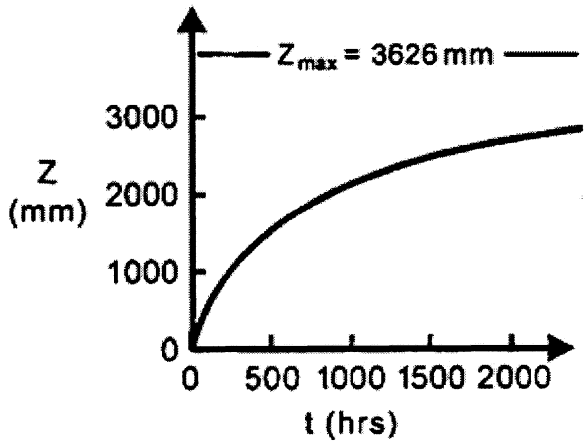

Figure 5.3: Example Graph of Scour Depth Verses Time from SRICOS Method (Briaud et al., 2004).

where t is time in hours, $\dot{z}_i$ is the initial erosion rate, y_s is the maximum possible scour depth calculated using the above equations and y_{final} is the anticipated scour depth after time, t. The time for the storm is obtained from the ADCIRC data from

the Computational Hydraulics Group at UT-Austin, as is the water velocity, and the initial erosion rate is determined based on soil type as given in Section 5.2.1 below.

5.2.1. Uncertainties in Input Parameters and Bias in the Model

With the base equations of the deterministic method presented, one unique component of this study is to account for the uncertainties in the input data, along with bias and model error, thereby yielding a probabilistic scour depth instead of a deterministic output. The uncertainties in the input data are given in Table 5.1 below. Most of the structural parameters are taken as deterministic because piers and piles are often pre-cast and made off-site, allowing for greater certainty in the values of the pier width and length. Additionally, as soil type and pier type are discrete parameters, they are also adopted as deterministic values. It is acknowledged that assignment error is feasible, but not accounted for in this study. The attack angle of the water to the pier is taken to have a uniform distribution with +/- 5 degrees variation based on engineering judgment and review of plans relative to field studies. It is noted that the ultimate fragility curves are not conditioned upon storm duration or water depth, since preliminary sensitivity studies found the models to be relatively insensitive to these parameters. Given the significance of water velocity in affecting the scour depth, the fragility models developed in Section 5.2.3 of this chapter are conditioned upon water velocity. However, in the case study hurricane scenario events presented in Chapter 6, a uniform distribution of +/- 5-10% is adopted for water velocity, water depth and storm duration to account for potential model error associated with the hurricane simulations. An alternative

approach could be to fully decouple this hazard intensity variability and integrate the scour fragilities with random variables of water velocity.

Water, Storm and Soil Parameters					
			Distribution Parameters		
Variable	**Symbol**	**Distribution**	**1**	**2**	**Unit**
Water Depth	y_1	Uniform	$0.9* y_1$	$1.1* y_1$	m
Water Velocity	V_1	Uniform	$0.95* V_1$	$1.05* V_1$	m/s
Critical Water Velocity	V_c	Normal	Varies by soil type. See Table 5.3		m/s
Attack Angle of Water	θ	Uniform	θ- 5	θ+5	Degrees
Initial Erosion Rate	$\dot{z}_i$	Uniform	Varies by soil type. See Table 5.3		mm/hr
Soil Type		Deterministic	-	-	-
Duration(time)	t	Uniform	$0.95 *t$	$1.05*t$	hrs
Structural parameters					
Width	a	Deterministic	-	-	m
Pier Type	--	Deterministic	-	-	-
Length		Deterministic	-	-	m
Pier Spacing		Deterministic	-	-	m
Prediction models' error					
SRICOS Model Error	ε_1	Lognormal	$\kappa = 0$	$\zeta = 0.698$ for sand, 0.353 for clay	-

Table 5.1: Variables and Distributions with Uncertainties Accounted for in Probabilistic Pier Scour Model.

The critical water velocity, V_c, and initial erosion rate, $\dot{z}_i$, are dependent upon the soil type. In ideal cases the critical water velocity and initial erosion rate are obtained by collecting a site specific soil sample from each bridge and testing it in the erosion function apparatus (EFA). To obtain these parameters without requiring a soil sample from each bridge site, Briaud et al. (2009) presented "erodibility charts" for each soil type, based on 81 EFA tests, which give rough boundaries to the initial erosion rate and the mean and coefficient of variation (COV) of the critical water velocity. However, using the bounds for initial erosion rate and the given

mean and COV of critical water velocity introduces additional uncertainty to the analysis.

The hand-sketched bounds for initial erosion rate presented in the erodability charts by Briaud et al. (2009) are estimated as power laws (linear in the log-log space) herein, and the equations for the upper and lower bounds are shown in Table 5.3 below. The one exception of the form of the bound is the lower bound of soil type SP (see Table 5.2 below for definition) which fit a quadratic equation better. Therefore, the initial erosion rate used in this study is taken as a random value from a uniform distribution between the upper and lower bound, where the bound is a function of the water velocity, V_1. The critical water velocity, V_c, is represented by a normal distribution with mean and COV listed in Table 5.3 for each soil type (Briaud et al., 2009). It is noted that some assumptions are made when mapping from the erodability charts and critical water velocity estimates presented by Briaud et al. (2009) to the soil types in the case study region. For example, there are seven different soil types listed in the Houston/Galveston bridge database (given in Table 5.2 below); however, the erodibility charts only consider soil types CH, CL, SC and SP. Thus, the parameter estimates are extrapolated to other soil types in the region based on figures presented in Govindasamy et al. (2008) which plots EFA results for all soil types but does not include the hand-drawn initial erosion rate estimates. Based on a review of the few soil samples of CL-ML given in Govindasamy et al. (2008), CL-ML is assumed to have the same properties of CL for both V_c and $\dot{z}_i$. CH-CL, as a combination of fat and lean clays, is assumed to have a COV of V_c of 0.51, the mean of V_c equal to the average of the CH and CL means, an upper bound of $\dot{z}_i$

taken from CL and lower bound taken from CL. Finally, ML-SP is assumed to have the same parameters as SC.

Specific Soil Type
CH- Fat clays
CL- Lean Clays
CH-CL- Generic clay
CL-ML- Clay- Silt
ML-SP- Silty-Sand
SC- Sandy Clay
SP- Sand

Table 5.2: Definitions of Soil Types Found in the Houston/Galveston Region.

Soil Type	Normal Distribution for Critical Water Velocity (V_c)		Uniform Distribution for Initial Erosion Rate ($\dot{z}_i$)	
	μ_{V_c}(m/s)	COV_{V_c}	Lower Bound	Upper Bound
CH	0.73	0.51	$\dot{z}_i = 0.1128 * V_1^{2.8431}$	$\dot{z}_i = 9.8209 * V_1^{3.611}$
CL	0.51	0.52	$\dot{z}_i = 0.2262 * V_1^{3.4814}$	$\dot{z}_i = 31.687 * V_1^{4.636}$
CH-CL	0.62	0.51	$\dot{z}_i = 0.1128 * V_1^{2.8431}$	$\dot{z}_i = 31.687 * V_1^{4.636}$
CL-ML	0.51	0.52	$\dot{z}_i = 0.2262 * V_1^{3.4814}$	$\dot{z}_i = 31.687 * V_1^{4.636}$
ML-SP	0.63	0.45	$\dot{z}_i = 0.1042 * V_1^{3.0013}$	$\dot{z}_i = 44.03 * V_1^{5.0854}$
SC	0.63	0.45	$\dot{z}_i = 0.1042 * V_1^{3.0013}$	$\dot{z}_i = 44.03 * V_1^{5.0854}$
SP	0.17	0.24	$\dot{z}_i = 570948 * V_1^2 - 33.355 * V_1 + 5.0166$	$\dot{z}_i = 10267 * V_1^{4.527}$

Table 5.3: Assumptions on Critical Water Velocity Values and Bounds for Initial Erosion Rate (Briaud et al., 2009).

In addition to the uncertainty in the input parameters, the inherent bias in the SRICOS method, called SRICOS model error in Table 5.1, is taken into account based on the work of Bolduc et al. (2008). In this work, Bolduc et al. (2008)

compared the maximum scour depth obtained by the SRICOS method with the actual maximum scour depth observed at bridges in the field within three databases. Based on those databases, Bolduc et al. (2008) found that for bridges built in cohesive soils, the bias was roughly 0.955 with an error estimator that has a lognormal distribution. For bridges built in sand, the bias was 0.447 with the same error estimator. The following equations present the bias removal and introduction of error estimate for the scour prediction equations of clay and sand sites respectively:

$$y_{sm}(clay) = 0.955 * y_s * \varepsilon$$

$$y_{sm}(sand) = 0.447 * y_s * \varepsilon$$

Equation 5.8: Scour Depth Calculation with Bias Removal and Model Error Estimator (Bolduc et al., 2008).

where y_s is the maximum scour depth calculated by SRICOS, and ε is the error estimator with parameters given in Table 5.1.

5.2.2. Capacity Limit States for Fragility Analysis

With the methodology presented above, the probabilistic scour depth at a pier can be established given a scenario event or conditioned upon a hazard parameter such as water velocity. However, to support decision making, these probabilistic estimates of scour depth are compared to capacity limits at which TxDOT would usually repair or rebuild a bridge for pier scour. For this analysis, based on guidance from the geotechnical division of TxDOT (Delphia, 2011), the limit state for repair is

taken as $^1/_8$ of the embedded pile depth as given by TxDOT inspection files and as-builts, or 2.75 ft if no pile depth is available. These numbers are based on the maximum allowable scour for a pile being half of the embedment depth (total pile length minus height from ground to bridge), and that TxDOT districts usually install countermeasures at about $^1/_4$ of the maximum allowable depth. For failure (meaning TxDOT would close the bridge to repair/replace it), the limit state is taken as $^1/_4$ of the pile depth based similar arguments above except that many districts would begin to close bridges with half or more of the maximum allowable scour depth in order to replace them (Delphia, 2011). When pile depth is not given, 5.5 ft is taken as the critical scour depth based on a generic 22 ft pile embedment length. This approach to limit state analysis is rooted in the identification of prescriptive capacity limits beyond which repair or closure of the bridge is anticipated.

5.2.3. Fragility Analysis of Piers in the Houston/Galveston Bay Area

Prior to conducting the regional case study analysis for various hurricane scenario events, fragility curves for all the bridges in the Houston/Galveston bay area were developed. These fragility curves state the probability of limit state exceedance given water velocity. Similar to the storm surge fragility modeling, Monte Carlo simulation is conducted with 7000 samples, using Latin hypercube sampling, of the random variables in Table 5.1 to compare realizations of the scour depth to the prescriptive limit states. From the point estimates of failure probability a fragility function is derived from regression analysis based on the least squares method. The results show that following a region of nearly zero failure probability, an

exponential regression model provides a good fit to the fragility point estimates for about half of the bridges in the inventory. In some cases a quadratic or a power regression provided a better description of the fragility for the few bridges that did not fit an exponential regression. The parameters of fragility curves for all bridges can be found in Appendix C. All of the regressions given in Appendix C have an R^2 over 0.81 with most coefficients of determinations over 0.97.

Two example fragility curves are shown below for exceedance of the pier scour limit state (Figures 5.4 and 5.5). For most of the bridges, a discernible failure probability (limit state exceedance) does not occur until the water velocity is over 1 m/s. Figures 5.4 and 5.5 show the points point estimates of failure probability for pier scour of bridges 10 and 122 respectively, with the associated fragility curve fitted to them. These two bridges were chosen to show the difference in fragility curves for bridges in sandy soils (Bridge 10) and in clay soils (Bridge 122). Note that the failure probability becomes non-negligible at different water velocities depending on the soil type (about .7 m/s for Bridge 10 and 1.5 m/s for Bridge 122), and that the two fragility curves have different shapes.

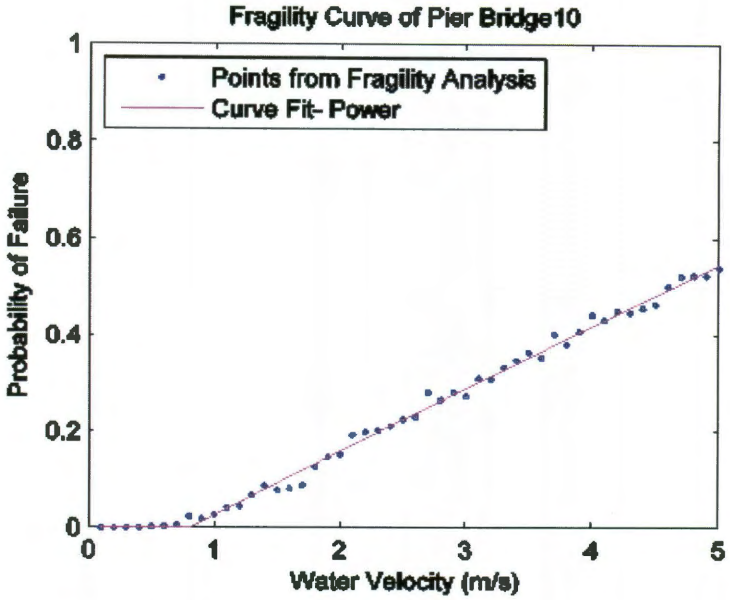

Figure 5.4: Fragility Curve Fitting for a Bridge Pier in Sandy Soil.

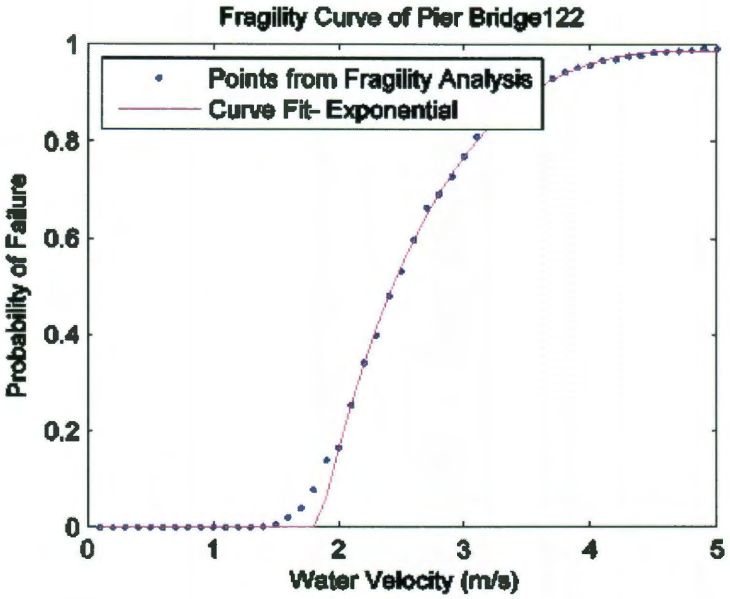

Figure 5.5: Fragility Curve Fitting for a Bridge Pier in Clay Soil.

The median value, or water velocity associated with 50% probability of limit state exceedance is 4.64 m/s for Bridge 10 and 2.43 m/s for Bridge 122. This

statistic does provide some insight on the fragility, indicating that while the bridge in clay soil requires a higher velocity to initiate scour, once scour is initiated the probability of limit state exceedance increases quickly when compared to the bridge in sandy soil. However, extreme values are often of interest in structural safety and risk analyses. The fragility curves reveal that the 5th percentile and the 95th percentile for the bridge in sandy soil (Bridge 10) are 1.17 m/s and greater than 5 m/s respectively. In comparison, they are 1.89 m/s and 3.87 m/s for the bridge in clay soil (Bridge 122). These fragility curves are predicated on the water velocity varying from 0 m/s to 5m/s and therefore any water velocity outside of this range (unlikely to occur in a hurricane event) cannot be predicted through extrapolation. The increased range between the 5th and 95th percentiles in the bridge in sandy soil highlights the increased uncertainty in the scour performance assessment of Bridge 10.

To further investigate the sensitivity of scour depth estimates, and hence introduction of variability in fragility analyses, tornado plots were created for each of the bridges, see Figures 5.6 and 5.7 below, to determine the greatest source of uncertainty in the scour estimates. The seven random variables previously presented in Table 5.1 were considered at their extreme (5th and 95th percentile values for normal and lognormal distributions, lowest and highest values for uniform distributions) and median values. For the analysis of scour depth sensitivity, one factor at a time is changes to its upper or lower level while the other variables are held at their median values.

The tornado plots reveal the relative importance of different sources of uncertainty, indicating the variation in pier scour depth estimates due to a range of potential parameter realizations relative to the median value case. To be consistent with the fragility analysis, the tornado plots were evaluated at the set water depth and storm duration for which the fragility analysis was conducted, and across a range of water velocities to determine if variation in the assumed velocity changes the relative importance of the variables. The values in the tornado plots do vary with smaller water velocities but converge after 1 m/s; thus, only one tornado plot is shown for each bridge taken at velocity 5 m/s. For the case studies presented, the scour depth estimate when all variables are at their mean value is 14.43 ft for Bridge 10 and 11.48 ft for Bridge 122.

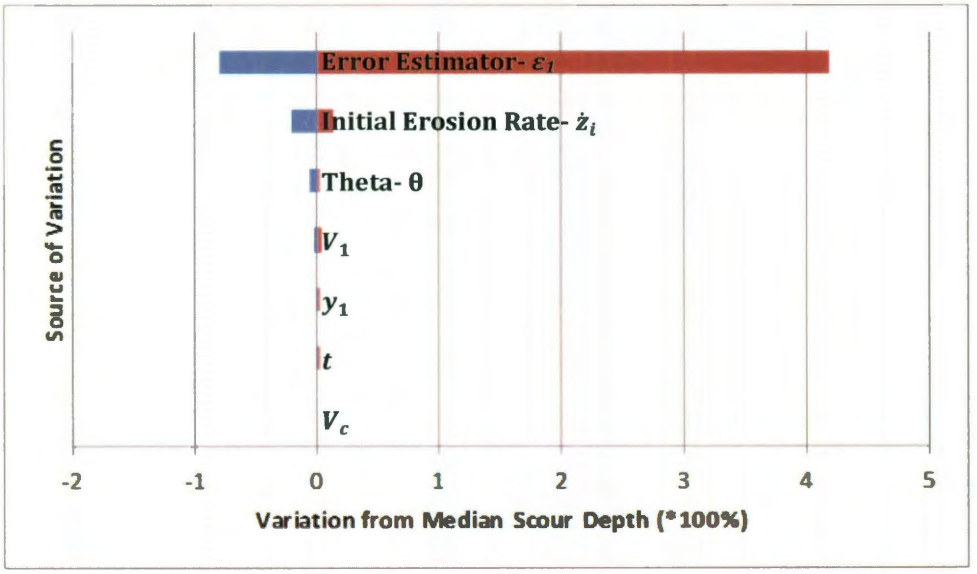

Figure 5.6: Tornado Plot of Sources of Uncertainty in Bridge 10.

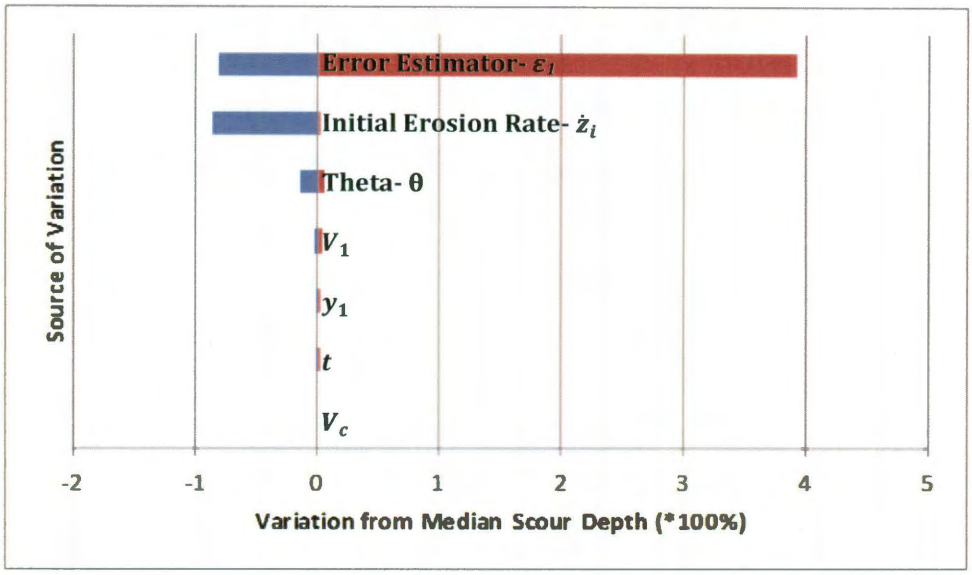

Figure 5.7: Tornado Plot of Sources of Uncertainty in Bridge 122.

Based on the tornado plots, the error estimator from the bias removal term provided the largest source of uncertainty in all the bridges when the water velocity exceeded that which would initiate scour. Before that water velocity (0.7 m/s and 1.5 m/s for Bridges 10 and 122 respectively), the initial erosion rate provided the most uncertainty about the scour depth estimate, but did not contribute enough uncertainty to cause the probability of limit state exceedance to change. At higher water velocities, all other variables (including initial erosion rate) added much less variation to the pier scour estimate than the error estimator. One explanation for this may be due to the fact that the original scour model is based on coefficients and a small change in the input variables does not change the coefficient used due to the categorical nature of the analysis. Also, while the duration (time) and initial erosion rate are not tempered by the coefficients, they are not directly proportional to the

scour depth. However, the error estimator affects the scour depth directly and has the widest range, due to its lognormal distribution.

From Figures 5.6 and 5.7 above, the error estimator accounted for the most variability in both bridges, although the magnitude of variation in scour depth (both absolute and with respect to the median value estimate) is larger for the bridge in sandy soil due to the uncertainty in the input parameters. This helps explain the fundamental difference in the fragility functions presented in Figures 5.4 and 5.5 which reveal a signature of larger uncertainty modeled by the fragility of Bridge 10 than of Bridge 122. Furthermore, these results indicate that reducing uncertainty in the bias removal error estimator can improve future fragility models of bridge pier scour and improve accuracy in subsequent risk assessments.

5.3. Probabilistic Abutment Scour Modeling

While pier scour is the most common outside of extreme coastal events and leads to the failure of many bridges every year, it is not a major contributor to failure during hurricane events based on studies of damages from previous hurricanes (Froehlich and Fisher, 2000). During hurricanes, it has been seen that abutment scour is a more common occurrence and leads to more drastic failures than pier scour alone (DesRoches, 2006). However, as noted in the literature review, there is very little consensus on how abutment scour is to be modeled (Chiew, 2008). Thus, to be consistent across the scour analysis and as it holds the most feasibility for a regional study, the simplified SRICOS method is also applied to abutment scour. Abutment

scour occurs when the soil at the toe of the bridge abutment erodes, which can lead to the collapse of the abutment and the bridge structure. Figure 5.8 below shows how the flows around the abutment can lead to scour hole formation.

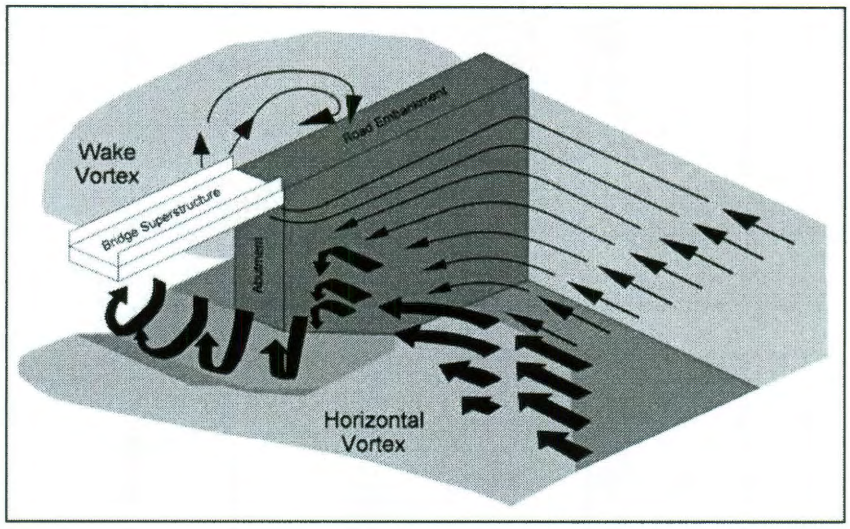

Figure 5.8: Schematic of Abutment Scour Vortexes (Ayres, 2004).

Since the SRICOS method is used for abutment as well as pier scour, many of the equations and inputs are similar; thus, the uncertainties for the shared inputs will remain the same as previously reported in Sections 5.2.1. The maximum abutment scour depth is estimated via an empirically driven equation in the SRICOS method presented by Briaud and Oh (2010) as:

$$y_s = y_{fl} * K_1 * K_2 * K_L * K_G * K_P * 243 * Re_{f2}^{-.28} * \left(1.65 * Fr_{f2} - Fr_{fc}\right)$$

Equation 5.9: Maximum Abutment Scour Equation from Briaud and Oh (2010).

where y_s is the maximum scour depth, y_{fl} is the floodplain water depth (which for this study is the same as approach water depth, y_1), K_1 is the correction factor for the shape of the abutment, K_2 is the correction factor for the angle the abutment makes

with the flow of water, K_L is the factor that corrects for the setback of the abutment from the water, K_G is the correction factor for the channel type, K_P is the correction factor for the pressure flow, $Re_{f2}$is the Reynold's number of the water flow, and $Fr_{f2}$and Fr_{fc} are the Froude numbers for the flow based on approach water velocity and critical water velocity respectively. The equations for all of the factors, the Reynolds number and the Froude numbers are as follows. The abutment shape factor is given as:

$$K_1 = \begin{cases} 1.22, & for\ VW \\ 1.0, & for\ WW \\ 0.73, & for\ ST \end{cases}$$

Equation 5.10: Correction Factor for Abutment Shape (Briaud and Oh, 2010).

where *VW* is a vertical wall abutment type, *WW* is a wing wall abutment, and *ST* is a sloping spill through. The term vertical wall for abutments is self-explanatory; the abutment consists of a vertical wall that meets the water. A wing wall abutment is usually accompanied by a vertical wall at the bridge-water interface but has a "wing" of material (usually concrete) attached to it, either parallel, perpendicular or at an angle to the wall. A sloping spill through is somewhat the opposite of a wing wall; the spill through has concrete sloping from the approach embankment to the water's edge. Figure 5.9 presents an illustration of each abutment type:

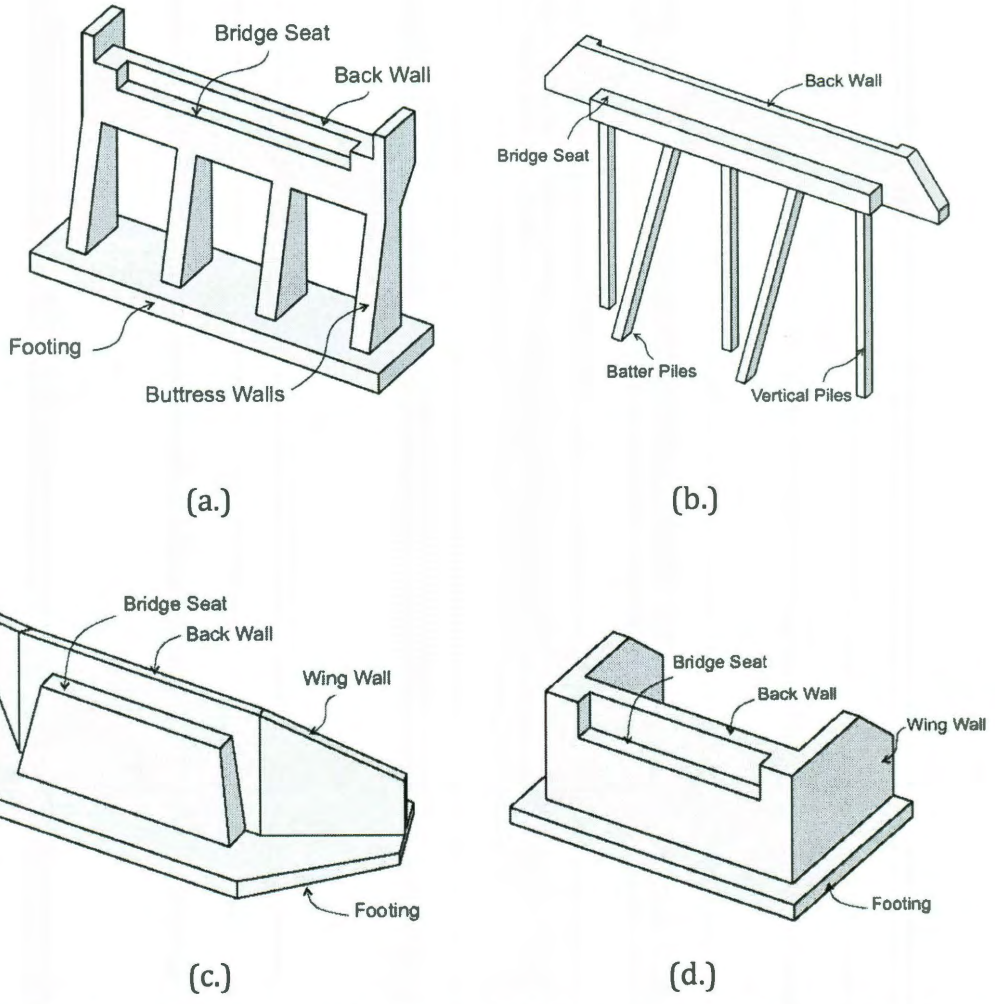

Figure 5.9: Examples of Abutment Types (a.) Sloping Spill Through; (b.) Vertical Wall; (c.) Wing Wall with Angled Wings; and (d.) Wing Wall with Perpendicular Wings (Nielson, 2005).

The abutment angle factor, K_2, takes into account the angle that the abutment makes with the flow of water, which can increase or decrease erosion rates. For this study, where the data was not available for the abutment angle, the attack angle of the piers was used. The corrections for K_2 are given as:

$$K_2 = \begin{cases} 1 - .0005 * |\theta - 90°|, & for\ 60° \leq\ \theta \leq 120 \\ 0.85, & otherwise \end{cases}$$

Equation 5.11: Correction Factor for Abutment Angle, K_2 (Briaud and Oh, 2010).

where θ here is the abutment angle. K_L is defined as:

$$K_L = \begin{cases} -0.37 * \left(\frac{L_f - L}{y_1}\right), & for \left(\frac{L_f - L}{y_1}\right) < 1.5 \\ 1.0, & otherwise \end{cases}$$

Equation 5.12: Correction Factor for Abutment Setback from Water (Briaud and Oh, 2010).

where $\frac{L_f - L}{y_1}$ is the relative setback of the abutment from the water; L_f is the length from the water's edge to the end of the abutment, and L is the length of the abutment. For this study, when the setback amount is not known, a generic setback is given based on as-built estimations. K_G, the correction factor for the channel type is defined as:

$$K_G = \begin{cases} 1.0, & for\ compound\ channel \\ 0.42, & for\ rectangular\ channel \end{cases}$$

Equation 5.13: Correction Factor for Channel Type (Briaud and Oh, 2010).

Most of the channels are compound, natural channels; however there are some concrete-lined rectangular channels which greatly reduce the susceptibility to scour. K_P is the factor for the flow pressure and is given as follows:

$$K_P = \begin{cases} 2.75 * \frac{d_1}{h} + 1, & for\ \frac{d_1}{h} < .33 \\ 1.83 * \left(\frac{d_1}{h}\right)^2 - 3.76 * \frac{d_1}{h} + 2.97, & for\ .33 \leq \frac{d_1}{h} \leq 1.0 \\ 1.0, & for\ \frac{d_1}{h} > 1.0 \end{cases}$$

Equation 5.14: Correction Factor for Flow Pressure (Briaud and Oh, 2010).

where d_1 is the distance between the water surface and the low chord of the bridge and h is the distance from the bridge deck to the toe of the abutment. The Reynolds number for the stream or channel is based on the density, velocity, viscosity and depth of the water. The equation is given below:

$$Re_{f2} = \frac{\rho * y_1 * V_1}{\mu}$$

Equation 5.15: Reynold's Number Equation for Channel (Briaud and Oh, 2010).

where ρ is the density of water, V_{f2} is the velocity of the water, and μ is the viscosity of the water. The last parameters of equation 5.9 are the Froude numbers which are defined as follows:

$$Fr_{f2} = \frac{V_1}{\sqrt{g * y_1}}$$

$$Fr_{fc} = \frac{V_c}{\sqrt{g * y_1}}$$

Equation 5.16: Froude Numbers for Assumed Velocity, V_1, and Critical Velocity, V_c (Briaud and Oh, 2010).

where V_{fc} is the critical water velocity defined above in the simplified SRICOS method, y_1 is the approach water depth, and g is the gravitational constant (9.81 m/s). From Equations 5.9-5.16, the final scour depth at abutments can be determined with the hyperbolic function (Equation 5.7) presented in Section 5.2. The duration of the storm and the initial erosion rate of the soil are both determined in the same way as in the pier scour analysis. With the equations all defined, the

uncertainties for the input parameters must be taken into account once more, as with the pier scour.

5.3.1. Uncertainties in the Input Parameters

While most of the input uncertainties remain the same as presented in the probabilistic pier scour (i.e. random variables for all of the hydraulic parameters for water depth and velocities as these remain consistent throughout the scour analysis, see Table 5.1), some additional parameters have to be taken into account for abutment scour. For example, since the abutment scour model requires the calculation of the Reynolds number at the abutment (the pier scour model does not), the uncertainty in the density and viscosity of water must be accounted for. For this project, the distribution for the density of water ρ is taken as uniform and varying between 1000 kg/m^3 and 1025 kg/m^3 to account for the uncertainty in the saline content of the water as sea water from the surge mixed with the fresh water. Currently, the density of fresh or sea water can be taken as a constant; however, there have been no studies on the distribution of saline content as the two types of water mix as they do during hurricanes. Also, while the viscosity of water at a certain temperature is constant, this study adopts a +/-5% uniform distribution around the viscosity of water at 80° Fahrenheit to account for changes in the temperature of the water (Kestin et al., 1978). Additionally, the abutment setback, $(L_f - L)$ and the height above water, d_1, are both given a uniform distribution with 10% and 5% uncertainty respectively, based on engineering judgment and comparison of plans to field data. All of the additional parameters for abutment

scour (not previously defined for pier scour) and their probability distributions are given in Table 5.4 below.

Water and Soil Parameters					
			Distribution Parameters		
Variable	Symbol	Distribution	1	2	Unit
Water Density	ρ	Uniform	1000	1025	Kg/m^3
Water Viscosity	μ	Uniform	0.9* μ	1.1* μ	kg/m*s
Structural parameters					
Distance between water and bridge	d_1	Uniform	0.95* d_1	1.05* d_1	m
Distance between abutment and bridge	h	Uniform	0.95* h	1.05* h	m
Abutment Setback	$(L_f - L)$	Uniform	0.9* $(L_f - L)$	1.1* $(L_f - L)$	m

Table 5.4: Variables and Distributions with Uncertainties Accounted for in Probabilistic Abutment Scour Model.

As none of the abutment scour models have been fully validated with field evidence, neither has the SRICOS method for abutment scour been analyzed for the inherent bias in the method. Because of this, the inherent bias is not removed for this study and the abutment scour depth obtained from this method is considered conservative. This limitation provides a key area of future research need, requiring field data and statistical analysis of bias and model error.

5.3.2. Capacity Limit States for Abutment Fragility Analysis

As with pier scour, capacity limit states must be determined in order to predict the probability of failure or repair of the abutments. The Connecticut Department of Transportation (ConnDOT), in giving guidance to acceptable scour depths, says that the scour depth for an abutment on a spread footing should not exceed the embedment depth of the footing and for abutments on pile foundations, the piles must still be stable without any express guidance as to an appropriate scour depth

(DOT, 2000). Since all of the bridges in this study area are considered to have pile foundations, the piles dominate the scour depth considerations here as they did for pier scour. However, for most of the bridges, the pile depth under the abutments is unknown and thus a set, prescriptive limit state must be assumed. Also, because damage from abutment scour can occur more easily at lower scour depths than damage from pier scour, the limit state should be less than that for pier scour.

To that end, the limit states are set at 1.4 ft of scour for repair and 2.75 ft for complete failure, corresponding to half the assumed values for piers and in conjunction with reasonable estimates of when TxDOT would take actions against scour (Delphia, 2011). This consists only of scour at the toe of the abutment and not the scour of the embankment which can cause failure with even smaller scour depths. With these limit states, the probability of exceeding these limit states, leading to the repair or failure of the bridge abutments for a given hurricane event or a range of water velocities can be established. As with pier scour, these abutment limit states are prescriptive limits upon which bridge owners anticipate repair actions or closure of the bridge.

5.3.3. Fragility Analysis of Abutments in the Houston/Galveston Bay Area

Fragility curves for abutment scour were also calculated for all of the bridges in the abutment subset of the Houston/Galveston bay area. The same strategy for probabilistic analysis, sampling and regression analysis is conducted for the abutment fragility analysis as described for the pier scour fragility in Section 5.2.3. From these curves, it seems that the failure probability (limit state exceedance) is

reached quickly over water velocities of 0.75-1 m/s depending on the bridge. The abutment fragility curves show much less uncertainty about the median values when compared to pier scour, possibly due to lower limit states, and to the lack of bias removal and error estimator used in pier scour. It is noted that this model error was a primary source of uncertainty in the pier scour analysis, but estimates of model error for abutment scour are lacking to date.

Two fragility curves for abutment scour are given in Figure 5.10 and 5.11 below for the same bridges as considered in the pier fragility analysis in Section 5.2.3. The abutment regressions were fitted in the same way as the piers, with the exponential regression used for most, and all of the regressions have an R^2 over 0.98. The prarameters for these regressions can be found in Appendix D.

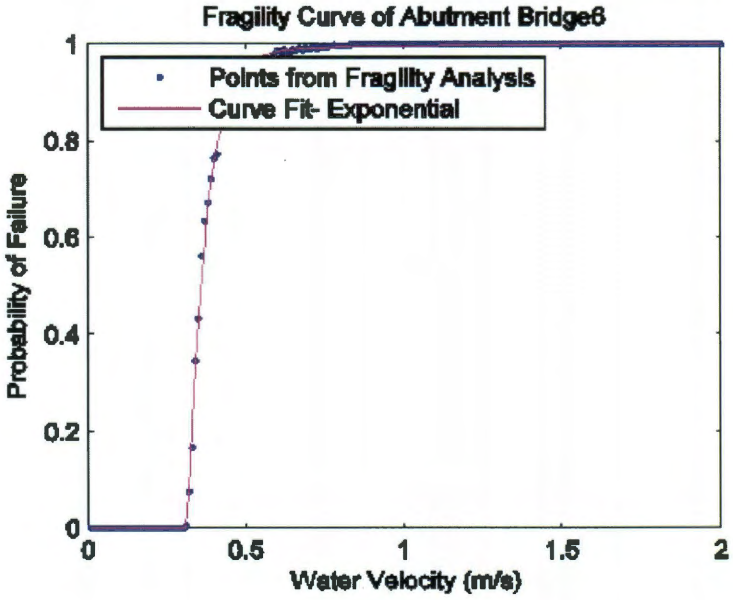

Figure 5.10: Fragility Curve Fitting for a Bridge Abutment in Sandy Soil.

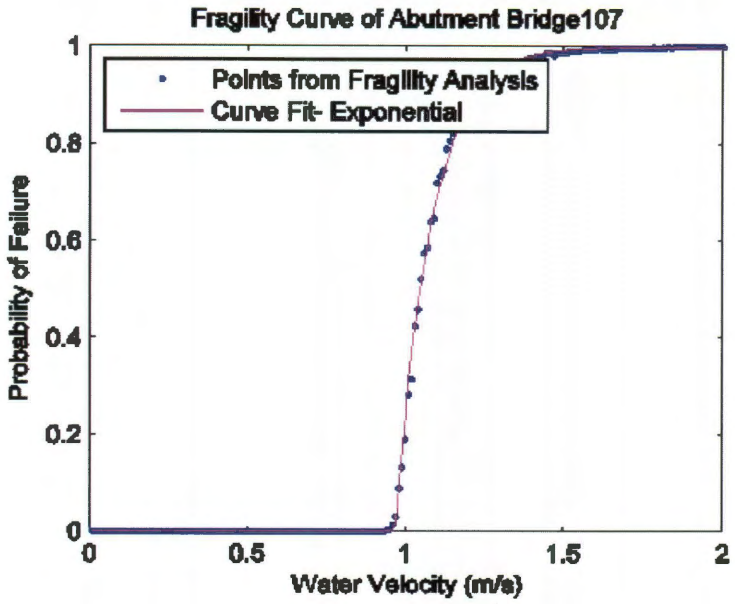

Figure 5.11: Fragility Curve Fitting for a Bridge Abutment in Clay Soil.

As with the pier scour fragility curves, the failure probability is negligible until about .3 m/s for Bridge 6 (Bridge 10 for pier), and about .95 m/s for Bridge 107 (Bridge 122 for pier). Unlike the pier fragility curves, the abutment fragility curves exhibited the same regression form regardless of soil type. The median value and 5th and 95th percentile values are 0.36 m/s, 0.32 m/s, 0.50 m/s for Bridge 6 and 1.05 m/s, 0.97 m/s, and 1.3 m/s for Bridge 107. These three values indicate both that the bridge in sandy soil is more vulnerable to abutment scour than the bridge in clay soil, as anticipated, and that there is less uncertainty about the abutment scour estimates when compared to pier scour, as noted above.

5.4. Qualitative Approach to Embankment Scour

Embankment scour is somewhat difficult to define as various authorities have used it to mean different things over the years. In the scope of this work, however, embankment scour will mean any scour that occurs behind the abutment (i.e. beneath a sloping spill through or behind a vertical wall) or under the roadways to undermine the approach span support. Several examples are given in Figure 5.12 below to give a better idea of what embankment scour can include.

(a.)

(b.)

(c.)

Figure 5.12: Examples of Embankment Scour (a.) and (b.) behind Abutments and under Approach Spans; and (c.) under Roadways (DesRoches, 2006).

With this definition, embankment scour encompasses the widest range of scour possibilities and also has been the most documented form of scour seen in hurricane events (DesRoches, 2006). Despite being the most documented form of scour in Hurricane Katrina, no previous models determine risk from embankment scour let alone a scour depth for a given storm. With this in mind, this research develops new risk levels for bridges based on the water velocity of a given storm and the soil composition at the embankment. Rather than conduct a fully quantitative probabilistic analysis of embankment scour, this study adopts a simplified qualitative approach to provide indicators of risk due to embankment scour. Future work can address this open area of study and produce quantitative models for abutment scour.

5.4.1. Qualitative Risk Levels for Embankment Scour Assessment

Four risk levels were determined based on informal solicitation of experienced geotechnical engineers, principles of soil mechanics and empirical evidence from past hurricanes (Briaud, 2011, Briaud et al., 2001). First, a bridge can have a "very low" risk level for embankment scour if the bridge is not inundated and the average storm water velocity is less than the critical water velocity. The reasoning for this comes from past experience that if the storm surge does not reach the roadway level, then embankment scour is unlikely to occur (Briaud, 2011). Inundation here is determined by taking the elevation of the roadway and comparing it to the surge height. If the bridge is not inundated and $V_a < V_c$, it is given a risk level of "0."

The rest of the bridges that are inundated fall into three additional categories: low, medium, and high risk. These risk levels are determined based on the critical water velocity of the soil the bridge is on and the velocity of the storm surge. A risk level of "1" is given when the bridge is inundated but the maximum water velocity is less than the critical velocity, or when the bridge is not inundated but the average velocity is greater than the critical velocity (meaning that erosion could initiate). A risk level of "2" is assumed if the bridge is inundated, the maximum water velocity is greater than the critical velocity, but the average velocity is less than the critical velocity. Finally, a risk level of "3" is given if the bridge is inundated and the average velocity is greater than the critical velocity. This is shown in the following equations:

$$Risk\ Level\ 0(very\ low) = \begin{cases} not\ inundated \\ V_a < V_c \end{cases}$$

$$Risk\ Level\ 1(low) = \begin{cases} not\ inundated \\ V_a > V_c \end{cases} \ or \ \begin{cases} inundated \\ V_{max} < V_c \end{cases}$$

$$Risk\ Level\ 2(medium) = \begin{cases} inundated \\ V_{max} > V_c \\ V_a < V_c \end{cases}$$

$$Risk\ Level\ 3(high) = \begin{cases} inundated \\ V_a > V_c \end{cases}$$

Equation 5.17: Embankment Scour Risk Levels.

The same uncertainties in the inputs used in pier and abutment scour are used in embankment scour for the critical water velocity and the storm water velocity. Because of this, a bridge could be given different risk levels based on the

varying inputs. To account for this and provide a cogent risk assessment for embankment scour, average, or expected value, risk level most of the simulations belong to will be the risk level assigned to the bridge.

With all of the models now described, the next step in this research is to apply those models to the Houston/Galveston bay area and assess the risk from various hurricane events, as will be presented in the next chapter.

Chapter 6

Case Study of the Houston/Galveston Bay Area Bridge System

Once all the fragility models described in the previous two chapters were developed, a case study of the Houston/Galveston Bay Area was conducted. This assessment was conducted for various hurricane scenario events ranging in intensity and landing position. This chapter presents the case study scenarios and applications of surge and scour fragility models for risk assessment of the bridge infrastructure.

6.1. Case Study Methodology

6.1.1. Definition of the Houston/Galveston Bay Area

The Houston/Galveston Bay Area was first defined in Chapter 2 as the entirety of Galveston Island and Bolivar Peninsula as well as everything within a one-mile radius of the Houston Ship Channel and the various bays. Thus, all the bridges

analyzed in the case study (155 bridges) are in the Houston/Galveston bay area and were considered to be in the potential region affected by coastal surge. Figure 6.1 presents the overall Houston/Galveston bay area and shows the spatial distribution for the height above water of each bridge.

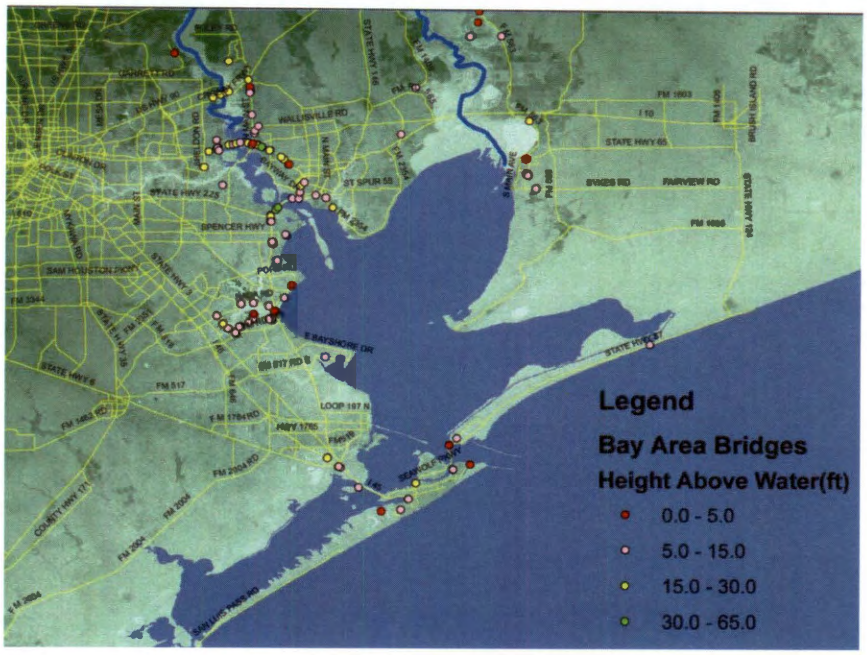

Figure 6.1: Map of the Houston/Galveston Bay Area with Bridges Characterized by Height above Water

6.1.2. Definitions of Scenario Events

In order to understand the vulnerability of the Houston/Galveston bridge network to a variety of possible hurricane events, three scenarios were chosen as potential events along the Texas coastline from a suite of events analyzed by the Computational Hydraulics Group at UT-Austin as part of the SSPEED Center project to understand the lessons of Hurricane Ike and help prepare the Houston/Galveston area better prepare for future hurricane events (CHG 2010; Bedient, Blackburn, and

Sebastian 2011). The first event, Hurricane Ike, is simply a hind cast model of Hurricane Ike that landed in September 2008. This scenario is used as a baseline reference for the damage seen and as a validation or sanity-check of the values obtained in the fragility models. The remaining two scenarios consider a hurricane with 30% stronger wind speeds hitting the Houston coastline. One, called "Ike + 30%" has the same trajectory and landing position as the original Ike, but with the 30% stronger winds. The other scenario, called "Super Ike", has the 30% stronger wind speeds and a more southern landing position that would impact both Houston and Galveston more directly. Super Ike was the strongest of the scenarios run by the CHG and is considered a worst-case scenario for the Houston area. Figure 6.2 shows the two landing positions considered in this study for the various scenarios.

Figure 6.2: Map of Houston/Galveston Bay Area Denoting Hurricane Scenario Landing Points

6.2. Results of Case Study Analysis

In order to obtain a better understanding of the bridge network immediately after a storm event, several vulnerability models were used to determine the risk to the study bridges. In the sections following, short term damage or inaccessibility is modeled using inundation maps. Such inundation maps represent the current state of the art in risk mapping, although some studies just limit the identification of "high risk" bridges to those in the surge zone without considering deck elevation. This case study extends the analysis to more holistic risk analysis considering uncertainty in long-term damage such as structural damage and erosion, which is studies through the bridge deck uplift and scour models presented in Chapters 4 and 5. After considering each failure mode individually, pier and abutment scour are combined together to form local scour risk, and both the local scour and uplift are combined in an overall risk map which presents the highest likelihood of damage and the failure mode that would cause it.

Overall risk maps are presented for each of the three scenario events, while the individual vulnerability maps are only presented for the "Super Ike" scenario here; the full list of vulnerability maps are available in Appendix E.

6.2.1. Bridge Inundation Results

Currently for hurricane risk assessment, inundation maps are used to determine which bridges are vulnerable. However, inundation, which refers to whether or not a bridge is likely to be submerged in water at any time during the hurricane, does

not yield an understanding of the structural damage a bridge will face; instead, it gives an idea of the impassibility of a bridge immediately following the storm. Additionally, these inundation maps rarely use the actual elevation of the bridge and instead just look at the surge levels; if a bridge is in the surge zone, it is considered at a high risk.

Despite the seeming drawbacks of current inundation maps, accurate inundation maps, which compare the elevation of the bridge deck with the likely surge at that point, can yield great insight into the state of the bridge system after a hurricane in terms of easy accessibility. As such, it is the first step in the case study of the Houston/Galveston bay area, both to compare with older surge zone based inundation maps and to compare with the bridge deck uplift model which shows long-term structural damage.

Inundation maps were developed for each of the three hurricane scenarios based on the data obtained from the CHG at UT-Austin, as well as LiDAR elevation data and bi-annual inspections. From this, it was seen that not all the bridges in the surge zone are at risk of inundation due to the high clearance of some bridges. However, in the "Super Ike" event, over half the bridges were considered inundated at some point during the simulation and thus, there could be issues using some of those bridges as re-entry routes.

While inundation is a good first pass of risk assessment, it does not give enough information as to whether or not a bridge will fail merely because it was submerged.

Figure 6.3 below shows the distribution of the inundated bridges during the "Super Ike" scenario. From Figure 6.3, it is evident that during the "Super Ike" scenario all the bridges on Galveston Island and Bolivar Peninsula would be inundated at some point. Additionally, Table 6.1 shows that 46 out of the 107 bridges with surge were inundated in the Ike scenario, while 76 out of 115 were in the "Ike + 30" scenario and 93 out of 126 were in the "Super Ike" scenario. These results show that being in the surge zone does not imply inundation for a bridge deck. In order to have a better understanding of the short-term impassability of a bridge, inundation maps must take into account the elevation of the bridge deck. However, even with the elevation of the bridge decks taken into account, inundation maps do not provide a measure of the vulnerability of a bridge to long-term structural damage.

Hurricane Scenario Event	Number of Bridges		
	Inundated	Not Inundated	In "Surge Zone"
Ike	46	109	107
Ike + 30%	76	79	115
Super Ike	93	62	126

Table 6.1: Number of Bridge Inundated, Not Inundated and in the Surge Zone for Each of the Three Scenario Events

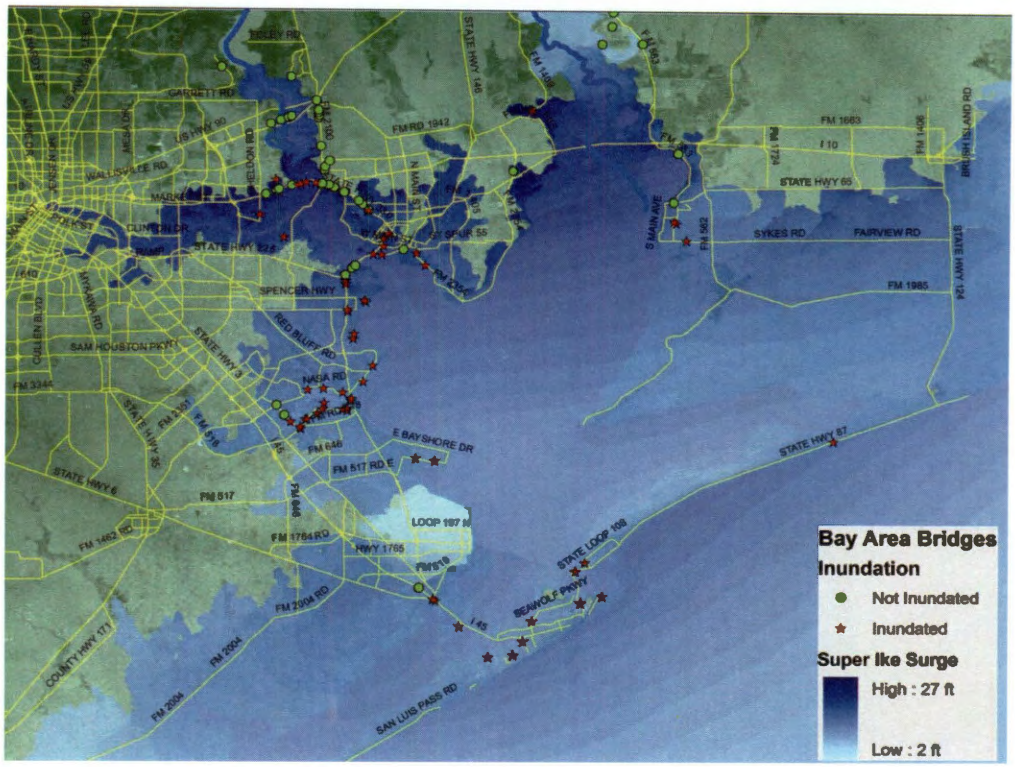

Figure 6.3: Map of Inundated Bridges in the "Super Ike" Scenario.

6.2.2. Bridge Deck Uplift Results

The bridge deck uplift fragility surfaces described in Chapter 4 are applied to the case study bridges to determine a quantitative assessment of the risks of structural damage for three scenarios. This model compares the actual capacity of the bridge to resist vertical surge and wave forces with the maximum surge and wave forces experienced during a scenario event. The results of the uplift model were first compared with the Ike scenario as a sanity check to determine if the results were valid and the model working. While a full validation cannot be conducted with such a limited data set, the Ike scenario shows great consistency with the actual damages

seen during Hurricane Ike in 2008 and lends greater confidence to the results of the other two scenarios.

Table 6.2 below gives the number of bridges in each range of failure probability for each scenario. As mentioned earlier, only 136 bridges were used in this specific vulnerability model. The risk ranges are as follows: very low (0-5% Failure Probability), low (5-25% Failure Probability), medium (25-75% Failure Probability) and high (75-100% Failure Probability).

Hurricane Scenario Event	Failure Probability (%)			
	0 – 5	5 - 25	25 - 75	75 - 100
Ike	127	5	1	3
Ike with 30% Stronger Wind Speeds	106	4	7	19
"Super Ike"	69	7	8	52

Table 6.2: Number of Bridges in Each Failure Category for Each Hurricane Scenario Event from Bridge Deck Uplift.

From Table 6.2, it is evident that the Houston/Galveston bay area bridge network can withstand a hurricane of Ike's magnitude without much damage, but with a stronger and more direct storm, over one third of the bridges have a high likelihood of failure. Bridges that had a high probability of failure in these scenarios tend to have low clearance over mean sea level (see Table 6.3) and little or no connectivity between the substructure and superstructure of the bridge. This was also seen in the empirical evidence from Hurricane Katrina (Padgett, Spiller, and Arnold 2009). Figure 6.4 shows the spatial distribution of damage from the Super Ike scenario; seen in the figure, all the bridges on Bolivar Peninsula and about half on Galveston Island have a high failure probability. Additionally, several bridges in

the Clear Lake region and across the Houston Ship Channel exhibit a high failure probability.

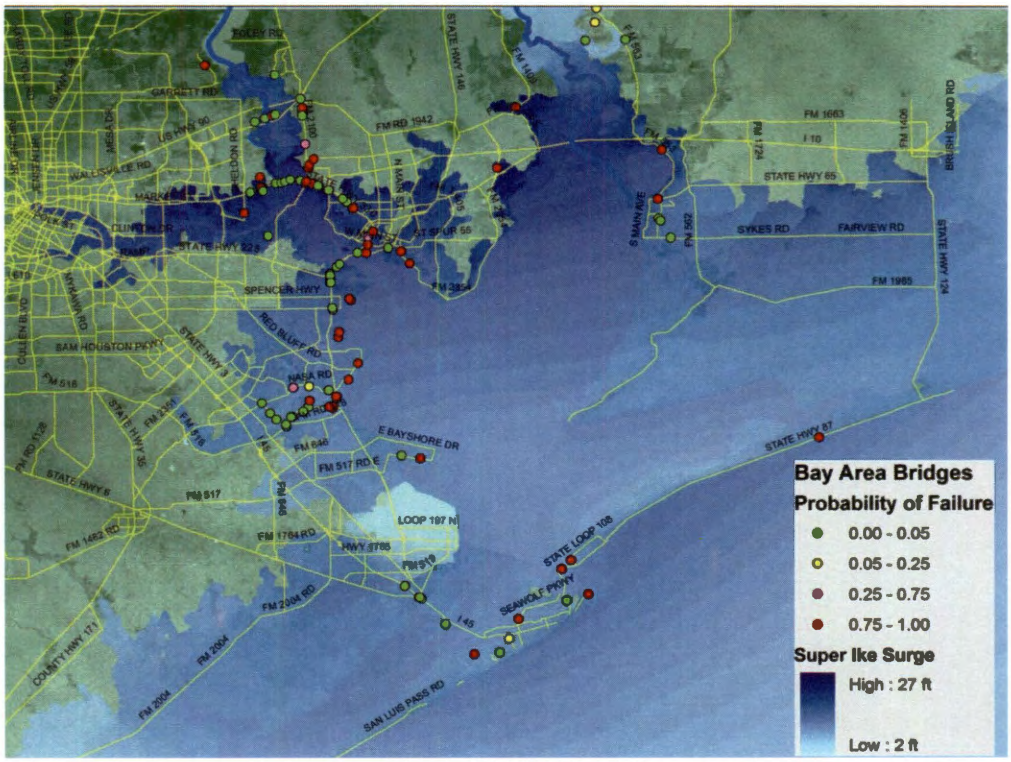

Figure 6.4: Map of Bridge Deck Uplift Failure Probabilities in the "Super Ike" Scenario.

Failure Probability (%)	Height from Low Chord of Bridge to Water (ft)			
	0 – 5	5 - 10	10 - 20	20 - 30
0 – 5	8	23	32	6
5 - 25	2	4	1	0
25 - 75	1	4	3	0
75 - 100	24	17	10	1

Table 6.3: Number of Bridges in Each Failure Probability by Height above Water in the "Super Ike" Scenario.

As an illustration of the distribution of bridges in the "Super Ike" scenario in particular, Table6.3 above gives the number of bridges that have a particular failure

probability range and height above water. This height above water is the difference between the water level and the low chord of the lowest elevation span because the bridge failure probability is predominated by the highest vulnerability span. Evident in the table is the conclusions above in that most of the bridges in the "high" failure probability range are less than 10 ft above mean water level, while more than half the bridges in the "very low" failure probability range are greater than 10 ft above mean sea level. The surge for the Super Ike scenario ranges from 11 ft to 27 ft at the bridge locations.

6.2.3. Comparison of Bridge Deck Uplift and Inundation Results for Structural Damage

To compare the current state of the art in transportation risk assessment with the new probabilistic methods for bridge deck uplift; a simple comparison of the inundation maps to the failure probability map of unseating is conducted. From a direct comparison of the number of bridges inundated verses "high" failure probability, it appears that the inundation maps overestimate the true damage state of the system after a hurricane. In the Super Ike scenario, for example, 93 bridges were considered inundated and only 62 bridges had a high failure probability. However, a closer look at each of the bridges, shown in Figure 6.5 below, reveals that not all the bridges that have a high failure probability were inundated in the scenario and vice versa. This phenomenon should be explored further in future research. One explanation, however, is the fact that inundation maps do not reflect wave heights that may impose significant loads on bridge decks. Furthermore, it has

been shown in previous experimental studies that, after a certain amount of submergence of the bridge span, the maximum vertical uplift force actually decreases; thus, a bridge that is inundated could experience a smaller demand force than one that is not inundated (Marin and Sheppard 2009).

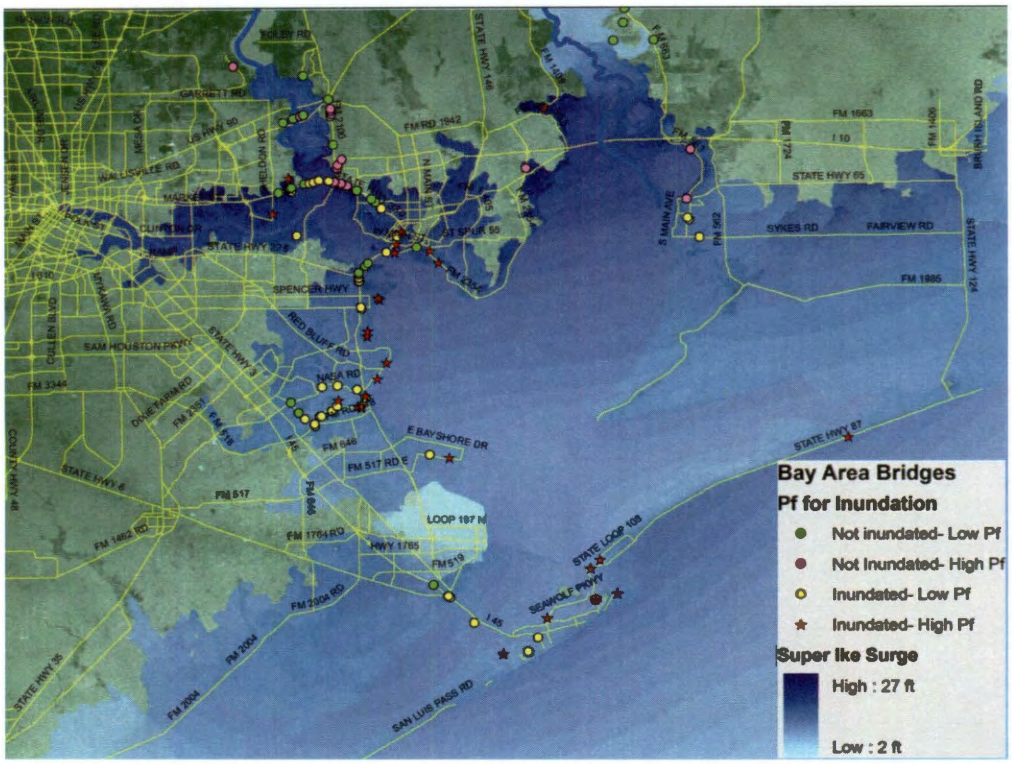

Figure 6.5: Map Comparing Bridge Deck Uplift Failure Probability and Inundation for the "Super Ike" Scenario.

6.2.4. Pier Scour Results

Following the method outlined in Chapter 5 of this thesis, the failure probability of pier scour was calculated for each of the 123 bridges in the pier scour subset for each scenario event. This estimates the probability distribution of scour depth at each pier during the 20-60 hours of hurricane surge. The scour depth is then compared to the limit states for pier scour (1/8 of the embedment length for repair,

¼ of the embedment length for failure with 2.75 ft and 5.5 ft respectively assumed if no pile length is recorded) to determine risks of scour leading to repair or to failure and replacement. Tables 6.4 and 6.5 below show the number of bridges in each failure probability category for each scenario event. Again, as with the uplift model, there is not enough data at this time to perform a full validation of the scour model; however, the results for the Ike scenario follow generally with the empirical evidence from Ike. In Ike, while many smaller, locally or privately owned bridges experienced scour, there was little documented pier scour and no major bridges were closed due to pier scour following Ike. Even in the stronger scenario events, a bridge might need repairs but there are no high failure probability bridges. This conforms to what Froelich and Fisher (2000) saw in North Carolina after Hurricane Floyd, that pier scour was not the dominant failure mode.

Hurricane Scenario Event	Failure Probability (%)			
	0 – 5	5 - 25	25 - 75	75 - 100
Ike	123	0	0	0
Ike with 30% Stronger Wind Speeds	122	1	0	0
"Super Ike"	122	1	0	0

Table 6.4: Number of Bridges in Each Failure Category for Each Hurricane Scenario Event from Pier Scour.

Hurricane Scenario Event	Repair Probability (%)			
	0 – 5	5 - 25	25 - 75	75 - 100
Ike	122	0	1	0
Ike with 30% Stronger Wind Speeds	122	0	1	0
"Super Ike"	122	0	1	0

Table 6.5: Number of Bridges in Each Repair Category for Each Hurricane Scenario Event from Pier Scour.

The spatial distribution of pier scour is shown in Figure 6.6 below. Even in the worst case scenario, only one bridge has a non-negligible failure probability, and that bridge, Rollover Pass, also experienced the highest average water velocity in each of the three scenarios. Rollover Pass is also the bridge that experienced bridge deck unseating during Hurricane Ike in 2008 and had a high failure probability for bridge deck uplift in each of the three scenario events.

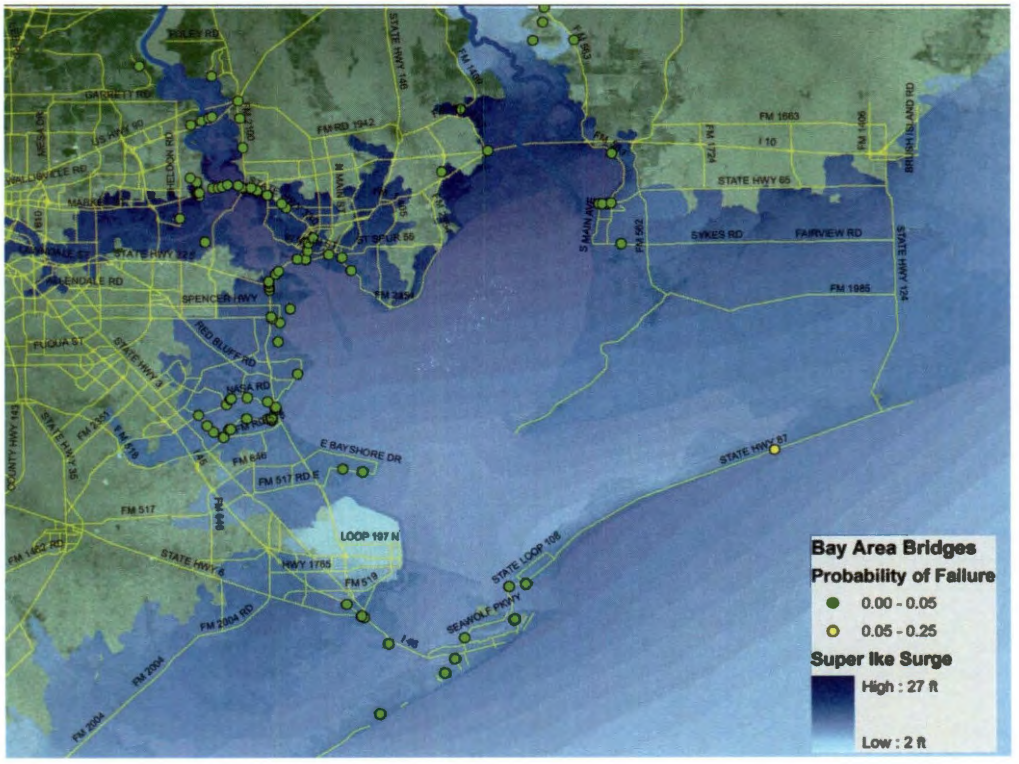

Figure 6.6: Map of Pier Scour Failure Probabilities in the "Super Ike" Scenario.

6.2.5. Abutment Scour Results

A risk assessment for abutment scour was conducted for each of the three hurricane scenarios using the probabilistic models presented in Chapter 5. In each of the three scenarios, one bridge had a "high" failure probability (Rollover Pass, see Figure 6.7)

due to the higher velocities it experienced. This again follows with the evidence from Ike that while small, locally owned bridges failed from scour, not many large state-owned bridges did. Tables 6.7 and 6.8 below give the number of bridges in each failure/ repair probability category for each scenario event. Figure 6.7 shows the locations of the bay area bridges along with their failure probabilities for the "Super Ike" scenario; only Rollover Pass bridge showed a high failure probability.

Hurricane Scenario Event	Failure Probability (%)			
	0 – 5	5 - 25	25 - 75	75 - 100
Ike	106	0	0	1
Ike with 30% Stronger Wind Speeds	106	0	0	1
"Super Ike"	106	0	0	1

Table 6.6: Number of Bridges in Each Failure Category for Each Hurricane Scenario Event from Abutment Scour.

Hurricane Scenario Event	Repair Probability (%)			
	0 – 5	5 - 25	25 - 75	75 - 100
Ike	106	0	0	1
Ike with 30% Stronger Wind Speeds	105	1	0	1
"Super Ike"	104	0	1	2

Table 6.7: Number of Bridges in Each Repair Category for Each Hurricane Scenario Event from Abutment Scour.

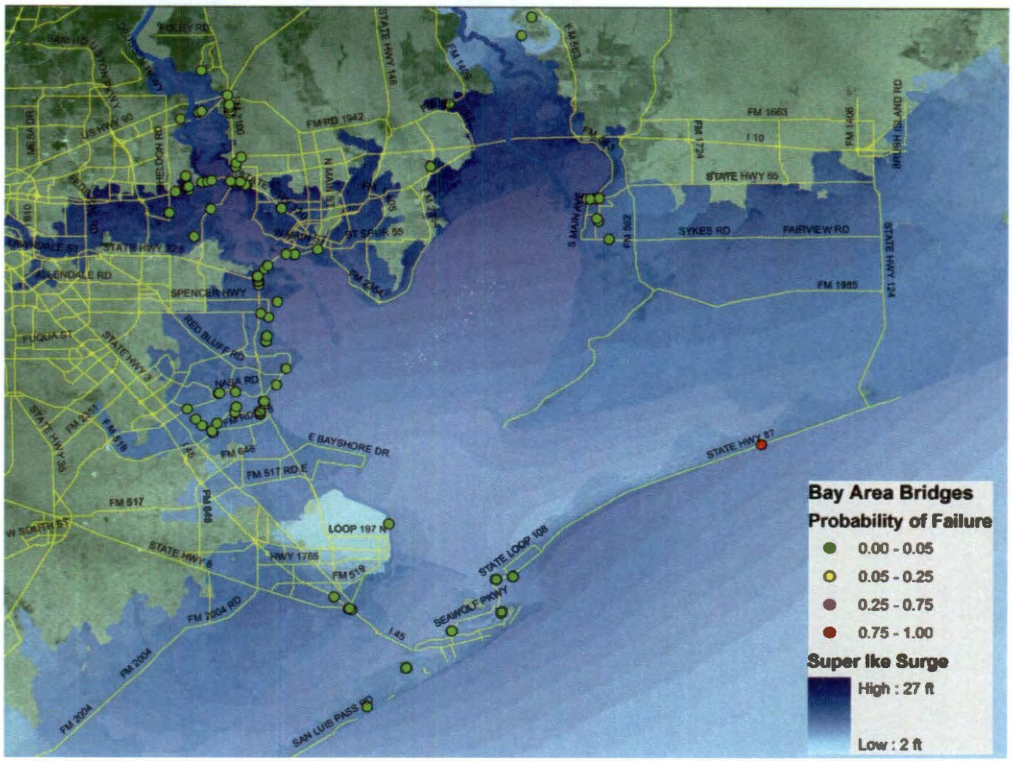

Figure 6.7: Map of Abutment Scour Failure Probabilities in the "Super Ike" Scenario.

6.2.6. Local Scour Risk from Pier and Abutment Scour

To convey scour risk more coherently to emergency officials, pier and abutment scour are combined into one local scour category. This is done by treating the two scour types as a series system (implying that failure due to either location indicates overall failure of the system) where the failure probability of each bridge equals:

$$P_f = 1 - \prod_{n=1}^{2}(1 - P_{f,n})$$

Equation 6.1: Upper Bound Series Estimation of Local Scour Risk.

where P_f is the total failure probability from scour and $P_{f,n}$ is the failure probability from pier and abutment scour. Understanding the dependent or independent nature

of pier and abutment scour is outside the scope of this thesis, however, the above equation is instituted for local scour to give an upper bound on the failure probability. Tables 6.8 and 6.9 give the number of bridges in each failure and repair probability range respectively. Since the bridges with a failure or repair probability are the same in pier and abutment scour, there is still only one bridge with a high failure probability in local scour (Rollover Pass), and two bridges with high repair probability (Rollover Pass and one of the Galveston Ferry Slips). These bridges also experienced the highest average water velocities during the "Super Ike" scenario, 1.15 m/s and .23 m/s respectively, and were based in sandy or silty soil, both soil types known to erode more quickly than clay.

Hurricane Scenario Event	Failure Probability (%)			
	0 – 5	5 - 25	25 - 75	75 - 100
Ike	146	0	0	1
Ike with 30% Stronger Wind Speeds	146	0	0	1
"Super Ike"	146	0	0	1

Table 6.8: Number of Bridges in Each Failure Category for Each Hurricane Scenario Event from Local Scour.

Hurricane Scenario Event	Repair Probability (%)			
	0 – 5	5 - 25	25 - 75	75 - 100
Ike	146	0	0	1
Ike with 30% Stronger Wind Speeds	145	1	0	1
"Super Ike"	144	0	1	2

Table 6.9: Number of Bridges in Each Repair Category for Each Hurricane Scenario Event from Local Scour.

6.2.7. Embankment Scour Results

The embankment scour model is a qualitative risk model that assigns risk levels (ranging from very low/no risk to high risk) to the bridges based on the water velocity at the bridge and the critical water velocity of the soil type found at the site.

As this is a qualitative measure, the exact scour depth is not derived as part of this study and is recommended as an area for future work. Further work in embankment scour can quantify the amount of scour given a water velocity as well as determine the allowable scour for embankments (which remains a challenge given the broad definition of embankment scour).

To that end, the risk levels for the bridges in each of the scenarios are given in Table 6.10. In the Ike scenario, one bridge has a high risk of embankment scour, while most of the bridges are not expected to have significant concern regarding embankment scour. With increasing severity of hurricane scenario, greater numbers of bridges are at a medium or high risk of embankment scour (Figure 6.8). Embankment scour, due to its qualitative nature, will remain a separate risk map from the other models that give a failure probability. This simplified indicator of risk based on anticipated water velocity and soil properties can serve as a basis for targeting more refined quantitative analysis of embankment scour potential.

Hurricane Scenario Event	Risk Level			
	Very Low (0)	Low (1)	Medium (2)	High (3)
Ike	108	34	11	1
Ike with 30% Stronger Wind Speeds	77	59	14	4
"Super Ike"	61	68	20	5

Table 6.10: Number of Bridges in Each Risk Level for Each Hurricane Scenario Event from Embankment Scour.

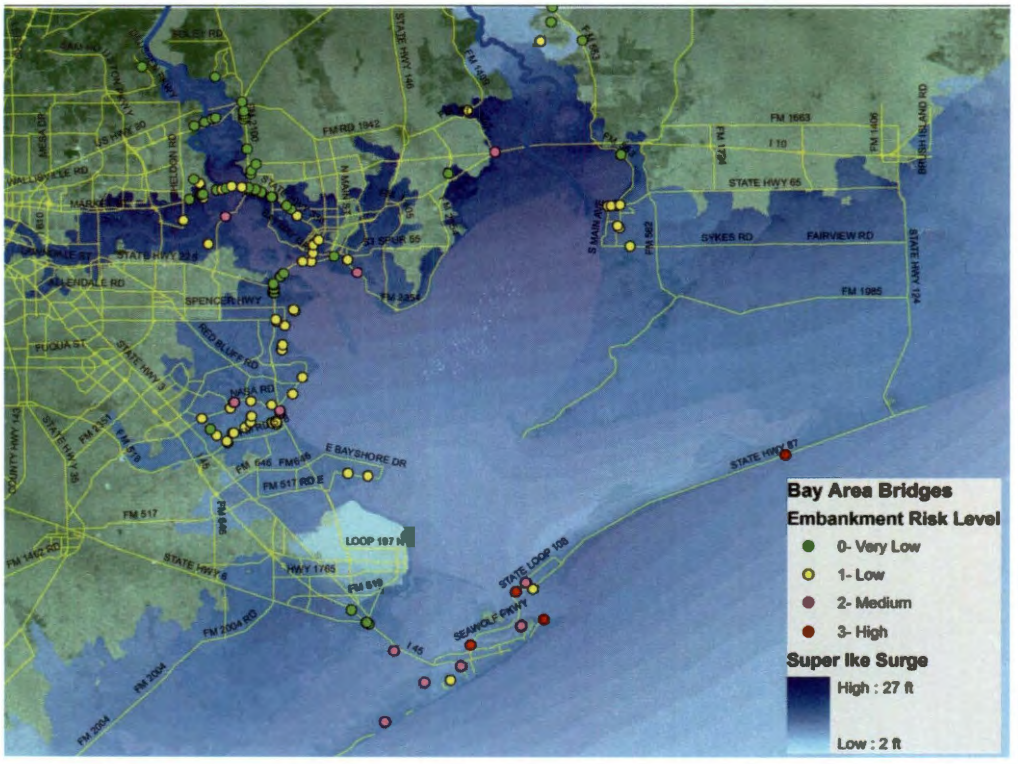

Figure 6.8: Map of Embankment Risk Levels for the "Super Ike" Scenario.

6.3. Overall Risk Maps for the Houston/Galveston Case Studies

Because the number of maps presented here and those in Appendix E can become overwhelming, a single cogent risk map was created that encompasses the greatest risk factor to each bridge. Each map was made by determining the failure mode which has the highest failure probability; this is then mapped in a similar fashion to

the previous maps but the failure mode is denoted by differing shapes. If there are two failure modes that both have a high failure probability, that is denoted by a separate shape. These maps are not intended to show the failure probability of both failure modes acting simultaneously on the bridge; rather the overall risk maps are composite maps of the local scour and bridge deck uplift risk maps.

As can be seen in Figure 6.9-6.11 below for each of the scenario events, bridge deck uplift dominates the failure modes in all the scenario events. In the Ike scenario, very few bridges have a high failure probability. This one map per scenario, along with the embankment map shows the risk from bridge deck uplift and three types of scour and gives guidance as to what type of risk each bridge faces.

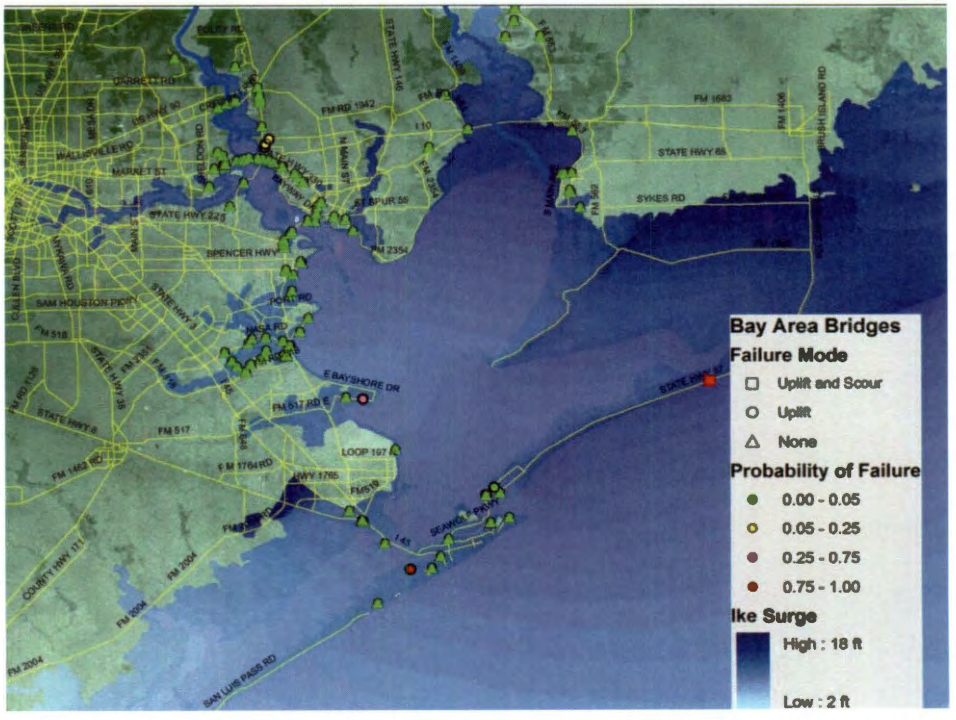

Figure 6.9: Map of Risk from Uplift and Local Scour in the Hurricane Ike Scenario.

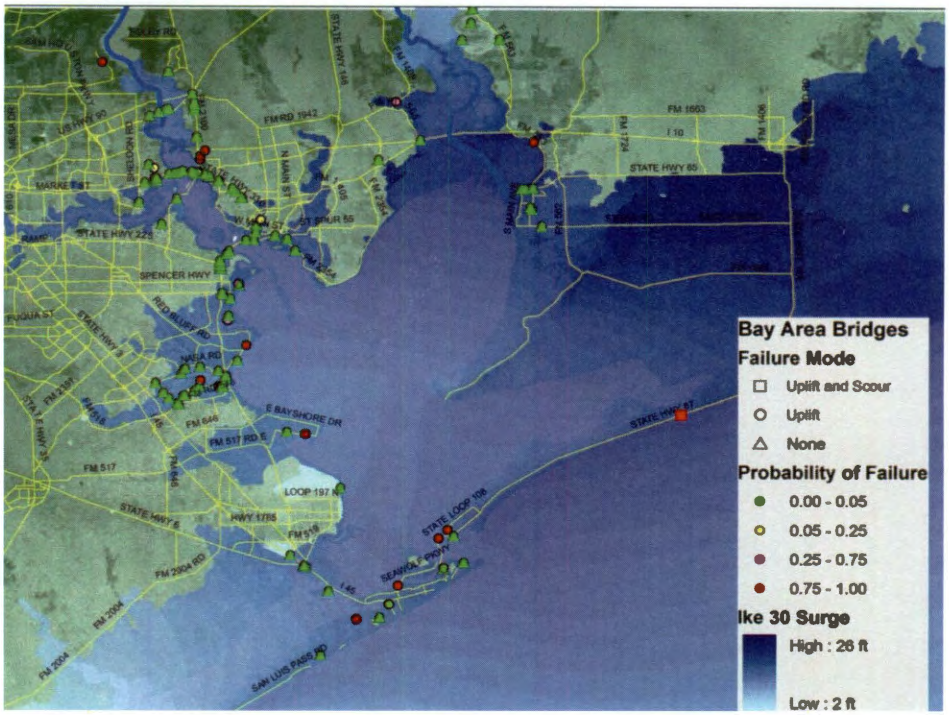

Figure 6.10: Map of Risk from Uplift and Local Scour in the Ike +30% Scenario.

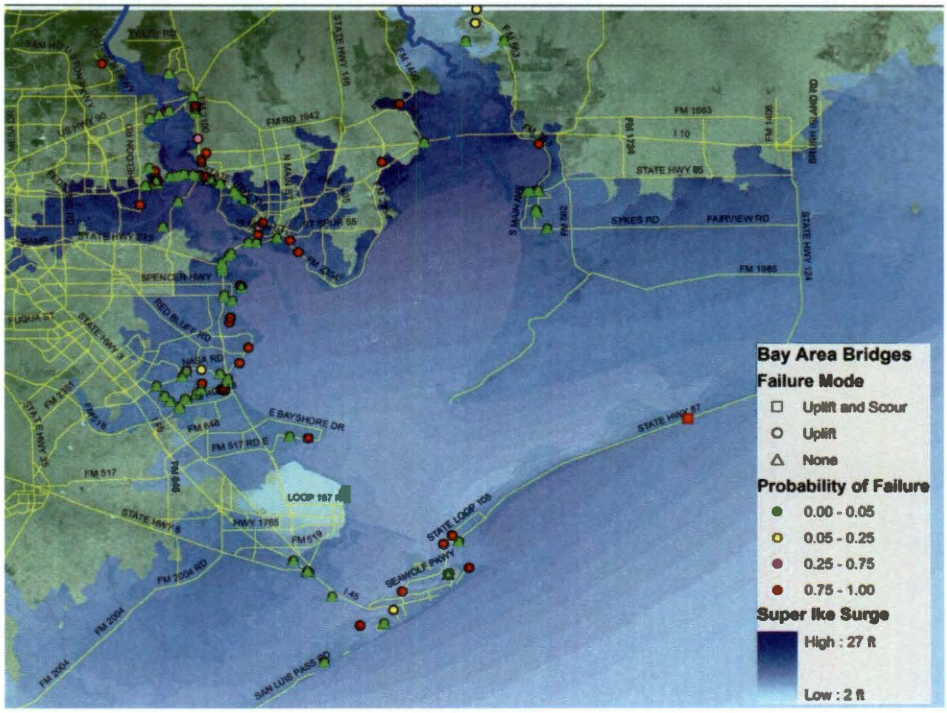

Figure 6.11: Map of Risk from Uplift and Local Scour in the "Super Ike" Scenario.

6.4. Conclusions from the Case Study Results

This chapter has presented all the results from five different views of risk during hurricane events, using probabilistic models for bridge failure modes and scenario hurricane events. Inundation was shown as a measure of short-term inaccessibility and compared to the indicator of long-term damage, bridge deck uplift. Three different types of scour were investigated and presented here, with pier and abutment scour being integrated into one local scour failure mode. Finally, the overall risk is shown for each scenario. While scour did not play as large of a role in these scenario events, it is clear from the fragility curves presented in Chapter 5 that with a larger water velocity at the bridge sites, scour could easily become the controlling failure mode.

Although the bridges in the Houston/Galveston bay area reveal low risks in a Hurricane Ike type storm, if a hurricane had stronger wind speeds or hit Houston more directly, the damage, both structural and scour (depending on velocity), could be severe. A significant portion of the inventory, 52 bridges, exhibited a high failure probability in the "Super Ike" scenario, implying that over a third of the region's bridges have a high risk of damage during a stronger hurricane event. In the next chapter, the applications of these models for various risk mitigation efforts will be discussed.

Chapter 7

Applications of the Houston/Galveston Bay Area Risk Assessment

This Houston/Galveston bay area risk assessment lends itself to three major applications: re-entry route assessment, predictive modeling of the transportation system and retrofit prioritization. These applications are listed roughly in order from short to long-term applications. In this chapter, these three main applications are discussed with some ideas for future work being presented herein.

7.1. Assessment of the Viability of Post-Event Re-Entry Routes

The most immediate application of this risk assessment is the ability to rank routes into and out of areas most impacted by hurricane forces before a hurricane hits the Texas coast. This assessment of re-entry routes is greatly beneficial to emergency planners as the coordinate post-event rescue and recovery efforts. The list of routes

in Table 7.1 below and their possible inaccessibility are not supposed to be taken as an end-all for decision making but provide an additional tool for an official to consider when determining how to enter a community after a storm. Local officials have indicated the priorities and importance of accessing regional hospitals, along with other critical facilities, and common consideration of major highways and evacuation routes as re-entry routes (Clark, 2011, EMA, 2011).

For this study, three main regions were chosen: Galveston Island, Bolivar Peninsula and Clear Lake/Johnson Space Center. These three regions were chosen because of the devastation past hurricanes have inflicted upon these areas or their importance to the City of Houston. As such four major routes/ highways and five hospitals were chosen as representative of the area: I-45 into Galveston Island, SH87 on Galveston Island and Bolivar Peninsula, SH146 from Galveston Island to Clear Lake, SH Spur 330 in the Clear Lake Region, University of Texas- Medical Branch (UTMB), the Shriner's Hospital and Galveston Emergency Services in Galveston and CHRISTUS St. John's Hospital and MD Anderson in Clear Lake. These routes and hospitals are listed in shown in Figure 7.1 below with the Hurricane Ike scenario surge overlaid.

Figure 7.1: Map of Overall Failure Probabilities from Hurricane Ike Scenario with Major Routes Overlaid.

With the important routes and locations determined, each scenario was inspected to determine if the route was anticipated to be clear or possibly blocked by bridge damage. These accessibility rankings are given for each major re-entry route and route to hospital (with the route taken in parenthesis) in Table 7.1. Regarding the considerations of accessibility in Table 7.1, since this risk assessment only includes bridges listed in the NBI database (consisting of all state-owned or operated bridges but not locally or privately owned and operated bridges), the designation of "likely accessible" or likelihood of inaccessibility is based on such bridges. Bridges that are not required to be reported to the National Bridge Inventory Program are not considered in this analysis. Additionally, for the hospitals

only the main route to the hospital was checked since, in a storm event, if a smaller road has a damaged bridge there is usually more than one way to get to the hospital. Given the scope of the risk assessment presented herein, accessibility designations on re-entry routes or major routes to hospital consider bridge unseating, pier, abutment scour and embankment scour. It is noted that debris is not considered herein and is often a major barrier to roadway accessibility.

The considered for evaluating accessibility based on bridge performance are also typical primary routes for debris removal. An accessibility designation is assigned based on the failure probability of each failure mode for the bridges along the route. "Likely Accessible" is assigned if all the bridges along the route had a failure probability of 0-0.05 and had no more than a low risk level from embankment scour. "Low Probability of Inaccessibility" was assumed if any of the bridges along the route had a failure probability of 0.05-0.25 for unseating or scour or had bridges with a medium risk level from embankment scour. "Medium Probability of Accessibility" was given if the failure probability of any of the bridges on a given route were between 0.25 and 0.75 or if any of the bridges had a high risk from embankment scour. Finally, "High Probability of Inaccessibility" was assigned if any of the bridges on a route had a failure probability over 0.75 and a high risk to embankment scour. This work on assessment of critical routes is but a precursor to network reliability studies where the hospitals can be modeled as destinations in a typical Origin- Destination matrix and alternative routes, beyond the designated route assessed here, can be considered.

Route/Hospital	Ike	Ike-30	Super Ike
I45	Likely Accessible	Likely Accessible	Likely Accessible
SH146	Likely Accessible	Low Probability of Inaccessibility	Medium Probability of Inaccessibility
SH87	High Probability of Inaccessibility	High Probability of Inaccessibility	High Probability of Inaccessibility
SH Spur 330	Likely Accessible	Medium Probability of Inaccessibility	High Probability of Inaccessibility
UTMB (I45 to SH87 to UTMB)	Likely Accessible	Likely Accessible	Low Probability of Inaccessibility
Shriner's Hospital (same route as UTMB)	Likely Accessible	Likely Accessible	Low Probability of Inaccessibility
Galveston Emergency Medical Services (I45 to SH87 to 25th St)	Likely Accessible	Likely Accessible	Low Probability of Inaccessibility
CHRISTUS St. John's Hospital (I45 to Nasa Rd.1)	Likely Accessible	Low Probability of Inaccessibility	Medium Probability of Inaccessibility
MD Anderson near Clear Lake (same route as St. John's)	Likely Accessible	Low Probability of Inaccessibility	Medium Probability of Inaccessibility

Table 7.1: Matrix of Routes Analyzed for Each Hurricane Scenario Event with Likely Accessibility Rating.

From Table 7.1 above, it is clear that I-45 is the most viable route onto Galveston Island. Bolivar Peninsula could be difficult to enter from the north because Rollover Pass has a high failure probability in every scenario and would also be difficult to enter from the south by ferry as many of the ferry slips also have a high failure probability. The Clear Lake region is accessible from the major highways in most of the events, however there could be damaged bridges along SH-146 or SH Spur- 330 in a stronger event scenario. Figure 7.1 above and Figures 7.2 and 7.3 below show each of the scenarios graphically with the hospitals denoted by

stars and the critical routes highlighted. The figure for each scenario event also includes the highest failure probability of each of the vulnerability models; a composite map of the failure modes without the failure modes overlaid for clarity.

Figure 7.2: Map of Overall Failure Probabilities from Ike + 30% Scenario with Major Routes Overlaid.

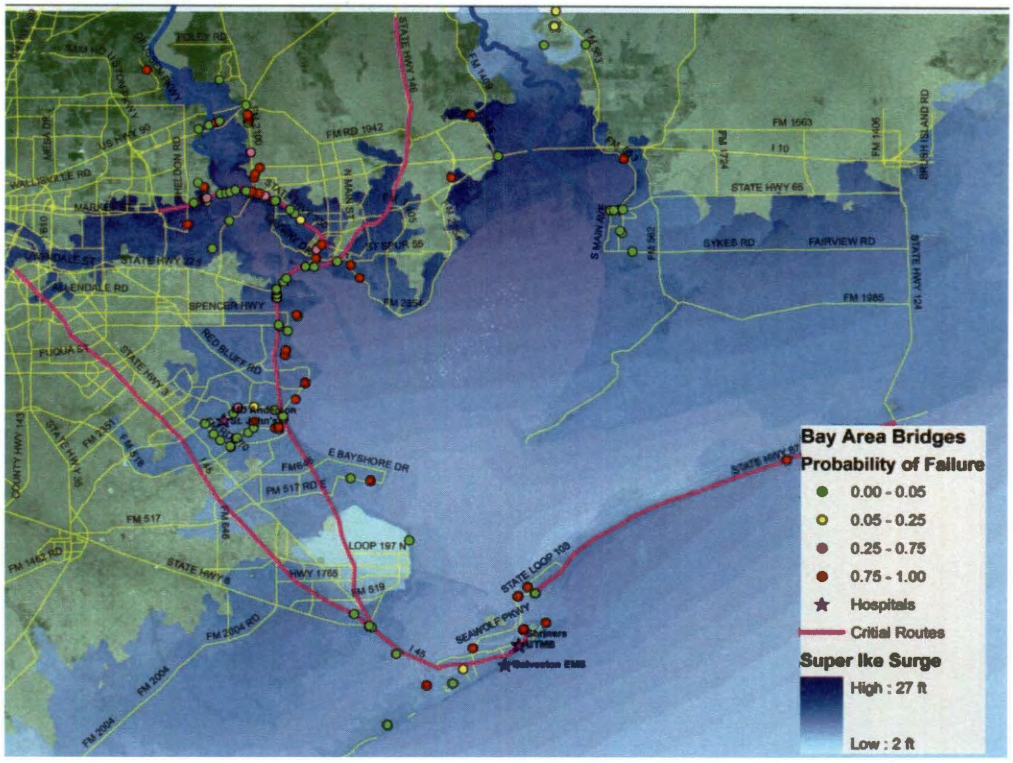

Figure 7.3: Map of Overall Failure Probabilities from "Super Ike" Scenario with Major Routes Overlaid.

Additionally, while not on the major route list for post event re-entry, some passages across the Houston Ship Channel could be blocked in a stronger hurricane event, such as Ike +30 or Super Ike. This could affect recovery work on important industries in the Ship Channel. Table 7.1 and Figures 7.1-7.3 give two media which emergency managers could use to help with decision making.

7.2. Predictive/Real-Time Risk Assessment

The second application of the risk assessment presented in this thesis is real-time predictive modeling of bridge failure as a storm approach the Texas coast. All the models discussed in previous chapters are fully automated so as to allow for

predictive modeling of the possible bridge failures in the Houston/Galveston bay area. The algorithms have been developed in MATLAB (Mathworks, 2009b) and interface to a text bridge database file. They can enable streamlined updating of bridge and soil data, as well as refinement of modeling assumptions such as probability distributions or model error and bias estimates if new field data is collected and analyzed.

The Computational Hydraulics Group (CHG) at UT-Austin can currently model the trajectory and strength of an impending hurricane as it moves through the Gulf of Mexico based on NOAA information. With the output of the CHG or other researchers as inputs to the bridge deck uplift and scour models, the current risk assessment can be conducted for any scenario event. The input needs from storm simulation include surge elevation, wave height and period, water velocity and storm duration at each bridge site. Additionally, the fragility curves for bridge deck unseating, pier and abutment scour can estimate the failure probability given input storm parameters. The advantage of developing fragility models for each bridge in the inventory and failure mode as conducted in this study (pier scour, abutment scour and unseating) is readily apparent in real time modeling. This negates the requirement to conduct any additional simulations or probabilistic analyses in support of the real or rapid risk assessment. Instead the failure probabilities can be directly computed from the fragility models given the hazard input.

This provides invaluable information for emergency managers when planning re-entry routes because they can have access to real-time, predictive maps

of the distribution of damage and not rely solely on pre-set scenario events. Thus, this application ties into the assessment of re-entry routes but gives better, more detailed information for the specific storm, as well as a safety assessment to begin prioritizing likely bridges in need of post-event inspection. Such an analysis can highlight structure with high damage potential for deployment of inspection crews. This approach has been adopted by the California Department of Transportation via a tool Shake Cast, used to notify inspectors of priority bridges in near real time following earthquake events on the basis of projected hazard intensities and bridge fragility estimates (Turner and Padgett, 2011).

7.3. Retrofit Prioritization and Aids to Mitigation Efforts

Last, the tools developed to support this risk assessment can aid in prioritizing bridges in need of retrofit or rebuilding efforts. There are several retrofit measures currently used in earthquake prone areas which may have applicability in increasing a bridge's capacity to withstand hurricane surge and wave forces, and several studies have proposed potential retrofit measures for coastal bridges susceptible to surge and wave loading (Padgett et al., 2008, Sawyer, 2008). That being said, the nature or extent of the retrofitting measures for bridges against hurricane forces is beyond the scope of this thesis; however, once a suite retrofit or mitigation measures have been determined, the risk assessment presented here can provide valuable information as to which bridges would benefit the most mitigation actions.

For a holistic risk based prioritization of bridges for retrofit, analysis beyond the three scenarios is required. Probabilistic storm surge and wave information are ideally integrated to reveal the risk of damage to bridges considering uncertainty in bridge vulnerability (quantified herein) couple with uncertainty in hazard potential. Furthermore, recent research has also proposed prioritization approached in which network topology and network reliability are considered in addition to bridge vulnerability (Rokneddin et al., 2011). Such approaches can provide an advanced basis for prioritizing bridges for retrofit in coastal regional, particularly if preferences beyond bridge damage, such as transportation network performance or accessibility of major destinations and critical facilities, are of primary interest.

7.4. Application Conclusions

This chapter presents three main potential applications for the Houston/ Galveston bay area. One application, assessment of re-entry routes, has been explored to some extent, but the possibilities are endless for testing various routes on the scenario maps. This work is prime for network reliability studies. Additionally, two future applications of the risk assessment are provided, real-time modeling and retrofit prioritization. These two applications can be utilized as new hurricanes threaten the Texas coast or as mitigation measures are chosen. The next chapter presents the overall conclusions of this work along with ideas for future research.

Chapter 8

Conclusions and Opportunities for Future Work

8.1. Summary and Conclusions

As shown through many hurricanes, from the 1900 storm in Galveston to Hurricane Irene in 2011, coastal regions are extremely vulnerable to damage from hurricane forces. This is also true of coastal transportation systems, which experienced high levels of damage in Hurricanes Katrina, Ike and Irene, to name a few. In order for emergency managers and infrastructure owners to be better prepared for possible damage and plan mitigation activities, this thesis implements the first Houston/ Galveston bay area hurricane risk assessment to bridges under multiple failure modes: bridge deck uplift and bridge scour.

This thesis lays the groundwork for regional risk assessments of bridge and roadway infrastructure in any coastal area through the detailed information of the

database compiling and methodology for the probabilistic uplift and scour models. The precise information necessary for the risk assessment models was presented in Chapter 3. Methodologies for determining bridge deck uplift and scour were presented in Chapters 4 and 5, including a new approach to scour fragility modeling of bridges and the adaptation of unseating fragility analysis for the regional portfolio. Additionally, three case study scenario event hurricanes were tested on the study bridges using the methodologies in Chapters 4 and 5 to determine the failure probability of each bridge from each failure mode. The results of this case study are presented in Chapter 6, revealing the distribution of damage to bridges in the Houston/Galveston area associated with each event. Last, several applications building upon this Houston/Galveston bay area risk assessment were introduced in Chapter 7, including re-entry route assessment, real-time predictive modeling and retrofit prioritization.

The work presented in this study is unique in that no probabilistic assessment of bridges under multiple hurricane induced failure modes has been conducted as of yet. Granted, in the scenario events considered, unseating tended to control the failure mode of the bridges. Since the embankment scour model is still qualitative, the risk from embankment scour cannot be compared directly to the risk from uplift or pier/abutment scour; however, the results reveal a potential threat of this failure mode in several key areas.

Some key conclusions from this research and observations from the case study analysis include:

1.) In the Houston/Galveston bay area bridge infrastructure 68% of the bridges are less than 15 ft above the mean water level and 68% of the bridges are multi-span simply supported bridge types which have revealed vulnerability in past hurricane events

2.) Bridge specific unseating fragility analysis under storm surge and wave loading is data intensive, yet most of the information required to support the analysis can be found in publicly available databases coupled with in-house inspection reports and as-built plans. Resulting unseating fragilities are influenced by bridge type (simply-supported vs. continuous, girder vs. slab or box beam), material type (steel vs. concrete) and connectivity between the deck and substructure of the bridge.

3.) Probabilistic analysis of hurricane induced bridge scour can enable fragility models of bridges with probability of failure conditioned upon storm water velocity. The dominant sources of uncertainty in these probabilistic models are model error from the SRICOS predictive models, as well as uncertainty in the initial erosion rate of the soil due to assumptions made on the basis of soil type at bridge sites.

4.) Bridge deck uplift was the predominant failure mode in most of the bridges for the scenario events considered in the case study. While the Houston/Galveston bay area bridge network endured the Hurricane Ike scenario with little damage predicted (3 out of 155 bridges with an estimated failure probability over 0.75), a stronger hurricane such as the "Super Ike"

scenario could inflict far greater damages to the bridge network (52 out of 155 bridges with an estimated failure probability over 0.75).

5.) While pier and abutment scour did not affect the bridges in the scenario events greatly (typically only 1 bridge with appreciable probability of either pier or abutment scour), a stronger storm with higher water velocity could cause increased scour damage, especially to abutments. The scour fragility analyses reveal median values of water velocity leading to repair or closure on the order of 0.36 m/s for bridge abutments in clays and 1.05 m/s bridge abutments in sands.

8.2. Suggestions for Future Work

The field of hurricane risk assessment of transportation infrastructure is still relatively young and as such there is a great deal of future research that can branch from that presented in this thesis; a few of these suggestions are enumerated below.

1. To allow better input to the risk models, site specific soil samples can be obtained and tested for each bridge. This would greatly reduce the uncertainty in the scour models.
2. While model bias and model error were considered for bridge deck unseating and pier scour in this work, sufficient statistical analysis of empirical data versus model estimates has not been conducted to enable such considerations within the abutment fragility modeling, highlighting a future research opportunity.

3. Further research on a quantitative estimate of embankment scour is needed to fully understand the risk embankment scour poses to both roadways and bridges.
4. The hurricane risk assessment conducted herein provide failure probability estimates of bridges across a region and can form a foundation for future system reliability analysis considering connectivity or flow reliability at the transportation network level.
5. As indicated in Chapter 7, numerous opportunities arise for application of the models in supporting risk mitigation and planning in coastal regions, with associated research needs. Key intellectual challenges remain, such as integration of hazard models with vulnerability models for real time or rapid assessment. Furthermore, simplified or rigorous network-level prioritization of bridges for upgrade can integrate the models proposed herein. However, the viability of various retrofit options are yet to be fully explored, particularly in a risk based fashion.

References

AASHTO 2008. Guide Specifications for Bridges Vulnerable to Coastal Storms.

ACI 2005. *318 - Building code requirement for structural concrete*, American Concrete Institute (ACI).

AGUÍÑIGA, F., MATAKIS, K., ESTRADA, H., SAI, J., LEELANI, P. & SHELDEN, J. 2008. Report Synthesis of Wave Load Design Methods for Coastal Bridges. *Report No. 0-5516-2.* Texas A&M University- Kingsville.

ALIPOUR, A., SHAFEI, B. & SHINOZUKA, M. 2010. Failure Estimation of Highway Bridges under Combined Effects of Scouring and Earthquake. *Bridge Maintenence, Safety, Management and Life-Cycle Optimization.* Philadelphia, PA: CRC Press.

AP, A. P. 2011. *Hurricane Irene: State-by-state damage* [Online]. Politico. Available: http://www.politico.com/news/stories/0811/62276.html 2011].

ATAEI, N. & PADGETT, J. E. 2010a. IM Study for Probabilistic Modeling of Coastal Bridges Susceptible to Hurricane Events. *International Symposium on Reliability Engineering and Risk Management (ISRERM2010).* Shanghai, China.

ATAEI, N. & PADGETT, J. E. 2010b. Probabilistic Modeling of Bridge Deck Unseating during Hurricane Events. *ASCE Journal of Bridge Engineering.*

AYRES 2004. Field Manual- Scour Critical Bridges. Federal Highway Administration (FHWA).

BASOZ, N. & KIREMIDJIAN, A. S. 1999. Development of empirical fragility curves for bridges. *Technical Council on Lifeline Earthquake Engineering Monograph,* 693-702.

BASOZ, N. & MANDER, J. 1999. *Enhancement of the Highway Transportation Module in HAZUS,* Washington D.C, National Institute of Building Sciences.

BEA, R. G., IVERSEN, R. & XU, T. 2001. Wave-in-deck forces on offshore platforms. *Journal of Offshore Mechanics and Arctic Engineering,* 123, 10-21.

BEA, R. G., XU, T., STEAR, J. & RAMOS, R. 1999. Wave forces on decks of offshore platforms. *Journal of Waterway, Port, Coastal and Ocean Engineering,* 125, 136-144.

BLAKE, E. S., LANDSEA, C. W. & GIBNEY, E. J. 2011. The Deadliest, Costliest and Most Intense United States Tropical Cyclones from 1851 to 2010 (and Other Frequently Requested Hurricane Facts). *NOAA Technical Memorandum NWS NHC-6.* Miami, FL: National Hurricane Center.

BOLDUC, L. C., GARDONI, P. & BRIAUD, J.-L. 2008. Probability of Exceedance Estimates for Scour Depth around Bridge Piers. *JOURNAL OF GEOTECHNICAL AND GEOENVIRONMENTAL ENGINEERING,* 134, 175-184.

BRADNER, C., SCHUMACHER, T., COX, D. & HIGGINS, C. 2011. Experimental Setup for a Large-Scale Bridge Superstructure Model Subjected to Waves. *Journal of Waterway, Port, Coastal, and Ocean Engineering,* 137, 3-11.

BRIAUD, J.-L. 2006. Bridge Scour. *Geotechnical News,* 24, 54-56.

BRIAUD, J.-L., CHEN, H. C., TING, F. C. K., KWAK, K., HAN, S.-W., NURTJAHYO, P., CAO, Y. & LI, Y. Measuring the erodibility of cohesive soils. 2004 Minneapolis, MN, United states. American Society of Civil Engineers.

BRIAUD, J.-L., GOVINDASAMY, A. V., KIM, D., GARDONI, P., OLIVERA, F., CHEN, H.-C., MATHEWSON, C. & ELSBURY, K. 2009. SIMPLIFIED METHOD FOR ESTIMATING SCOUR AT BRIDGES. College Station, TX: Texas Transportation Institute.

BRIAUD, J.-L. & OH, S. J. 2010. Bridge Foundation Scour. *Geotechnical Engineering Journal of the SEAGS & AGSSEA,* 41, 16.

BRIAUD, J. L. 2011. *RE: Thoughts on Embankment Scour.* Type to ARNOLD, C.

BRIAUD, J. L., CHEN, H. C., KWAK, K. W., HAN, S. W. & TING, F. C. K. 2001a. Multiflood and Multilayer Method for Scour Rate Prediction at Bridge Piers. *JOURNAL OF GEOTECHNICAL AND GEOENVIRONMENTAL ENGINEERING,* 127, 114-125.

BRIAUD, J. L., TING, F. C. K., CHEN, H. C., CAO, Y., HAN, S. W. & KWAK, K. W. 2001b. Erosion Function Apparatus for Scour Rate Predictions. *JOURNAL OF GEOTECHNICAL AND GEOENVIRONMENTAL ENGINEERING,* 127, 105-113.

CCSP 2008. Impacts of Climate Change and Variability on Transportation Systems and Infrastructure: Gulf Coast Study, Phase I. *In:* SAVONIS, M. J., BURKETT, V. R. & POTTER, J. R. (eds.) *A Report by the U.S. Climate Change Science Program and the Subcommittee on Global Change Research.* Washington D.C, USA: Department of Transportation.

CHEN, Q., WANG, L. & ZHAO, H. 2009. Hydrodynamic Investigation of Coastal Bridge Collapse during Hurricane Katrina. *Journal of Hydraulic Engineering,* 135, 175-186.

CHEN, Q., WANG, L., ZHAO, H. & DOUGLASS, S. L. 2007. Predictions of storm surges and wind waves on coastal roadways in hurricane-prone areas. *Journal of Coastal Research,* 23, 1304-1317.

CHG 2010. Computational Hydraulics Group. University of Texas at Austin.

CHIEW, Y.-M. 2008. Scour and scour countermeasures at bridge sites. *Transactions of Tianjin University,* 14, 289-295.

CHOI, E., DESROCHES, R. & NIELSON, B. 2004. Seismic fragility of typical bridges in moderate seismic zones. *Engineering Structures,* 26, 187-199.

CUOMO, G., SHIMOSAKO, K.-I. & TAKAHASHI, S. 2009. Wave-in-deck loads on coastal bridges and the role of air. *Coastal Engineering,* 56, 793-809.

DAWSON, C. 2010. Advances in ADCIRC Storm Surge Models for Forecasting and Hindcasting Texas Hurricanes. *Hurricane Ike: What We Have Learned and Steps for the Future.* Houston, TX: Severe Storm Prediction, Education and Evacuation from Disasters.

DELPHIA, J. 2011. *RE: TxDOT Guidelines on Scour Depths.* Type to ARNOLD, C.

DENSON, K. H. 1978. Wave Forces on Causeway-Type Coastal Bridges. Mississippi State Univeristy: Water Resources Research Institute.

DENSON, K. H. 1980. Wave Forces on Causeway-Type Coastal Bridges: Effects of Angle of Wave Incidence and Cross-Section Shape. Mississippi State University: Water Resources Research Institute.

DESROCHES, R. (ed.) 2006. *Hurricane Katrina: Performance of Transportation Systems*: American Society of Civil Engineers.

DOT, C. 2000. *ConnDOT Drainage Manual* [Online]. Connecticut Department of Transportation. Available: http://www.ct.gov/dot/lib/dot/documents/ddrainage/9.B.pdf.

DOUGLASS, S. L., CHEN, Q., OLSEN, J. M., EDGE, B. L. & BROWN, D. 2006. Wave Forces on Bridge Decks. Washington D. C.

DOUGLASS, S. L., HUGHES, S. A., ROGERS, S. & CHEN, Q. 2004. The Impact of Hurricane Ivan on the Coastal Roads of Florida and Alabama: A Preliminary Report. Coastal Transportation Engineering Research and Education Center.

DUEÑAS-OSORIO, L., SUBRAMANIAN, D. & STEIN, R. 2010. *Hurricane Risk Assessment for Informed Evacuation Decision* [Online]. SSPEED Center. Available: http://sspeed.rice.edu/sspeed/Risk %20Assessment.html.

EL GHAMRY, O. A. 1963. Wave Forces on a Dock. *In:* LABORATORY, H. E. (ed.) *Institute of Engineering Research Technical Report HEL-9-1.* California: University of California, Berkeley.

ELIGEHAUSEN, R., MALLEE, R. & SILVA, J. F. 2006. *Anchorage in Concrete Construction,* Berlin, Ernst & Sihn.

ELLINGWOOD, B. & HWANG, H. 1985. PROBABILISTIC DESCRIPTIONS OF RESISTANCE OF SAFETY-RELATED STRUCTURES IN NUCLEAR PLANTS. *Nuclear Engineering and Design,* 88, 169-178.

ELLINGWOOD, B. R. & WEN, Y.-K. 2005. Risk-benefit-based design decisions for low-probability/high consequence earthquake events in Mid-America. *Progress in Structural Engineering and Materials,* 7, 56-70.

FEMA 2008. Hurricane Ike Impact Report. Federal Emergency Management Agency.

FHWA 1995. Recording and Coding Guide for the Structure Inventory and Appraisal of the Nation's Bridges. *In:* DIVISION, O. O. E. B. (ed.) *Report No. FHWA-PD-96-001.* Washington, DC: Federal Highway Administration.

FRENCH, J. A. 1979. WAVE UPLIFT PRESSURES ON HORIZONTAL PLATFORMS. *NASA Technical Paper,* 1, 187-202.

FROEHLICH, D. C. Local scour at bridge abutments. Proceedings of the 1989 National Conference on Hydraulic Engineering, August 14, 1989 - August 18, 1989, 1989 New Orleans, LA, USA. Publ by ASCE, 13-18.

FROEHLICH, D. C. & FISHER, P. F. 2000. Storm Surge Scour at Coastal Bridges: Documenting the Effects of Hurricanes Bonnie and Floyd in North Carolina. *Water Resources.*

GOVINDASAMY, A. V., BRIAUD, J. L., CHEN, H. C., DELPHIA, J., ELSBURY, K., GARDONI, P., HERRMAN, G., KIM, D., MATHEWSON, C. C., MCCLELLAND, M. & OLIVERA, F. Simplified method for estimating scour at bridges. 2008 New Orleans, LA, United states. American Society of Civil Engineers, 385-393.

HARRISON, L. J. & MORRIS, J. L. 1991. Bridge Scour Vulnerability Assessment. *National Conference on Hydraulic Engineering.* Nashville, TN.

JCSS 2001. JSSS Probabilistic Model Code. *In:* SAFETY, J. C. O. S. (ed.) *Part 3: Resistance Models.* Joint Committee on Structural Safety.

JOHNSON, P. A. 1995. Comparison of Pier-Scour Equations Using Field Data. *Journal of Hydraulic Engineering,* 121, 626-629.

JOHNSON, P. A. & DOCK, D. A. 1998. Probabilistic Bridge Scour Estimates. *Journal of Hydraulic Engineering,* 124, 750-754.

KANG, W. H., SONG, J. & GARDONI, P. 2008. Matrix-based system reliability method and applications to bridge networks. *Reliability Engineering and System Safety,* 93, 1594-1593.

KAPLAN, P., MURRAY, J. J. & YU, W. C. Theoretical analysis of wave impact forces on platform deck structures. Proceedings of the 14th International Conference on Offshore Mechanics and Arctic Engineering. Part 5 (of 5), June 18, 1995 - June 22, 1995, 1995 Copenhagen, Den. ASME, 189-198.

KESTIN, J., SOKOLOV, M. & WAKEHAM, W. A. 1978. *Viscosity of liquid water in the range ?8?°C to 150?°C,* NIST.

KIREMIDJIAN, A., STERGIOU, E. & LEE, R. 2007. Issues in seismic risk assessment of transportation networks. *Earthquake Geotechnical Enigneering,* 461-480.

LEE, Y. J., SONG, J., GARDONI, P. & LIM, H. W. 2011. Post-hazard flow capacity of bridge transportation network considering structural deterioration of bridges. *Structure and Infrastructure Engineering: Maintenance, Management, Life-cycle Design and Performanc,* 7, 509-521.

MARIN, J. & SHEPPARD, D. M. Storm surge and wave loading on bridge superstructures. 2009 Austin, TX, United states. American Society of Civil Engineers, 557-566.

MELVILLE, B. W. 1997. *Pier and Abutment Scour: Integrated Approach,* ASCE.

MORRIS, J. L. & PAGAN-ORTIZ, J. E. Bridge Scour Evaluation Program in the United States. Managing Water; Coping with Scarcity and Abundance, 1997 San Francisco, CA. International Association for Hydraulic Research, 110-116.

NBI 2010. National Bridge Inventory Database. Federal Highway Administration (FHWA).

NCRS. 2011. *Soil Data Mart* [Online]. Natural Resources Conservation Service. Available: http://soildatamart.nrcs.usda.gov/ 2011].

NIELSON, B. G. 2005. *Analytical Fragility Curves for Highway Bridges in Moderate Seismic Zones.* Doctor of Philosophy, Georgia Institute of Technology.

OH, S. J., CHEN, X., BRIAUD, J.-L., CHANG, K.-A. & CHEN, H.-C. 2009. The Effect of Abutment Length for Abutment Scour in Cohesive Soil: Initial Results.

OKEIL, A. M. & CAI, C. S. 2008. Survey of short- and medium-span bridge damage induced by Hurricane Katrina. *Journal of Bridge Engineering,* 13, 377-387.

PADGETT, J., DESROCHES, R., NIELSON, B., YASHINSKY, M., KWON, O.-S., BURDETTE, N. & TAVERA, E. 2008. Bridge damage and repair costs from Hurricane Katrina. *Journal of Bridge Engineering,* 13, 6-14.

PADGETT, J. E. & ARNOLD, C. Lessons in bridge vulnerability from hurricane Katrina: Reconnaissance findings and analysis of empirical data. 2009 Oakland, CA, United states. American Society of Civil Engineers, 47.

PADGETT, J. E., SPILLER, A. & ARNOLD, C. 2009. Statistical analysis of coastal bridge vulnerability based on empirical evidence from Hurricane Katrina. *Structure*

and Infrastructure Engineering: Maintenance, Management, Life-Cycle Design and Performance.

POWLEDGE, G. R., RALSTON, D. C., MILLER, P., YUNG, H. C., CLOPPER, P. E. & TEMPLE, D. M. 1989a. Mechanics of overflow erosion on embankments. I. Research activities. *Journal of Hydraulic Engineering,* 115, 1040-1055.

POWLEDGE, G. R., RALSTON, D. C., MILLER, P., YUNG, H. C., CLOPPER, P. E. & TEMPLE, D. M. 1989b. Mechanics of overflow erosion on embankments. II. Hydraulic and design considerations. *Journal of Hydraulic Engineering,* 115, 1056-1075.

RICHARDSON, E. V. & DAVIS, S. R. 2001. Evaluating Scour at Bridges. *Hydraulic Engineering Circular No. 18.* 4th ed. Washington D. C.: US Department of Transportation (DOT).

ROBERTSON, I. N., RIGGS, R. H., YIM, S. C. S. & YOUNG, Y. L. 2007. Lessons from Hurricane Katrina storm surge on bridges and buildings. *Journal of Waterway, Port, Coastal and Ocean Engineering,* 133, 463-483.

ROKNEDDIN, K., GHOSH, J., DUEÑAS-OSORIO, L. & PADGETT, J. 2011. Bridge retrofit prioritization for aging transportation networks subject to seismic hazards. *Structure and Infrastructure Engineering,* In Review.

SARPKAYA, T. & ISAACSON, M. 1981. *Mechanics of wave forces on offshore structures,* New York, Van Nostrand Reinhold Co.

STEARNS, M. & PADGETT, J. E. 2011. Impact of 2008 Hurricane Ike on Bridge Infrastructure in the Houston/Galveston Region. *Journal of Performance of Constructed Facilities,* 1, 139.

STEIN, S. M., YOUNG, G. K., TRENT, R. E. & PEARSON, D. R. 1999. Prioritizing Scour Vulnerable Bridges Using Risk. *Journal of Infrastructure Systems*, 95-101.

USGS 2009. Evaluation of Potential Bridge Scour in Missouri. United Stated Geological Survey.

USGS. 2011. *The National Map Seamless Server* [Online]. United States Geological Survey. Available: http://seamless.usgs.gov/Website/Seamless/viewer.htm [Accessed 2011.

YANG, C. S., DESROCHES, R. & PADGETT, J. E. Fragility curves for a typical california box girder bridge. 2009 ASCE Technical Council on Lifeline Earthquake Engineering Conference, TCLEE 2009: Lifeline Earthquake Engineering in a Multihazard Environment, June 28, 2009 - July 1, 2009, 2009 Oakland, CA, United states. American Society of Civil Engineers, 5.

ZHOU, Y., BANERJEE, S. & SHINOZUKA, M. 2010. Socio-economic effect of seismic retrofit of bridges for highway transportation networks: a pilot study. *Structure and Infrastructure Engineering: Maintenance, Management and Life Cycle,* 6, 145-157.

Appendix A- Definitions of Damage States

Table A.1: Definitions of Damage States, Adapeted from Padgett et al. (2008)

Damage State	Description
Slight	Minor cracking and spalling to the abutment, cracks in shear keys at abutments, minor spalling and cracks at hinges, minor spalling at the column (damage requires no more than cosmetic repair), minor cracking to the deck, or slight damage to operator house.
Moderate	Any column experiencing moderate (shear cracks) cracking and spalling (column structurally still sound), moderate movement of the abutment (<2"), extensive cracking and spalling of shear keys, any connection having cracked shear keys or bent bolts, keeper bar failure without unseating, rocker bearing failure, moderate settlement of the approach, moderate scour of the abutment or approach, damage to guardrails, wind and/or water damage to operator house resulting in switchboard or content damage.
Extensive	Any column degrading without collapse – shear failure (column structurally unsafe), significant residual movement at connections, or major settlement approach, vertical offset of the abutment, differential settlement at connections, shear key failure at abutments, extensive scour of abutments, or submerged electrical or mechanical equipment.
Complete	Any column collapsing or connection losing all bearing support, which may lead to imminent deck collapse, span unseating, tilting of substructure due to foundation failure.

Appendix B- Assumptions on Missing Data

While the subsets of bridges were determined based on restrictions to the applicable equations (i.e. the capacity model for uplift doesn't account for timber bridges, pier scour can only be determined on bridges with piers and abutment scour on bridges without riprap), even after determining the subsets of bridges, some data was missing despite the multitude of data sources. The missing data was usually attack angle of the water to the pier or abutment or the setback of the abutment from the water. When a bridge was missing a piece of data, rather than strike the bridge from the database, some assumptions were made about the missing data on order to run the vulnerability models on the bridge.

For pier scour, if the attack angle of the water to the pier was missing, the attack angle was assumed to be zero, as most of the bridges are aligned such that the water hits the bridge piers straight on. For a few bridges, pier type and size were missing; in those cases, a standard size of pier, 16 by 16 inches, was assumed until it can be replaced with more accurate data, and the pier type was assumed to be round-nose as most of the piers are of that type. Finally, as noted in the pier scour section of the scour chapter, if the pile lengths of a given pier were unavailable, as set limit state was used based on a 40ft pile length. Only 7 out of the 123 bridges had data pieces assumed, other than attack angle and pile length.

The data available for abutment scour was less completed than that for pier scour, but with some appropriate assumptions, all of the data for the 107 bridges

was obtained. As with pier scour, the attack angle of the abutment was the piece of data that was missing from the most bridges; in that case, the attack angle was assumed as zero in keeping with the pier scour assumptions and the data collected. Another piece of data missing from several bridges was the setback of the abutment from the water's edge. For setback, the assumed length depended on the abutment type: if the abutment type was vertical wall, then setback was assumed as 10ft, and if the abutment was a sloping spill through, the setback was assumed as 40ft. These numbers are based on the site visits conducted and the rest of the obtained data that suggested the setbacks were greater for sloping spill through bridges than for vertical wall ones. Similarly, if abutment type was missing (none of the bridges had setback, abutment length and abutment type missing), the type was assumed as vertical wall if the length of the abutment was less than 10ft, and as sloping spill through if the length was greater than 10ft. Finally, if the length of the abutment was missing, it was assumed to have 1 ft length as all the bridges with this were of a vertical wall abutment type. For abutment scour, 53 out of the 107 bridges tested had at least one piece of data assumed. This is keeping with abutment data being scarcer than the pier data.

Appendix C- Parameters of Fragility Curve Fitting for Pier Scour

Exponential Form: $P_f = a * e^{b*V_1} + c * e^{d*V_1}$

Quadratic Form: $P_f = a * V_1^2 + b * V_1 + c$

Power Form: $P_f = a * V_1^b + c$

Equation C.1: Forms of the Pier and Abutment Fragility Curves

Table C.1: Parameters of Fragility Curve Fitting for Pier Scour

Pier Bridge Number	$P_f = 0$ until $V_1 \geq$	a	b	c	d	Form
1	1	0.9902	-0.002283	-9.363	-1.974	Exponential
2	0.3	-0.04232	0.4207	-0.1827	N/A	Quadratic
3	0.3	0.9445	0.009071	-1.515	-1.233	Exponential
4	0.6	0.006733	0.03227	-0.03476	N/A	Quadratic
5	0.6	0.008782	0.02761	-0.02838	N/A	Quadratic
6	1.2	1.875	-0.1206	-5.606	-0.9191	Exponential
7	0.5	1.175	-0.03671	-2.905	-1.483	Exponential
8	1.2	0.000469	3	-0.00052	N/A	Power
9	1.2	0.000476	3.034	-0.00015	N/A	Power
10	0.7	0.1402	0.9626	-0.114	N/A	Power
11	0.5	0.08921	1.099	-0.06625	N/A	Power
12	1.2	1.53	-0.08651	-6.519	-1.145	Exponential
13	1.3	1.334	-0.06147	-10.08	-1.47	Exponential
14	1.3	1.454	-0.07567	-7.158	-1.184	Exponential
15	1.4	1.218	-0.04412	-23.83	-1.99	Exponential
16	1.4	1.213	-0.0432	-25.06	-2.025	Exponential
17	1.4	0.000423	2.133	-0.00037	N/A	Power
18	0.5	0.07777	1.153	-0.05269	N/A	Power
19	1.3	1.179	-0.03157	-9.969	-1.317	Exponential
20	1.3	-0.1008	0.9118	-1.11	N/A	Quadratic

Pier Bridge Number	$P_f = 0$ until $V_1 \geq$	a	b	c	d	Form
21	1.3	1.952	-0.1242	-5.655	-0.8606	Exponential
22	0.5	0.1795	0.9596	-0.1443	N/A	Power
23	2.2	-0.06783	0.8604	-1.672	N/A	Quadratic
24	1.4	-0.08534	0.8529	-1.169	N/A	Quadratic
25	1.2	1.232	-0.0453	-9.634	-1.582	Exponential
26	1.7	0.06681	1.635	-0.214	N/A	Power
27	1.5	1.98	-0.1386	-10.93	-1.158	Exponential
28	1.7	-0.08914	0.9489	-1.512	N/A	Quadratic
29	1.9	0.005483	2.789	-0.05278	N/A	Power
30	1.3	-0.07848	0.7751	-0.9879	N/A	Quadratic
31	1.5	0.05008	1.678	-0.144	N/A	Power
32	2.1	0.007813	2.678	-0.08928	N/A	Power
33	1.3	-0.04291	0.5486	-0.7709	N/A	Quadratic
34	1.5	-0.0507	0.6055	-0.8738	N/A	Quadratic
35	2.4	-0.06513	0.8843	-1.868	N/A	Quadratic
36	2.4	-0.05959	0.8454	-1.805	N/A	Quadratic
37	1.1	1.03	-0.007568	-1654	-6.173	Exponential
38	1.5	-0.06609	0.7865	-1.293	N/A	Quadratic
39	2.6	0.2526	1.182	-0.8463	N/A	Power
40	1.8	-0.1102	1.122	-1.837	N/A	Quadratic
41	1.7	0.008935	2.454	-0.05509	N/A	Power
42	1.9	0.03102	-0.04394	-0.05308	N/A	Quadratic
43	2.1	0.09882	1.499	-0.3399	N/A	Power
44	1.6	2.638	-0.1878	-10.88	-0.9875	Exponential
45	1.6	-0.1781	1.505	-2.137	N/A	Quadratic
46	2.2	0.1223	1.516	-0.4742	N/A	Power
47	1.3	1.639	-0.09513	-5.91	-0.9848	Exponential
48	1.7	2.276	-0.1609	-12.71	-1.083	Exponential
49	1.8	1.077	-0.01508	-94.22	-2.138	Exponential
50	1.8	2.893	-0.1789	-9.73	-0.7735	Exponential
51	1.8	-11.11	-0.9752	1.873	-0.1123	Exponential
52	1.8	2.738	-0.1715	-9.744	-0.7956	Exponential
53	2	-0.0743	0.8798	-1.588	N/A	Quadratic
54	1.5	-525.7	-13.28	1.005	N/A	Power
55	1.5	-1613	-15.79	1.004	N/A	Power

Pier Bridge Number	$P_f = 0$ until $V_1 \geq$	a	b	c	d	Form
56	1.7	1.247	-0.04851	-53.27	-2.11	Exponential
57	1.5	-517.4	-13.28	1.005	N/A	Power
58	1.1	-13	-15.18	1.002	N/A	Power
59	1	-4.695	-16.23	1.002	N/A	Power
60	1	-4.735	-16.31	1.002	N/A	Power
61	1.7	1.152	-0.03231	-218	-2.922	Exponential
62	1.8	-0.1283	1.222	-1.917	N/A	Quadratic
63	1.5	1.364	-0.06091	-22.19	-1.439	Exponential
64	1.3	1.155	-0.02634	-8.074	-1.177	Exponential
65	1.4	-0.08662	0.8305	-1.068	N/A	Quadratic
66	1.2	1.124	-0.02705	-22.51	-2.294	Exponential
67	2.2	0.06978	1.738	-0.3153	N/A	Power
68	1.7	-0.02515	0.4652	-0.8095	N/A	Quadratic
69	1.3	1.144	-0.03029	-19.2	-2.044	Exponential
70	1.8	-17.39	-1.267	1.347	-0.05567	Exponential
71	1.8	1.79	-0.1155	-15.15	-1.231	Exponential
72	1.2	1.051	-0.01169	-50.47	-3.016	Exponential
73	2.1	1.413	-0.07508	-200	-2.297	Exponential
74	1.7	2.159	-0.1454	-10.27	-0.9901	Exponential
75	1.8	-16.96	-1.248	1.374	-0.05937	Exponential
76	1.9	-12.93	-0.7537	4.321	-0.244	Exponential
77	2.1	1.448	-0.0803	-177.6	-2.234	Exponential
78	1.9	-0.09392	0.973	-1.605	N/A	Quadratic
79	1.8	-0.03859	0.5725	-0.9918	N/A	Quadratic
80	1.8	-0.0548	0.6936	-1.173	N/A	Quadratic
81	1.8	-0.05853	0.7215	-1.219	N/A	Quadratic
82	1.3	1.523	-0.07876	-5.135	-0.9269	Exponential
83	1.5	6.606	-0.284	-10.46	-0.5619	Exponential
84	1.6	-0.09784	0.9835	-1.484	N/A	Exponential
85	1.4	-5.715	-0.7624	1.846	-0.1024	Exponential
86	1.2	1.597	-0.09014	-5.163	-0.9522	Exponential
87	1.8	1.527	-0.06999	-6.818	-0.8303	Exponential
88	2.4	-0.08034	0.9906	-2.015	N/A	Quadratic
89	2.4	-0.07876	0.9807	-2.004	N/A	Quadratic
90	1.8	1.356	-0.0587	-19.95	-1.355	Exponential

Pier Bridge Number	$P_f = 0$ until $V_1 \geq$	a	b	c	d	Form
91	1.9	1.746	-0.1013	-13.57	-1.062	Exponential
92	1.4	6.35	-0.231	-8.491	-0.4199	Exponential
93	1.9	2.317	-0.1502	-14.28	-0.9722	Exponential
94	1.9	-20	-1.211	1.751	-0.1057	Exponential
95	2.2	-0.2268	2.029	-3.52	N/A	Quadratic
96	1.4	3.219	-0.2047	-7.209	-0.7247	Exponential
97	2.5	-0.04546	0.8281	-1.951	N/A	Quadratic
98	1.3	1.656	-0.09826	-6.242	-1.016	Exponential
99	2	1.499	-0.08714	-87.54	-1.995	Exponential
100	2.2	-0.1416	1.428	-2.608	N/A	Quadratic
101	1.3	1.746	-0.1065	-5.908	-0.9485	Exponential
102	1.3	1.651	-0.09601	-5.832	-0.9726	Exponential
103	1.5	-0.1053	0.9898	-1.364	N/A	Quadratic
104	1.2	1.232	-0.04742	-16.06	-1.945	Exponential
105	1.1	-7.065	-10.58	1.005	N/A	Power
106	1.8	-16.38	-0.5035	11.31	-0.3188	Exponential
107	1.3	1.081	-0.01877	-156	-3.555	Exponential
108	1.3	1.04	-0.009701	-1425	-5.206	Exponential
109	2.2	-0.1711	1.663	-3.036	N/A	Quadratic
110	2.4	-0.1525	1.592	-3.135	N/A	Quadratic
111	1	-3.233	-12.43	1.003	N/A	Power
112	1.3	3.517	-0.2038	-6.369	-0.6117	Exponential
113	1.2	1.094	-0.0217	-109.9	-3.497	Exponential
114	1.8	-0.02166	0.4437	-0.7689	N/A	Quadratic
115	1.3	3.498	-0.1874	-5.684	-0.5306	Exponential
116	2.1	-56.13	-1.578	1.38	-0.06208	Exponential
117	2	-160.9	-2.108	1.102	-0.01942	Exponential
118	1.3	2.05	-0.1323	-5.691	-0.8372	Exponential
119	1.9	3E-05	5.314	-0.00105	N/A	Power
120	1.5	-0.08141	0.837	-1.189	N/A	Quadratic
121	1.9	-0.07824	0.867	-1.469	N/A	Quadratic
122	1.5	1.64	-0.08516	-7.262	-0.8911	Exponential
123	1.3	1.904	-0.124	-6.328	-0.949	Exponential

Appendix D- Parameters of Fragility Curve Fitting for Abutment Scour

Table D.1: Parameters of Fragility Curve Fitting for Abutment Scour

Abutment Bridge Number	$P_f = 0$ until $V_1 \geq$	a	b	c	d	Form
1	0.86	0.9848	0.008098	-15000	-11.03	Exponential
2	0.26	0.998	0.001321	-7873	-33.33	Exponential
3	0.31	1.002	-0.001345	-22770	-31.25	Exponential
4	0.37	0.9897	0.006548	-1355	-18.46	Exponential
5	0.38	0.9887	0.007203	-1277	-18.3	Exponential
6	0.31	0.9864	0.008844	-214.1	-17.03	Exponential
7	0.31	0.9852	0.009669	-237.7	-17.37	Exponential
8	1	1.083	-0.04418	-3535	-7.99	Exponential
9	0.99	1.134	-0.06906	-1846	-7.367	Exponential
10	1	1.089	-0.04738	-3210	-7.891	Exponential
11	0.98	1.072	-0.03902	-3154	-8.008	Exponential
12	0.38	0.9899	0.006405	-1172	-18.07	Exponential
13	0.31	0.9863	0.008975	-228	-17.24	Exponential
14	0.87	0.9961	0.001572	-12800	-10.7	Exponential
15	0.87	0.9981	0.0004225	-12310	-10.64	Exponential
16	0.31	-9.302E-07	-12.1	1	N/A	Power
17	1.27	1.207	-0.09966	-709.9	-5.051	Exponential
18	1.33	4.024	-0.6307	-153.6	-3.33	Exponential
19	0.9	1.02	-0.01202	-10210	-10.05	Exponential
20	0.94	0.9849	0.007326	-7805	-9.434	Exponential
21	0.96	0.9914	0.003654	-9103	-9.365	Exponential
22	0.95	0.9804	0.009682	-8943	-9.449	Exponential
23	0.92	0.981	0.009588	-6447	-9.399	Exponential
24	1	1.113	-0.059	-2576	-7.652	Exponential
25	1.33	2.662	-0.4533	-220.1	-3.726	Exponential
26	0.92	0.9906	0.004129	-5520	-9.233	Exponential
27	0.92	0.9872	0.006028	-6045	-9.325	Exponential
28	1.26	1.349	-0.1523	-493.6	-4.77	Exponential
29	1.26	1.322	-0.1412	-488	-4.765	Exponential

Abutment Bridge Number	$P_f = 0$ until $V_1 \geq$	a	b	c	d	Form
30	0.91	0.986	0.006667	-5940	-9.399	Exponential
31	0.94	1.021	-0.01247	-3977	-8.628	Exponential
32	0.89	1.019	-0.01124	-8653	-9.975	Exponential
33	0.9	1	-0.0006527	-15870	-10.6	Exponential
34	0.94	1.003	-0.002816	-5825	-9.077	Exponential
35	0.95	1.021	-0.01296	-4600	-8.704	Exponential
36	0.95	1.003	-0.003062	-6428	-9.086	Exponential
37	0.95	1.01	-0.006505	-5442	-8.928	Exponential
38	0.92	0.9983	-0.00004957	-4805	-9.042	Exponential
39	1.21	1.109	-0.05857	-598.1	-5.183	Exponential
40	1.21	0.9911	-0.002495	-801.4	-5.47	Exponential
41	1.32	4.918	-0.7079	-119.5	-3.085	Exponential
42	1.28	1.398	-0.1689	-535.9	-4.761	Exponential
43	1.26	1.184	-0.08844	-637.4	-5.008	Exponential
44	1.33	3.422	-0.5672	-196.4	-3.564	Exponential
45	1.61	-0.3923	3.813	-5.196	N/A	Quadratic
46	1.32	7.449	-0.8728	-102.4	-2.825	Exponential
47	1.32	3.512	-0.5717	-158.5	-3.408	Exponential
48	1.33	3.662	-0.5914	-167.9	-3.425	Exponential
49	0.99	1.132	-0.06806	-1819	-7.353	Exponential
50	1	1.086	-0.04623	-3335	-7.928	Exponential
51	1	1.092	-0.04893	-2974	-7.815	Exponential
52	0.92	1.011	-0.006836	-3656	-8.758	Exponential
53	0.99	1.046	-0.02572	-5190	-8.458	Exponential
54	0.9	1.013	-0.007868	-9967	-10.06	Exponential
55	0.99	1.029	-0.01701	-6002	-8.63	Exponential
56	0.94	0.9898	0.004576	-7459	-9.341	Exponential
57	1.26	1.193	-0.09413	-732.4	-5.113	Exponential
58	0.94	1.011	-0.00727	-4863	-8.851	Exponential
59	1.24	1.089	-0.0487	-814.4	-5.312	Exponential
60	0.99	1.054	-0.02953	-4424	-8.299	Exponential
61	0.91	0.9844	0.007626	-5460	-9.352	Exponential
62	1.27	1.394	-0.1663	-477.2	-4.7	Exponential
63	1.22	1.299	-0.1336	-396.8	-4.746	Exponential
64	1.26	1.672	-0.2529	-313.1	-4.334	Exponential

Abutment Bridge Number	$P_f = 0$ until $V_1 \geq$	a	b	c	d	Form
65	1.26	1.279	-0.1262	-567.8	-4.891	Exponential
66	1.3	4.127	-0.6429	-130.5	-3.252	Exponential
67	1.25	1.029	-0.02132	-1032	-5.491	Exponential
68	1.22	0.9501	0.01744	-1081	-5.685	Exponential
69	1.27	1.655	-0.2483	-353.7	-4.404	Exponential
70	0.95	0.9903	0.004255	-6646	-9.155	Exponential
71	0.95	1.001	-0.001755	-6183	-9.033	Exponential
72	0.99	1.033	-0.0189	-6235	-8.662	Exponential
73	0.98	1.005	-0.004187	-8143	-9.072	Exponential
74	0.94	0.9809	0.009522	-8147	-9.453	Exponential
75	1.22	1.318	-0.1402	-383.8	-4.706	Exponential
76	1.32	13.69	-1.079	-87.34	-2.455	Exponential
77	1.32	22.19	-1.228	-89.62	-2.265	Exponential
78	1.31	-6.939	-6.368	1.067	N/A	Power
79	0.99	1.032	-0.01846	-5772	-8.587	Exponential
80	1.32	3.961	-0.6263	-155.3	-3.355	Exponential
81	1.33	2.991	-0.5075	-209.2	-3.662	Exponential
82	1.32	7.269	-0.8647	-105.8	-2.858	Exponential
83	0.9	1.016	-0.009418	-11040	-10.14	Exponential
84	1.33	4.037	-0.6329	-156.4	-3.342	Exponential
85	1	1.097	-0.05115	-2803	-7.761	Exponential
86	0.99	1.047	-0.02638	-4769	-8.376	Exponential
87	0.94	1.02	-0.01205	-3730	-8.579	Exponential
88	0.99	1.043	-0.02434	-5086	-8.446	Exponential
89	0.94	1.033	-0.01892	-3173	-8.391	Exponential
90	0.94	1.008	-0.005776	-5101	-8.905	Exponential
91	0.99	1.039	-0.02231	-5488	-8.535	Exponential
92	0.98	1.08	-0.04313	-2954	-7.934	Exponential
93	0.95	1.081	-0.04367	-6050	-8.947	Exponential
94	0.95	1.019	-0.01138	-4446	-8.673	Exponential
95	0.95	1.077	-0.04167	-5973	-8.937	Exponential
96	0.95	1.066	-0.03622	-6876	-9.109	Exponential
97	0.95	1.055	-0.03026	-8075	-9.275	Exponential
98	0.95	0.9946	0.001717	-7413	-9.261	Exponential
99	0.94	1.013	-0.008443	-4583	-8.798	Exponential

Abutment Bridge Number	$P_f = 0$ until $V_1 \geq$	a	b	c	d	Form
100	0.94	1.02	-0.01219	-4223	-8.716	Exponential
101	0.94	1.002	-0.002187	-5457	-8.986	Exponential
102	0.98	1.072	-0.03912	-3260	-8.051	Exponential
103	1.32	3.569	-0.5823	-169.1	-3.453	Exponential
104	1.32	4.767	-0.697	-126.3	-3.138	Exponential
105	1	1.096	-0.05072	-3081	-7.836	Exponential
106	0.99	1.054	-0.02962	-4525	-8.316	Exponential
107	0.95	1.017	-0.01068	-5300	-8.849	Exponential

Appendix E- Risk Maps of Houston/Galveston Case Study

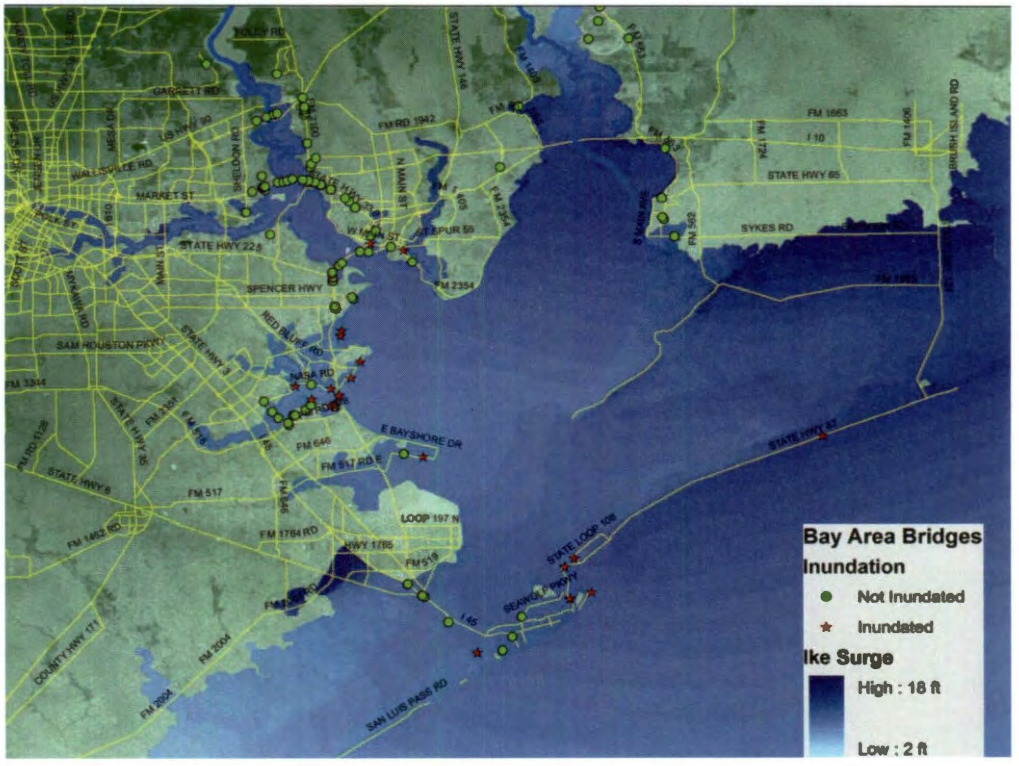

Figure E.1: Map of Inundated Bridges in the Hurricane Ike Scenario

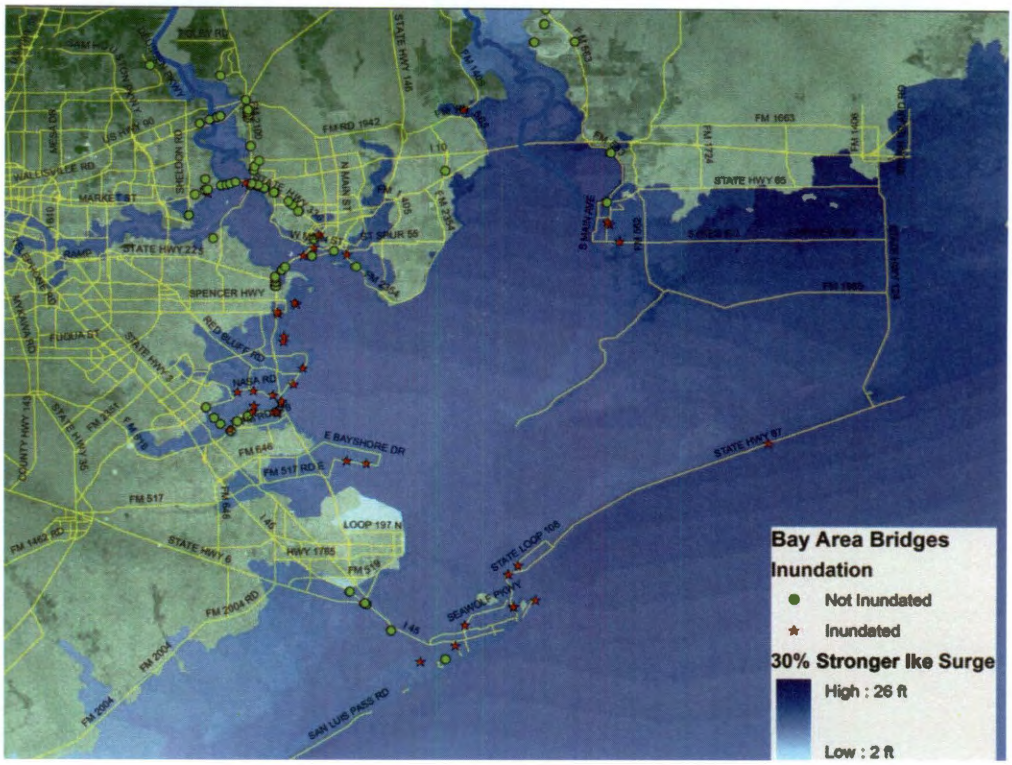

Figure E.2: Map of Inundated Bridges in the Ike + 30% Scenario.

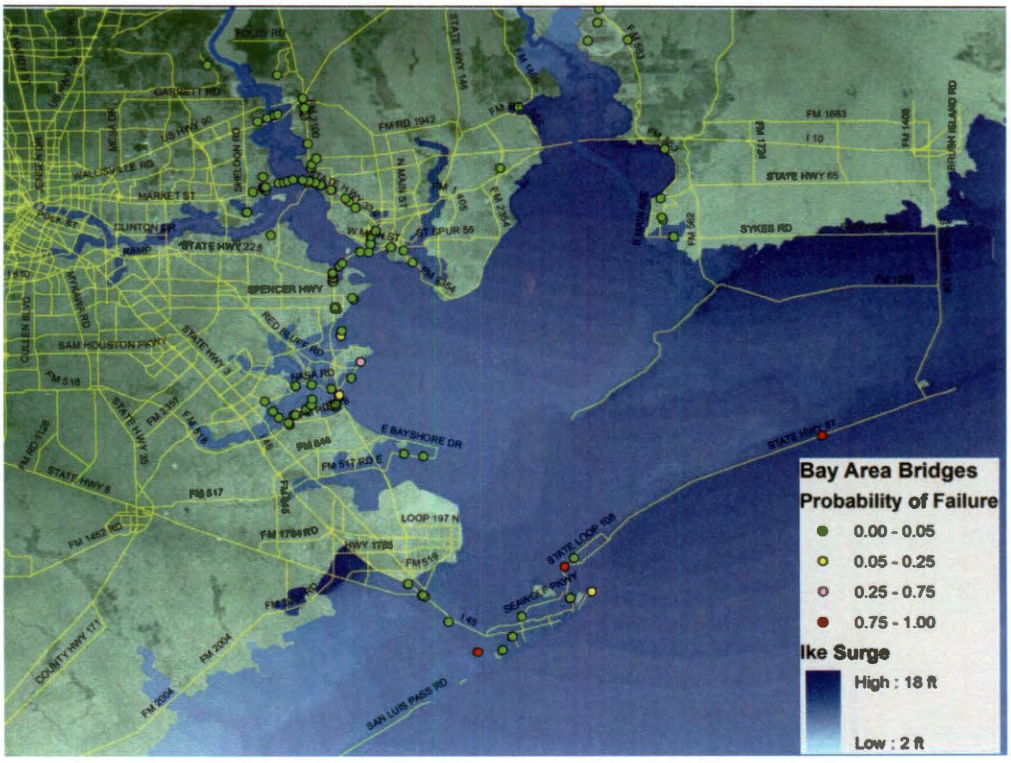

Figure E.3: Map of Failure Probabilities from Uplift in the Hurricane Ike Scenario.

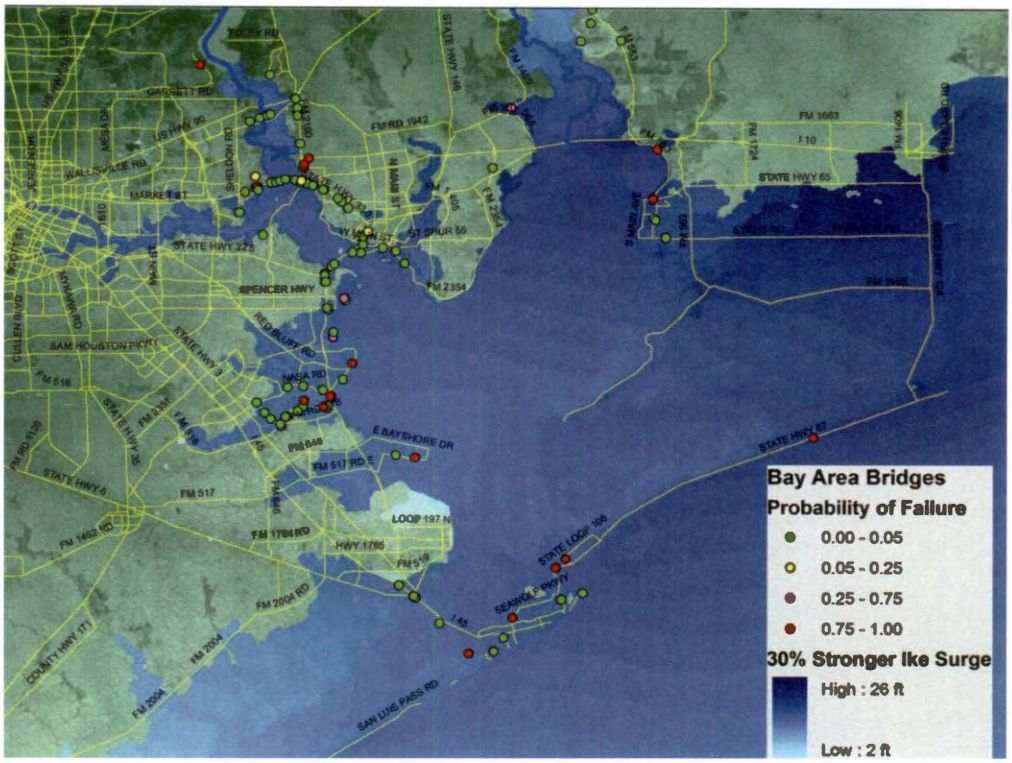

Figure E.4: Map of Failure Probabilities from Uplift in the Ike +30% Scenario.

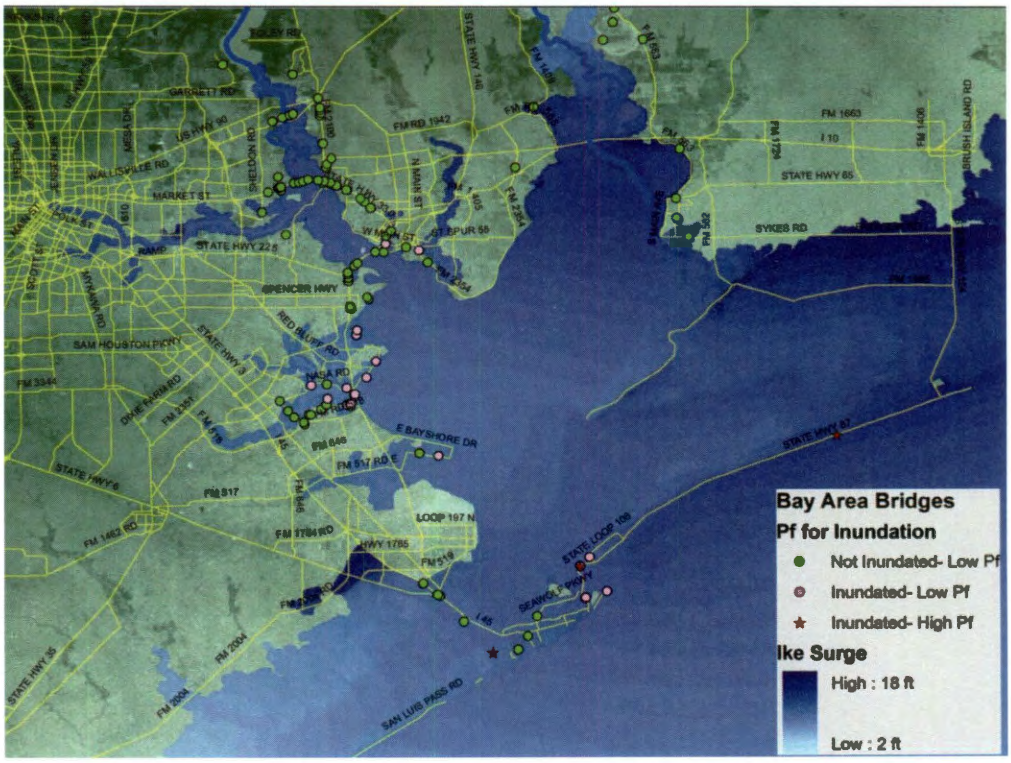

Figure E.5: Comparison Map of Uplift and Inundation for Hurricane Ike Scenario.

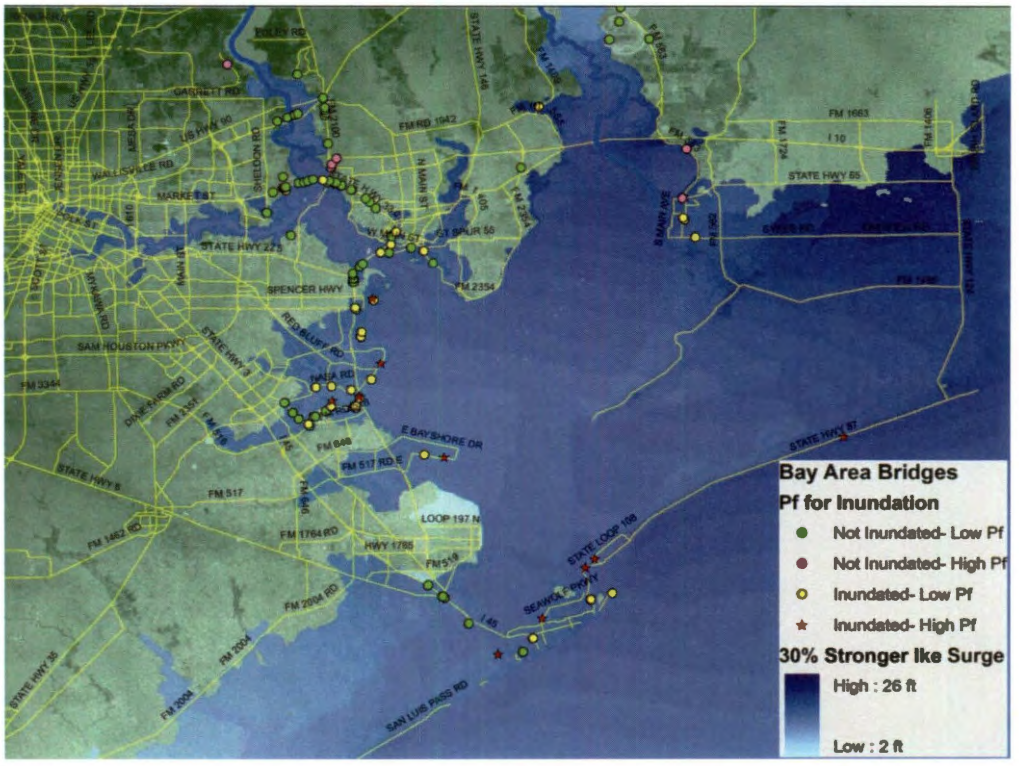

Figure E.6: Comparison Map of Uplift and Inundation for Ike +30% Scenario.

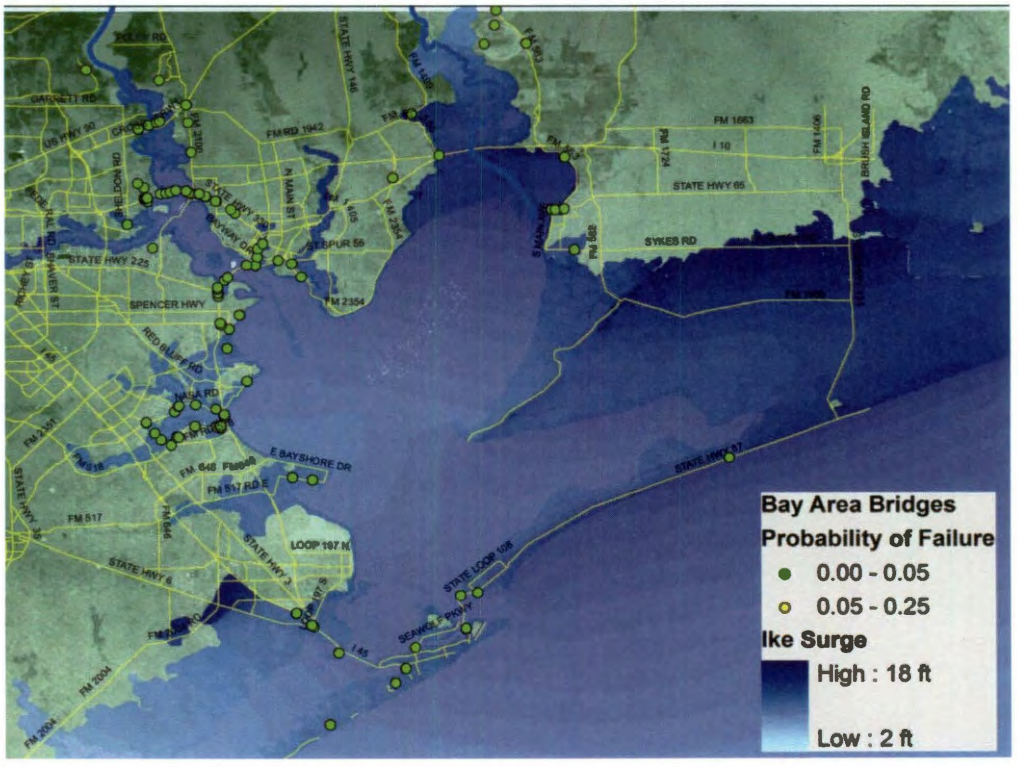

Figure E.7: Map of Failure Probabilities for Pier Scour in the Hurricane Ike Scenario.

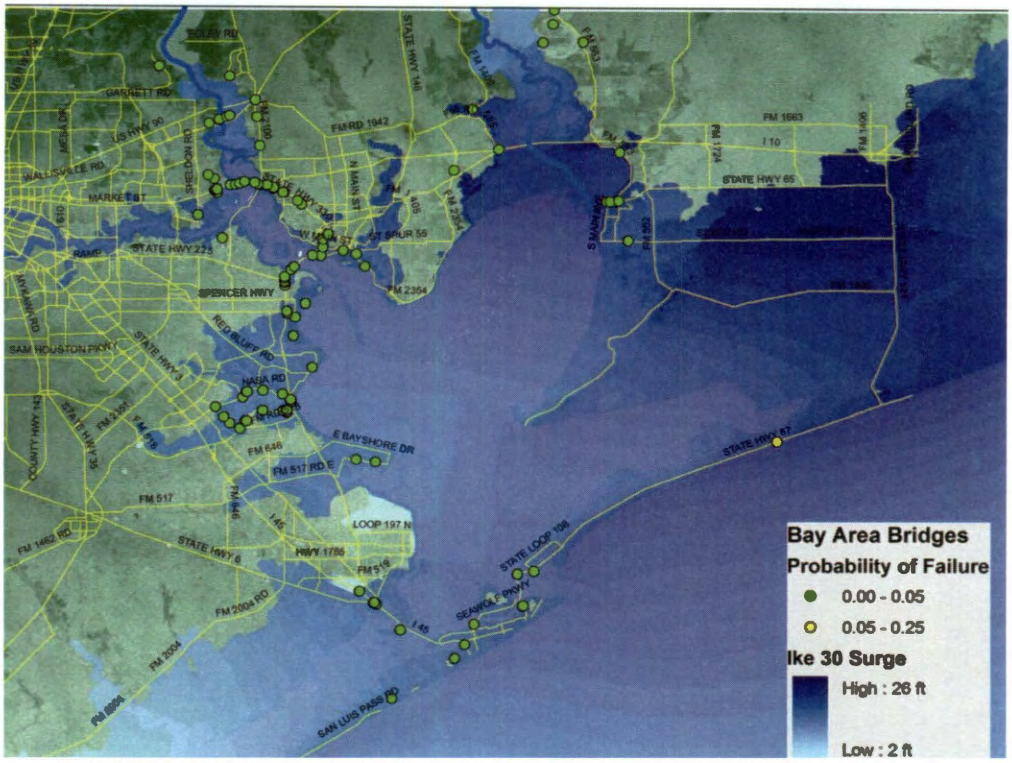

Figure E.8: Map of Failure Probabilities for Pier Scour in the Ike +30% Scenario.

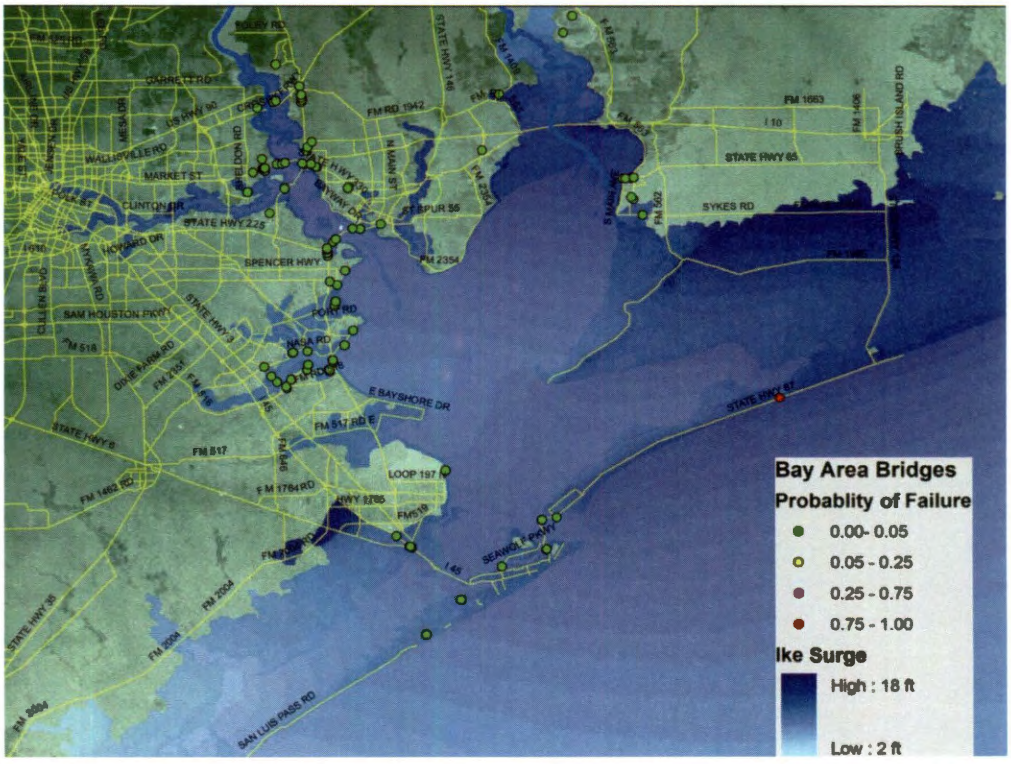

Figure E.9: Map of Failure Probabilities for Abutment Scour in "Ike" Scenario.

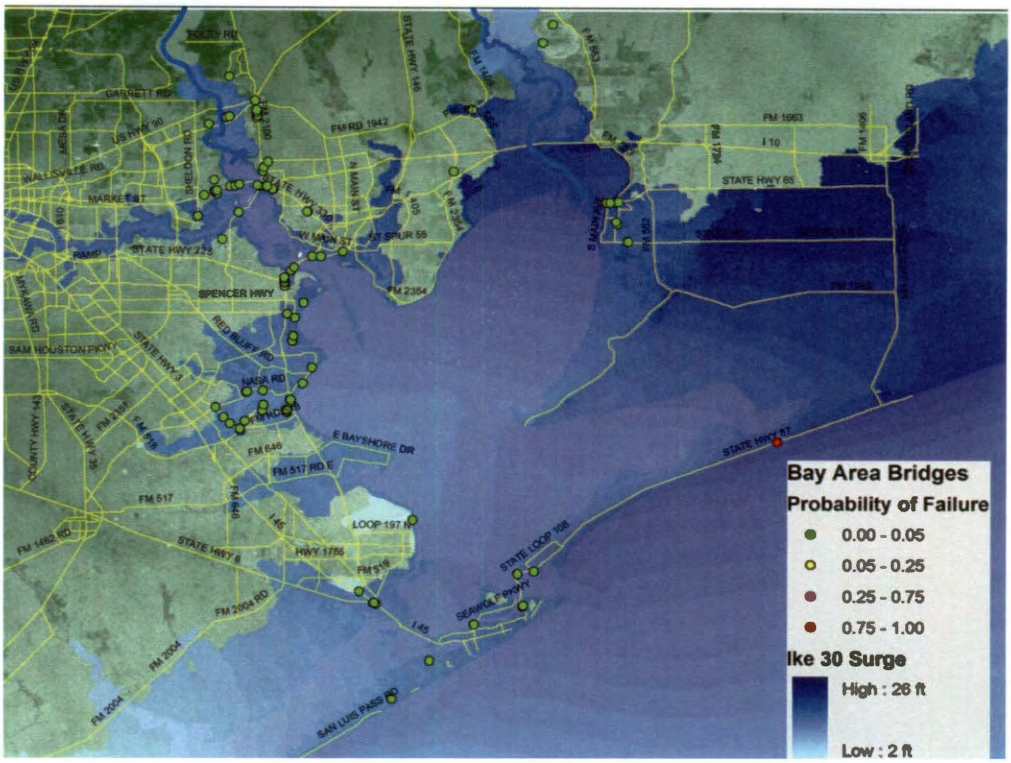

Figure E.10: Map of Failure Probabilities for Abutment Scour in Ike + 30% Scenario.

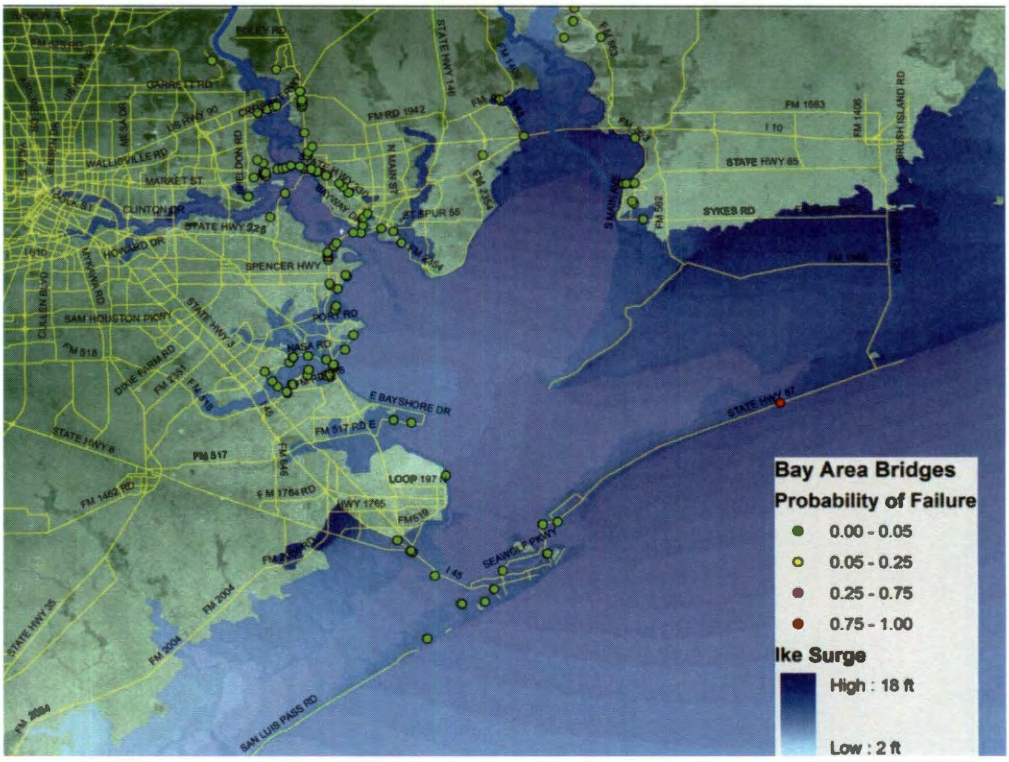

Figure E.11: Map of Failure Probabilities for Local Scour in Hurricane Ike Scenario.

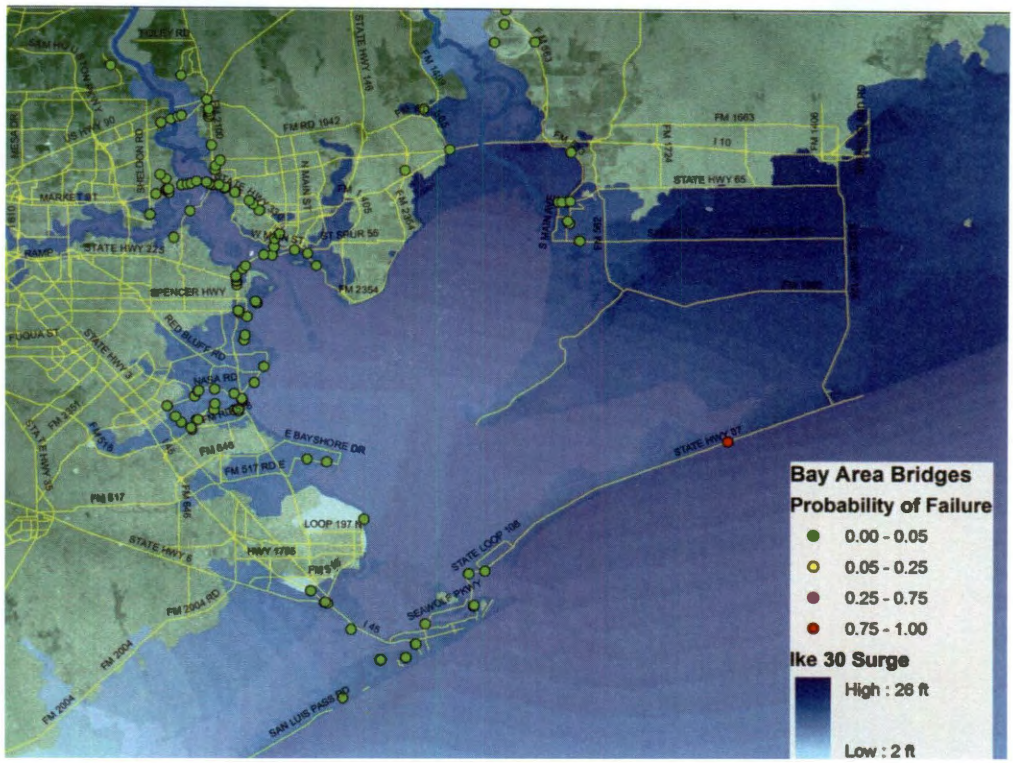

Figure E.12: Map of Failure Probabilities for Local Scour in Ike + 30% Scenario.

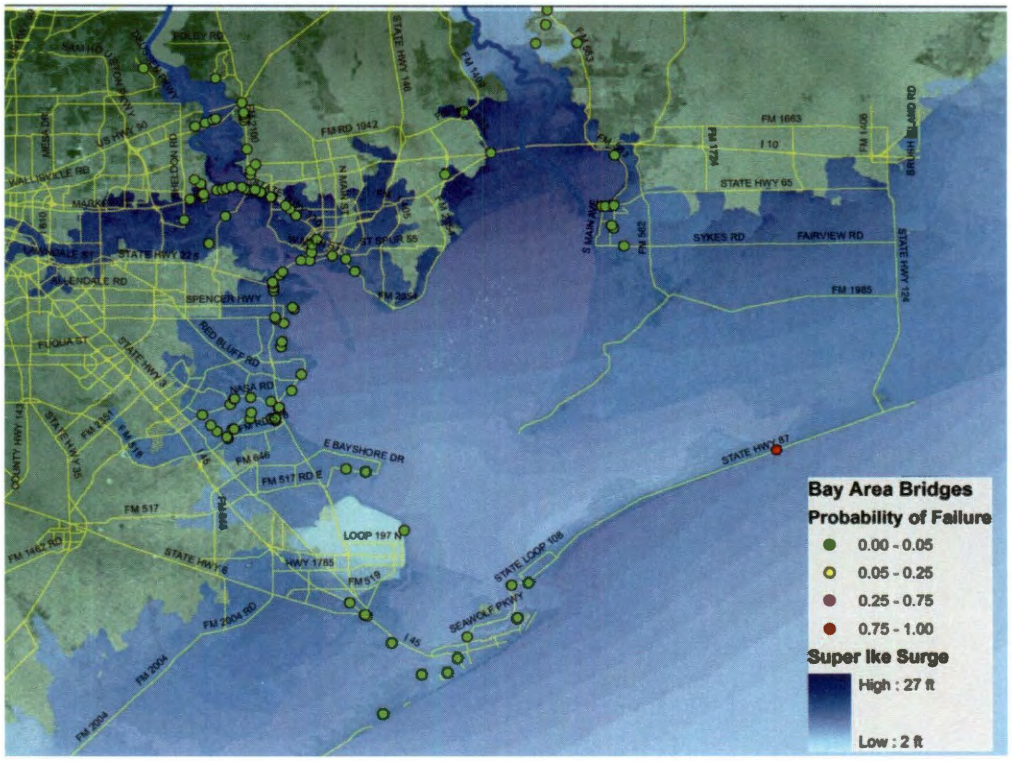

Figure E.13: Map of Failure Probabilities for Local Scour in "Super Ike" Scenario.

Figure E.14: Map of Embankment Scour Risk Levels for Hurricane Ike Scenario.

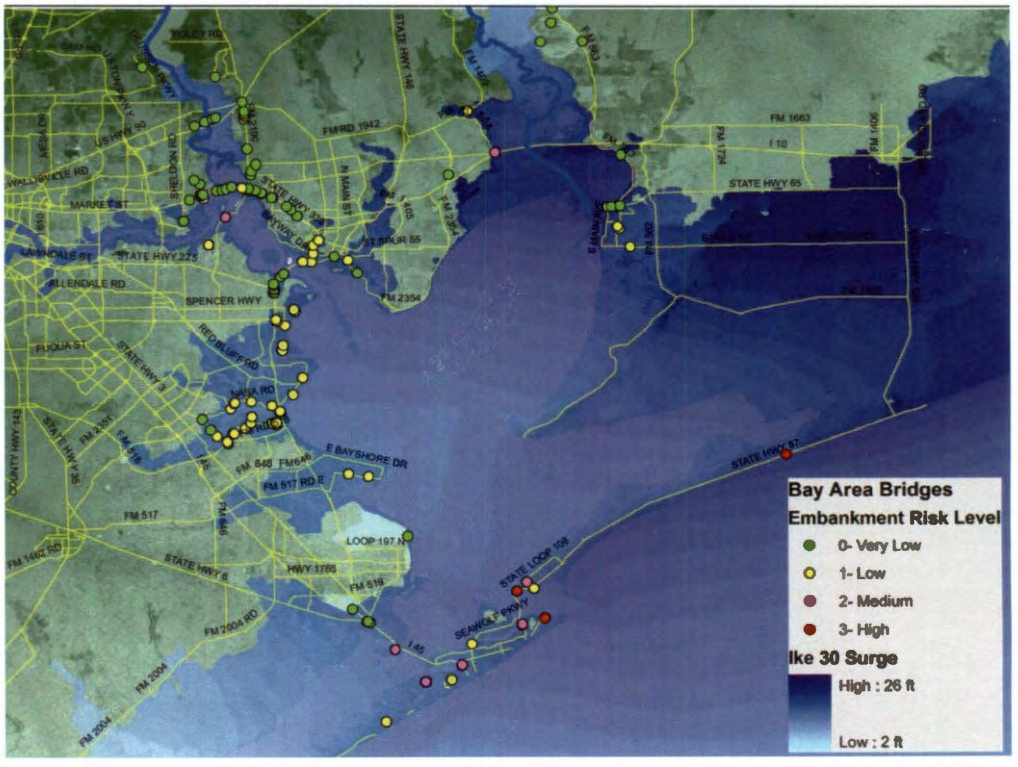

Figure E.15: Map of Embankment Scour Risk Levels for Ike + 30% Scenario.